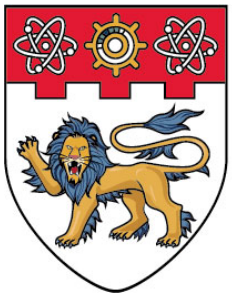

NANYANG TECHNOLOGICAL UNIVERSITY
SINGAPORE

AMPACITY AND THERMAL EQUIVALENT MODELING OF SUBSEA POWER CABLES FOR LONG DISTANCE POWER TRANSMISSION AND OPTIMIZATION

NISHANTHI DURAISAMY
SCHOOL OF ELECTRICAL AND ELECTRONIC ENGINEERING

2021

Ampacity and Thermal Equivalent Modeling of Subsea Power Cables for Long Distance Power Transmission and Optimization

Nishanthi Duraisamy

School of Electrical and Electronic Engineering

A thesis submitted to the Nanyang Technological University
in partial fulfillment of the requirement for the degree of
Doctor of Philosophy

2021

Statement of Originality

I hereby certify that the work embodied in this thesis is the result of original research, is free of plagiarised materials, and has not been submitted for a higher degree to any other University or Institution.

09-08-21

.....

Date

.....

Nishanthi Duraisamy

Supervisor Declaration Statement

I have reviewed the content and presentation style of this thesis and declare it is free of plagiarism and of sufficient grammatical clarity to be examined. To the best of my knowledge, the research and writing are those of the candidate except as acknowledged in Author Attribution Statement. I confirm that the investigations were conducted in accord with the ethics policies and integrity standards of Nanyang Technological University and that the research data are presented honestly and without prejudice.

09-08-21

. . . . . .

Date

. . . . . .

Assoc. Prof. H. B. Gooi

Authorship Attribution Statement

The thesis contains materials from one published journal paper and one paper submitted for potential publication, in the following peer-reviewed journals, where I was the first and the corresponding author.

Chapter 4 is published as: N. Duraisamy, H. B. Gooi, and A. Ukil "Ampacity Estimation for Submarine Power Cables Installed in Saturated Seabed - Experimental Studies," in *IEEE Transactions on Industry Applications*, vol. 56, no. 6, pp. 6229-6237, Nov.-Dec. 2020, doi: 10.1109/TIA.2020.3023398.

The contributions of the co-authors are as follows:

- I developed the concept, produced the results and prepared the manuscript.
- Assoc. Prof. Hoay Beng Gooi closely supervised all the research work, gave suggestions for the organisation of the manuscript and reviewed the manuscript for the final submission.
- Assoc. Prof. Abhisek Ukil reviewed the conceptualization and manuscript for the final submission.

09-08-21

. . . . . .

Date

. . . . . .

Nishanthi Duraisamy

To My Late Grandmother,

My Late Father, My Mother,

My Loving Family and My Teachers

Acknowledgement

I would like to take this opportunity to express my sincere gratitude towards my patient and encouraging supervisor **Associate Professor Hoay Beng Gooi** for his continued support and effort to help me reach significant level of progress in the research. It is a pleasure working with him and his attention to details inspired me to improve my approach towards the subject.

I am extremely grateful for being guided by Assoc. Prof. Abhisek Ukil who was my supervisor during the start of this PhD. Sincere thanks to him from the bottom of my heart for being exceptionally supportive even after he had to relocate to a different country. His overall insights in this field have made this an inspiring experience for me.

My sincere thanks to Energy Research Institute @ NTU (ERI@N) and Prof Subodh Mhaisalkar for all the support and funding given to me. I am grateful to have been associated with ERI@N that provided me with all the resources required for the research work including laboratory space, expert advice and guidance. I would like to thank Mr. Srinivasa Rao, Dr. Narasimalu Srikanth, Dr. Sriram and other colleagues of ERI@N FMS for their time and effort, and guidance provided to me. A special mention about my thesis advisory members - Dr Anshuman Tripathi, who had been a tremendous support throughout the PhD and Assistant Professor Xu Yan who extended their support and guidance for the research progress by providing constructive feedback during the TAC meeting sessions.

I would like to thank NTU for giving me this opportunity to pursue the studies and NTU libraries for being efficient and providing me access to resources and making special arrangements for those materials that were not under their subscription. I am grateful to Lloyd's Register Singapore Pte Ltd for supporting this studies and also Mr. Chen Fei from AIPEC Pte Ltd for his support to setup the experimentation.

I sincerely thank the field experts of this subject, researchers whose works formed a strong basis for this research work, and members of online forums who helped me readily with their subject knowledge.

Finally, my heartfelt thanks to my family and friends who have always been supportive of me and my efforts towards the PhD. Last but not least, I thank my wonderful and understanding son who had to sacrifice his time since he was a newborn.

Abstract

One of the defining aspects of life in the modern world is the convenience of access to a dependable and plentiful supply of electricity. This essential utility is delivered to consumers from power generating stations via an extensive and intricate network of cables. Submarine power cables are becoming increasingly important to modern power transmission strategies. There has been a large amount of recent investment in projects such as offshore wind farms and international “megagrid" initiatives, of which submarine power cables are essential components.

The installation and maintenance costs of such buried cables are far higher than the overhead lines due to the complexity involved. The cable construction and cooling system for the cables are not interchangeable with their overhead counterparts. The maximum allowable cable conductor temperature is limited to avoid cable failures. The maximum current carrying capacity (ampacity) of power cables depends on the heat transferability of its surrounding medium. Submarine power cable ampacity is calculated conventionally following the international standards defined for underground cables. This conservative approach results in the system over design and under-utilization of the cable capacity. In reality, the thermal behavior of submarine environments differs significantly from its underground counterpart as the porous sediments are constantly water-saturated.

The research aims to model the electrical and thermal characteristics of such long distance cables for accurately determining the effect of the factors that influence the ampacity and optimize the power flow. The cable ampacity analyses were

carried out using the standards defined in IEEE 835 and IEC 60287. Unrealistic simplifications used for calculating the heat dissipation from the cable limited the validity of the calculation to specific cable geometries. Consequently, the first challenge in this work was developing a general reliable numerical procedure for the analysis of thermal field characteristics of the subsea cable systems of any system geometry, backfill and submarine environment. The effect of the thermal circuit parameter variations was the main concern as it has a higher effect on the cable's thermal behavior and it may result in a significant difference in the cable ampacity . In this regard, special attention was paid in developing a sensitivity methodology of thermal field with respect to the thermal parameter changes. The difficulties have arisen since the model developed here was based on the exact finite element implementation and did not involve any simplification for the thermal heat modeling.

The finite element method (FEM) was used for determining the factors affecting ampacity of submarine power cables cable using the COMSOL Multiphysics software program. Complex multiple layered co-axial cables were analysed to determine the effect of sediment properties on the cables ampacity. Considerations of sediment properties to calculate external thermal resistance resulted in ampacity values significantly different from standard values. Lab-scale experimentation was conducted to validate the results. The inclusion of convective heat transfer obtained a more precise ampacity estimate compared to that of the standard methods. The findings are significant for submarine power cables where the occurrence of convective cooling is neglected in general.

Table of Contents

List of Tables

List of Figures

Nomenclature

Acronyms

AC	Alternating Current
DC	Direct Current
DTS	Distributed Temperature Sensing
FEM	Finite Element Method
GW	Giga Watts
HDPE	High Density Poly Ethylene
HPTE	High-performance Polypropylene Thermoplastic Elastomer
HVAC	High Voltage Alternating Current
HVDC	High Voltage Direct Current
IEC	International Electrotechnical Commission
IEEE	Institute of Electrical and Electronics Engineers
kV	kilo Volts
MW	Mega Watts
PDE	Partial Differential Equation
PRN	Parallel Resistance Network
RAM	Random Access Memory
SPRN	Series-Parallel Resistance Network
SRN	Series Resistance Network
TC	Thermo-couple
XLPE	Cross-linked Poly Ethylene

Symbols

α	Thermal diffusivity	m^2/s
β	Coefficient of thermal expansion	
$\Delta\theta x$	Critical temperature of the soil	°C
$\Delta\theta$	Temperature difference	°C
ϵ	Porosity	
κ	Intrinsic permeability	m^2
λ_1, λ_2	Sheath and armor ratio compared to the conductor losses	
μ	Kinematic viscosity	m^2/s
ρ	Density	kg/m_3
ρ_m	Bulk density	kg/m_3
ρ_s, ρ_f	Solid and fluid phase density	kg/m_3
θ_s, θ_f	Solid and fluid phase temperature	°C
θ_{amb}	Ambient temperature	°C
Υ	Ratio of the thermal resistivities of dry and moist soil	
$\vec{v}$	Fluid velocity vector	m/s
A	Cross-sectional area	m^2
C_m	Specific heat capacity of bulk component	J/kg/°C
C_p	Specific heat capacity at constant pressure	J/kg/°C
C_{ps}, C_{pf}	Specific heat capacity of solid and fluid at constant pressure	J/kg/°C
D_e	Overall diameter of the cable	m
g	gravitational acceleration	m/s^2
h	Heat transfer coefficient	$W/m^2{\cdot}$°C
K	Hydraulic conductivity	cm/s
k	Thermal conductivity	W/m·°C
k_s, k_f	Solid and fluid phase thermal conductivity	W/m·°C
k_{eff}	Effective thermal conductivity	W/m·°C
L	Cable depth of burial	m

Nomenclature

L_g	Overall length of the cable	m
n	Number of cables	
Nu	Nusselt number	
q	Heat flux	W/m^2
Q_{in}, Q_{br}	Volumetric heat	W/m^3
R	AC resistance of the conductor	Ω
R_0	AC resistance of the conductor at 20∘C	Ω
r_i, r_o	Inner and outer radius	m
Ra	Rayleigh number	
Re	Reynolds number	
s	Distance of separation between cables	m
T_1, T_2, T_3	Thermal resistances of non-metallic layers of the cable	°C·m/W
T_4	Thermal resistances of external environment	°C·m/W
T_{cond}	Conductive thermal resistance	°C·m/W
T_{cond}	Convective thermal resistance	°C·m/W
TR_a, TR_b	Thermal resistances of solid and fluid phase components	°C·m/W
TR_{er}	Equivalent thermal resistance	°C·m/W
W_d	Dielectric losses of insulator	W/m^3

Chapter 1

Introduction

The growing population and urbanization of the globe created enormous needs for electrical energy. The ever-increasing demand for electricity is a clear motivation for exploration of new forms of energy sources. The advent of renewable energy sources and oil explorations in faraway lands and sea beds bring new challenges in the overall efficiency of such systems in terms of power production, distribution, transmission and delivery. Electricity produced at one place is not completely consumed at the same place. The generated power is generally transmitted over long distances using transmission and distribution systems [7].

Traditionally, electricity generated at the power plants is transmitted through complex network – the grid consisting of substations, power lines, and distribution transformers. Power cables form a major part of the transmission and distribution system. The heating losses in the cables increase with the increase in length. In order to improve the efficiency of power production and delivery, the energy losses must be reduced.

World-wide, the transmission lines that are majorly overhead are now reconsidered to make them go underground. In addition to the aesthetic features, underground cables are well protected from damages caused by unforeseeable calamities that overhead lines undergo. However, this comes with overhead costs for installation

and high maintenance in case failure happens. As more and more power lines become underground, the reliability and efficiency of the system must be carefully investigated. The underground lines are not exactly similar to their overhead counterparts. These cables behave different than overhead lines as their capacitances are higher, typically by 25-70 times [8]. That results in higher charging currents that limit the maximum transferable active power through the cable. In addition, submarine power cables are subjected to harsh environmental conditions and during failures the possibilities of intervention are limited [9]. The difficulties of repair and maintenance of these cables are far more serious than overhead lines. Thus making them an expensive system not only to maintain but also to design, protect and install.

1.1 Background

Submarine cables are in use since long time. However, they are re-purposed overtime to cater different needs. Earlier, submarine power cables were mainly deployed to power offshore facilities that were isolated like lighthouses, infirmary ships, etc. In due course the cables were also used to supply power to islands located close the mainland [10].

The first known power cable that was installed underwater was a low-voltage natural rubber insulated cable that was laid across the Isar river of Munich, Germany in 1811 [11], [12]. Other insulation materials like lead sheathed paper insulation were also in use during those early stages. The advent of water-resistant components and synthetic insulating materials lead to the development of high voltages cables in mid 1900s [13]. Later, variants of paper insulated, lead sheathed cables and cables with synthetic dielectrics like polyethylene were introduced in the underwater applications. Spain-Morocco, a 26 km long interconnection for the transmission of 700 MW power from Spain to Morocco at 400 kV AC was installed in 1995. Fluid filled insulation was used in the cable construction. One of the peculiarities of the

link is the maximum water depth of 615 m [14].

In 1954, the first HVDC submarine power cable was installed to connect Gotland island to mainland Sweden. This is a 100-kV cable delivering 20 MW power and the cable spans 50 km underwater [15]. In 1996, a 160 km long interconnection for the transmission of 500 MW (bi-directional) by means of paper insulated mass impregnated cable having 1250 mm^2 conductor size and rated for voltage of 400 kV was used for power transmission between Italy and Greece. This link attained the maximum water depth for submarine power cables: 1000 m [14]. Today, myriad of developments have been made both in the cable materials and construction processes that improved the design and performance significantly.

Present day submarine power cables have numerous applications. Now, oil-and-gas companies exploring new oil resources in the seabed and increasing offshore wind, tidal and wave energy-harvest provides new quarters for submarine cables outside the earlier usage. There are more than 9000 km of HVDC submarine power cables in use and many new interconnections are under the planning phase [16]. Rapid expansions are expected for the submarine power cable network due to the advancements in the off-shore renewable energy systems. The international renewable energy agency (IRENA) predicted that the off-shore wind power capacity would reach 228 GW by the year 2030. Typical power cable systems for subsea oil fields and offshore wind farms are shown in Fig. 1.1 and Fig. 1.2

More importantly, wake of rapid development in the offshore renewable energy resources brought submarine power cables to the attention again. However, these cables have their own characteristics and peculiarities. The technical and economic feasibility of the offshore systems depend heavily on the cables. The cost of these cables are higher and can make up to forty percentage of the total cost of the project, and the installation, planning and execution have significant impact on the overall schedule and expenditure [10].

On the other hand, power distribution from the traditional grid with underground

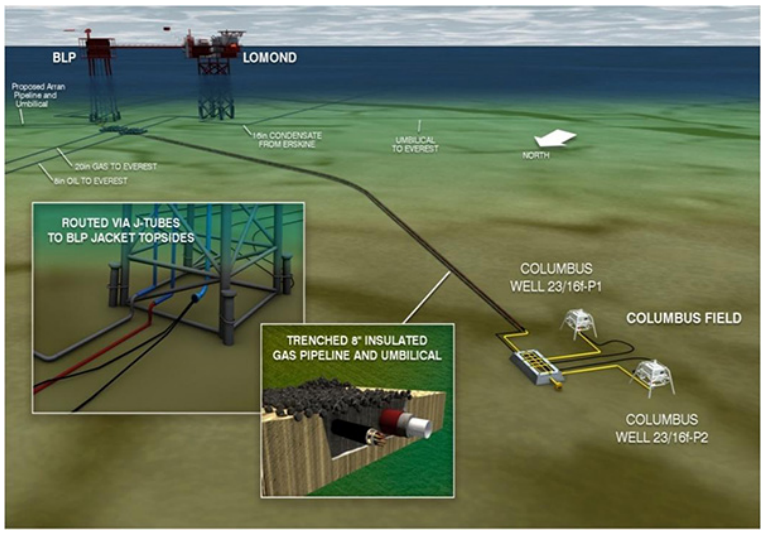

Figure 1.1: Cables in subsea oil field [1]

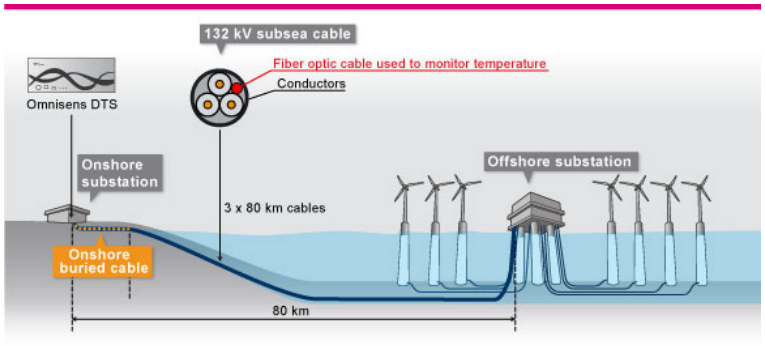

Figure 1.2: Omnisens cable for windfarms [2]

transmission lines, heavily relies on the health and reliability of the cable network as they are completely installed in the enclosed environment and failures will result in higher downtime due to difficulty in accessing these cables. Under these conditions frequent or prolonged duration of outages are undesirable.

The risk factors for buried cable systems in submarine environment results from factors like mining, damages due to cable breaking from digging or anchoring of ships, or incipient failure due to the cable components. As the cable repairing and downtime cost is much higher, the factors that can cause such cable failures are required to be minimized. The cable manufactures, utility companies, and investors of offshore systems try to limit incipient failures that may arise due to the cable manufacturing processes. In some cases, weak cable-spots may deteriorate

overtime even under normal operations. In order to achieve that, the cable system is over-designed hence they are not subjected to the full load capacity.

The current carrying capacity is called the ampacity of the cable [17] and it is determined from ampacity formulae and standards defined by IEC and IEEE which will be discussed in the sections below. The base ampacity is derated in order to prevent the cable from overloading and failures. Nevertheless, the maximum allowed ampacity of the cable is far lesser than the base ampacity due to pessimistic approach stated earlier.

1.2 Motivation

In 2020, annual renewable electricity capacity growth reached an all-time record at 167 gigawatt (GW), contributed mostly by wind (49 GW) and solar photovoltaics (PV) (109 GW) [18]. Efficient power transmission proves to be more economical than increasing the power production to compensate for losses [19]. Fig. 1.3 shows the various cable systems used in transmitting power from offshore wind farms to the grid onshore.

The maximum number of wind turbines that can be connected to a feeder is limited by the cable ampacity [20]. In the past, researches involved in cable power flow used the well-known derating approaches. The cable conductor size is decided based on the maximum current the cable is required to carry. Heat dissipation is an important factor considered while determining the maximum ampacity of the cable. The cable insulation thermal efficiency and the surrounding media contribute to the ability of the cable to dissipate the internal heat produced from the conductor. In addition to heat dissipation, there are few factors like load conditions, transient and short-circuit scenarios, and load factor also affect the allowable ampacity.

The most commonly used cables systems for power transmission from offshore

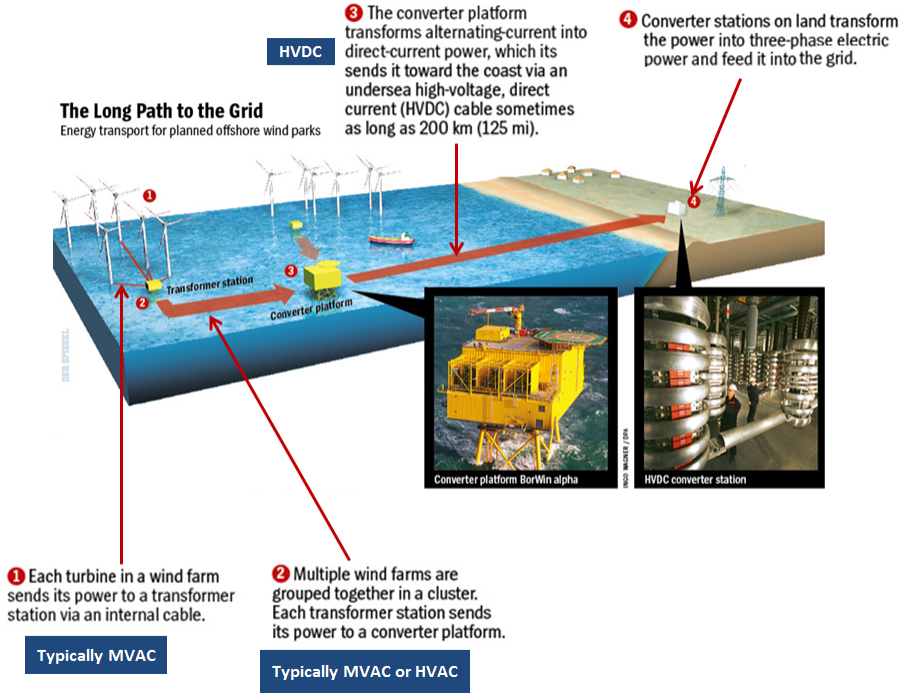

Figure 1.3: Offshore wind farm AC and DC cable system [3]

wind farms are HVAC, LFHVAC (Low Frequency HVAC) and HVDC [10]. The HVAC cable systems operate at 50 Hz frequency and LFHVAC operates at $16\frac{2}{3}$ Hz frequency. The AC cable systems consists of 3-core cables or 3 single-core cables arranged as bundle or equally spaced. The HVDC cables consists of monopolar or bipolar configurations. Table 1.1 shows the advantages and disadvantages of the various submarine power cables systems.

The power flow in the cable is directly related to the thermal and electrical characteristics of the cable and its surrounding. The standards assume the environmental conditions to be homogeneous and the thermal properties are uniform. However, the real-world conditions are different and the ampacity of cables in those conditions has to be determined considering the non-uniformity.

To ensure reliability and longer service life of the cables, it is essential to understand the thermal fields related to the cables and the installation environment. The efficiency of the surrounding medium to dissipate the heat generated in the cable determines the thermal capacity of the cable. The problem with buried ca-

Table 1.1: Comparison of various cable systems

System	Advantages	Disadvantages
HVAC	Conventional subsea cable technology Conventional topside hardware technology Lowest hardware costs	Cable electrical losses >100km Most subsea hardware not qualified
LFHVAC	Conventional subsea cable technology Conventional topside hardware technology Lower cable electrical losses compared to HVAC	Cable electrical losses >300km No qualified subsea hardware technology Higher hardware costs >HVAC
HVDC	Conventional subsea static cable technology Conventional topside hardware technology Lowest cable electrical losses	Subsea dynamic cable not qualified No qualified subsea hardware technology Highest hardware costs >LFHVAC

bles like submarine power cables is the medium in which they are buried, as some of the soil conditions does not enable efficient heat transfer which may result in high ampacity derating or overheating.

Better understanding of the thermal performance of the cable and different non-homogeneous conditions that it may be subjected to are needed for optimizing the power transfer and for determining the cable condition for better serviceability.

It will be useful to gain thorough knowledge about the environment that these cables might be exposed to and the thermal characteristic of the environment that may be different from the underground cable setting for maximising the efficiency, performance and lifespan of the cables. This insight will be valuable as the need for submarine power cables continues to grow.

1.3 Objective

Long-distance power transmission has traditionally been AC due to advent of transformers [9]. The losses in the underground AC network have been studied

for decades now. The existing knowledge of AC should suffice to work against the underground AC power network. Commonly followed standards consider submarine power cables in the same way as the underground cables though the burial medium is completely different.

The Ph.D. study mainly focuses on the detailed electro thermal analysis of submarine power cables for efficient power transfer and prevention of cable current over/under rating. The heat distribution in the cables was studied in detail using finite-element models and experimentation. Cable temperature monitoring was carried out in a lab-scale real cable environment. The objectives of the research involves,

- Maximizing the power cable capacity within safe limits.
- Accurate cable temperature corrections for ampacity calculations.
- Devising strategies for favorable cable installation conditions.

1.4 Major Contributions

This thesis presents the current rating model for submarine power cables considering all the factors that will affect the heat transfer in the porous water-saturated sea sediments. Particular emphasis was paid on the heat transfer mechanisms in submarine environment that will be different from that of the underground power cables. The mathematical description of the heat transfer involving conduction and convection for these specific conditions is presented in equation form.

1. A finite element method (FEM) model has been developed to analyse the factors that affect the heat transfer mechanisms of the submarine power cables. The porous nature of the sea sediments is recognized and the nature of heat flow is studied to implement them in the FEM model. This was achieved by combining the heat flow, heat-driven fluid flow, and temperature-dependent electrical parameters.

2. An analytical solution for the complex heat transfer in porous medium coupling the conduction and convection is developed. The solution also presents improvements to the present IEC 60287 for calculating the external thermal resistance T_4 that is used to determine the maximum current carrying capacity of submarine power cables. A comprehensive thermal network model of the submarine power cables with conduction, and convection thermal resistances was developed and verified with the detailed thermal analysis conducted using FEM simulations.

3. A lab-scale experimentation setup was developed in order to represent and understand the heat dissipation from an armored power cable in a water-saturated environment. The water-saturated sand is a representation of the submarine sediment. A corresponding 3D FEM model was developed to verify the experimental results and the analytical solution.

4. The FEM model initially designed to investigate the heat transfer problem has also been modified to determine how much influence certain sources of randomness in the burial environment can have on the temperature of the cable conductors. For example, to what extent will the mechanisms of heat transfer be affected by the velocities of the over-laying water.

1.5 Organization of the Thesis

The thesis is organised into seven chapters as follows. The background and motivation behind this study, the scientific contributions of the research work and the thesis outlines are presented in Chapter 1.

Chapter 2 presents a comprehensive overview of the power cable types and various methods for thermal ratings. A detailed comparison of various standards for rating power cables are reviewed providing a comparative overview of the methods. The significant difference between submarine and underground environment

is presented with the theoretical background and basis of heat transfer mechanisms in the porous domains.

Chapter 3 presents the conspicuous difference between the external thermal resistance calculation method for submarine power cables and underground power cables. Various thermal resistance calculation methods including contributions by convection heat transfer is proposed in this chapter. The chapter also discusses in details of the upper and lower limits for thermal resistance calculation and a novel series-parallel thermal resistance network (SPRN) for submarine power cable applications is proposed.

Chapter 4 presents the various factors affecting the submarine power cable ampacity. The significance of the factors are discussed in detail. A comparison of the IEC 60287 standards and the newly introduced influential factors and their effects are presented in this chapter.

Chapter 5 presents the effect of certain submarine conditions that will affect the assumptions discussed in the previous chapters. The influence of water velocity over the seabed and its effect on the power cable heat transfer. The finite-element model presented in the previous chapters are expanded to include the cross-flow and parallel flow above the embedded cable. An assessment was made whether the water movement above the seafloor is capable of significantly altering the thermal behaviour of submarine power cables.

Chapter 6 concludes the thesis with some recommendations for future research.

.

Chapter 2

Submarine Power Cable Types and Thermal Rating Methods

2.1 Submarine Power Cable Design

Subsea cables are in use from 19^{th} century onwards, though the initial application was primarily in long-distance wired communications. Later technological advancements and increased power demand paved way for subsea cable power transmission [21].

Though oil and gas industries were driving the development of subsea power cables for offshore oil rigs, the advent of offshore renewables paved way far HV transmission cables. Subsea cables contains multiple components such as power cores, optical fiber bundles for sensing and communication and other protective layers [22]. Both HVAC and HVDC cable systems are prevalent in offshore power transmission.

HVAC cables are limited by transmission distance, typically less than 80 km due to the losses and in the HVAC power transmission system, the cables behave like capacitive elements, creating reactive capacitive current in power transmissions

[23]. HVDC are used for longer distances and for system interconnection [4]. Fig. 2.1 shows typical HVAC and HVDC cables in subsea power transmission. HVAC cables used in subsea are typically three phase cables, they can be three separate cables for each phase laid at a distance from each other this is called flat formation and the cables are also bundled together called trefoil formation and cables with 3-core shown in Fig. 2.2 are also used. Similarly DC cable configurations are also present depending on the system. They are either mono-polar that uses single high voltage core conductor and a ground return or bi-polar with two cores, each core on a separate cable (one with positive polarity and the other with negative polarity) laid apart or bundled together or in a co-axial arrangement [24]. In normal operation, the mid point is grounded that allows current to circulate through the two high voltage conductors without ground current [25].

Figure 2.1: Modern HVDC and HVAC cables [4]

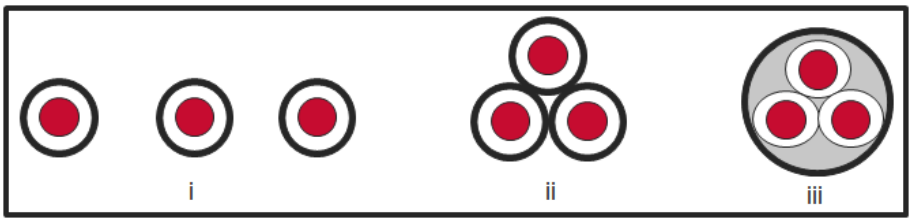

Figure 2.2: AC cable laying arrangements (i) Single-core cables in flat-formation (ii) Single cores in trefoil formation (iii) Three-core cable

2.1.1 Underground and Submarine Power Cables

On a broader note, when compared to overhead lines, submarine and underground power cables may appear to be closely similar with respect to the installation method. Both submarine and underground cables are buried and hence cable rating standards like IEC 60287 also consider them to be analogous in view of ampacity estimations. However, the apparent difference between the underground and submarine environments is the characteristic nature of the environment itself. The distinctive feature being the presence of large water body above the surface under which the submarine power cables are installed. In case of land cables, this will refer to air above the ground surface. The presence of water above the sediments may alter the heat transfer process in the regions surrounding the cables which may differ from the well-known heat transfer mechanism used for modeling underground cables. The water content in the subsea environment is much higher compared to the moisture content (considered for estimating underground cable thermal performance) in land. The weight of the large water body pushing down will exert excess pressure on the seafloor that will keep the sediments fully saturated.

The heat transfer process in the porous domains is complex and it is dependent on the configuration, volume and thermal properties of all the constituents of the medium. In soils with lower degree of water saturation, continuous heat flow will cause moisture migration or phase change of liquid water to vapour [26]. This will alter the thermal behaviour of the cables installed in it. The above phenomenon was considered and its effects on underground cables were investigated in many studies [27–30]. In porous medium, the soil structure determines the continuity of the pores and the pore-fluid connectivity. At lower saturation conditions, the heat transfer contributed by liquid phase is much higher than that of the vapour phase [31]. The hypothesis of the thermal flow in the presence of moisture/water content provides evidence that the heat dissipation from submarine power cables

to the surrounding medium will involve multi-phase heat flow and hence it should be modelled differently from the underground cables.

The specific heat capacity (the amount of heat required to raise the temperature of 1 gram of a substance by 1°C) of water is 4200 J/Kg/°C which is much higher than that of air (993 J/Kg/°C) that enables higher convective heat transfer for water [32–34]. Hence in the submarine environment, the overlying water and the water present in the porous sediments will efficiently transfer more heat compared to the underground setting. This phenomenon is significant as heat transfer at the seafloor will be higher than with the air medium over the ground surface. However, radiative heat transfer at the soil-air interface studied by [35–37] shows that presence of radiation heat transfer in the evolution of temperature in underground cable systems. On the contrary, radiative heat transfer is unlikely to occur in water as it has higher absorption of radiation at wavelengths of infrared range [38, 39].

Unlike the land regions, the submarine environment is much more dynamic in nature. The deep ocean waters are driven by water currents and the movement of large water bodies will induce pore pressure development in the sediments [40]. Basin-floor induced currents contribute to seabed migrations and cause sediment deposition. The sediment accumulation or sediments that are swept off might lead to alterations in the cable depth of burial and thus the distance from the heat sink [41, 42]. The sediment pore pressure changes will have implications on the convective heat transfer in the pore fluid as it has indirect effect on the buoyancy-driven flow.

2.1.2 Submarine Power Cable Components

The subsea cables are installed in harsh sea conditions, hence the cables should have good insulation for protection against thermal stress along with magnetic shield and mechanical armor for high stress resistance. These manufacturing fea-

tures ensure high efficiency in electrical transmission for these cable systems [9]. The composition of a HVAC subsea cable is shown in Fig. 2.3. The cables' structure includes a set of layers around the conductor. The cable conductors are mainly copper or aluminum for higher efficiency, heat resistance and favorable magnetic shielding [9].

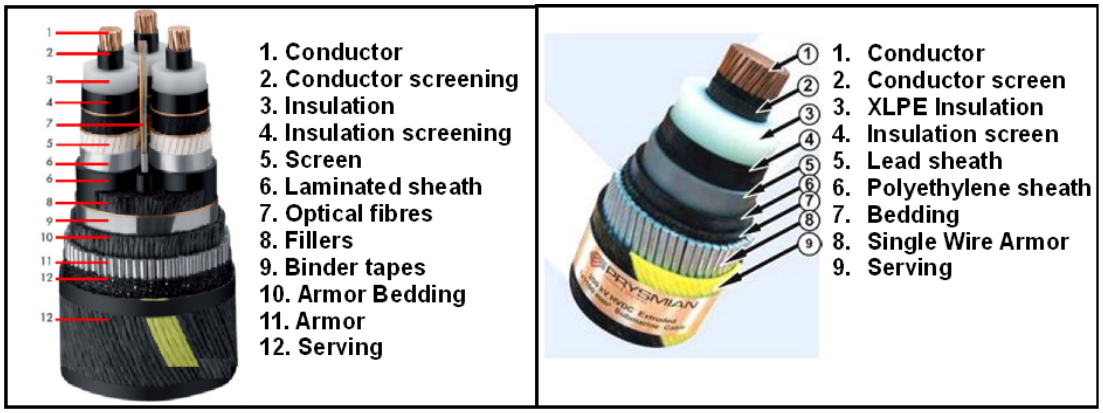

Figure 2.3: Typical cable components of (i) HVAC [5] subsea cables and (ii) HVDC subsea Cables [6]

Conductor

The centre of the cable is referred as "core" or "conductor" that allow the flow of electric current through its body along the cable. The conductors are selected based on the specific electric resistivity (that causes heat losses in the cable) to reduce transmission losses, and the raw material cost. The thermal conductivity of the materials is also of interest in order to reduce the thermal losses resulting from Joule heating.

Majority of submarine power cable conductors are made of copper as it has lower electric and thermal resistivity. Metals are good conductors and comparing the electric and thermal resistivities of metals such as gold ($2.4 \cdot 10^{-8}$ Ωm, 0.003 W/m·°C), silver ($1.59 \cdot 10^{-8}$ Ωm, 0.002 W/m·°C) [43], copper ($1.72 \cdot 10^{-8}$ Ωm, 0.002 W/m·°C) and aluminium ($2.80 \cdot 10^{-8}$ Ωm, 0.004 W/m·°C) [44, 45], it is worth to note that copper has a better balance between the thermo-electric property and cost of the material. Compared to aluminium, copper is expensive but

for the same current-carrying capacity the material required for aluminium conductor is 56% higher than that of copper. In addition, copper has lower coefficient of expansion and higher specific weight that is suitable for applications like deep sea installations. The metallic cable conductors will cause Joule heating due to the passage of electric current and in AC cables this will be reflected in the other metallic layers covering the cables.

Conductor Screening and Insulation screening

To minimize static current around the conductor surface and maintain uniform filed, semi-conducting tape are extruded on to the conductor surface that acts as conductor screen [46]. In cables with stranded conductors, the conductor screen smooths the imperfections on the conductor surface. It gives a smooth surface with dielectric properties similar to the insulation layer that follows the conductor screen [10]. The conductor screen reduces the electrical stress between the conductor and insulator.

Insulation

The primary function of the insulation is to prevent current flow in directions other than along the cable axis. It acts as a barrier between the conductor, and external surfaces with considerably lower electric potentials. The insulation layer of the cable should be even and free of voids or impurities. The insulation layer also adds mechanical strength to the cable structure and the dielectric properties of the insulation is essential for absorbing any potential gradient from the conductor. Hence the thickness of the layer is determined based on the operating voltages of the conductor. The insulation wall must be resistant to temperature and aging. There is no difference between the insulation materials for submarine and underground cables. Cross-linked polyethylene (XLPE) is the most commonly used insulation material for submarine cables [10]. In addition to XLPE, other extruded insulation technology - High Performance Thermoplastic Elastomer (HPTE) – Polypropylene

based insulation and mass impregnated paper insulation are other commonly used in submarine power cables [47].

Laminated sheath

The insulation layer is then covered by a layer of metallic sheath that is required to prevent any electric current leakages from the conductor. This also ensures that the field across the dielectric is uniform. They serve as long grounding path to dissipate fault currents to the surrounding soil and isolate any electro-magnetic interference. They also prevent moisture ingress reaching the insulation layer by providing additional barrier. This is essential for submarine power cables as they are installed in a high water content environment. The sheaths are generally made of copper, lead or aluminium.

Filler

The interstices of the sub-bundle (i.e. comprising power conductors, fibre optic bundle, hoses, etc) are typically filled with a soft polymer material such as polypropylene string or polyethylene [46].

Binder Tape

The binder tape is applied helically over the sub-bundle (i.e. comprising power conductors, fiber optic bundle, hoses, etc) to "maintain stability after laying up of the sub-components" [9].

Inner Sheath / Bedding

An inner sheath, typically a polymer like polypropylene or polyethylene, is applied over the taped bundle for "mechanical protection, bundle stability and to provide a bedding for the armor" [9]. For armored cables, the inner sheath is a requirement of ISO 13268-5.

Continuously extruded thermoplastic (e.g. polyethylene) in lieu of roving is required for dynamic applications [46].

Armor

As the name suggests, armor provides the mechanical strength for the cables against the damages arising from external factors. All the buried cables will have armors for protection. Armors also serve as earth continuity conductor and form a part of the overall earthing or grounding system. They are made of stranded metals wound in a helical manner around the cables. Armors cover the entire cables unlike the sheath which covers individual cores in a multicore cable. Magnetic and non-magnetic metallic armors are used based on the number of cores present in the buried cables. Commonly used materials for armoring are galvanized steel, stainless steel, aluminium and copper.

Metallic armors cause additional heating in the AC cables due to their magnetic properties. When the cable core is energized by an alternating current it induces magnetic field in the metal armor and it develops eddy currents. The eddy currents result in Joule heating in the armor.

Outer Sheath / Serving

An extruded polymer such as polyethylene or polypropylene yarn or extruded thermoplastic are used as outer covering for the cables [46].

2.2 Power Cable Thermal Rating

The amount of power that can be transferred using a power cable is determined by its maximum operating temperature and operating voltage. For insulated cables, the thermal limitations are set by the insulating material. To prevent thermal breakdown of the insulation, the allowable operating temperature of the conductors are set at a limit. For example, cables using XLPE insulation are required

to operate at or less than 90 °C to prevent the adverse effect on thermal ageing of the material [48]. The current capacity of the cable is determined based on this thermal limit which will allow the cable to operate within the safe limits. Emergency current ratings are calculated not to exceed the permissible emergency thermal limit for very short duration. These emergency current rating are scaled up steady-state current values. The IEC standards does not permit emergency scaling factor of more 2.5.

The current rating of the buried cables are calculated based on number factors that affect the cable thermal performances. The factors that are used for the calculation include thermo-physical properties of the cable components and its surrounding medium, ambient temperature, depth of burial and the presence of adjacent cables or other heat sources and their distance of separation. In case of cables that installed in conduits or ductbanks, the dimensions and heat transferability of these components are also included in the calculation.

Numerous calculation methods and procedures have been formulated for determining the thermal current rating of underground power cables that are installed in various configurations and arrangements. In buried cable scenarios, assumptions are made to solve the heat transfer equations and to arrive at an analytical solution. The values for the parameters involved in the calculation are ascertained using empirical data. For underground power cables, international standards provide data for typical cable configurations and installation methods.

The standard approaches overly simplify the cable thermal modeling based on several assumptions. The assumptions of homogeneity and ignoring apparent difference in various cable installation environment and methods make this research relevant. The thermal properties of the parameters and the nature of the interaction among these parameters significantly vary the cable thermal transfer capability compared to the standard methods. Commercial software was initially used to understand the calculation of cable thermal ratings including the factors

and their approximations set by the standards. When compared to the detailed procedures (explained in the following chapters), the approximations made by the traditional analytical models result in significant discrepancies in cable rating due to the accumulation of several assumptions.

Many alternate approaches have also been practised for calculating the current rating without the need for using overly simplified analytical methods. These are performed by solving the relevant partial differential equations using multidimensional numerical methods like finite element, finite volume etc., These approaches are complex and time consuming but advantageous as they eliminates the need for several assumptions made in the analytical method.

2.3 Ampacity Calculation Methods

Ampacity is the maximum sustained current that the cable is allowed to carry under favorable condition. This characteristic parameter of the cable is influenced by cable properties and other parameters like installation conditions and surrounding medium and its thermal characteristics. In long-distance power transmission and distribution network using underground cables, e.g., in Singapore and many other cities, there are instances where the power cables passes through areas of thermally unfavorable conditions, e.g., regions having local heating that increase the ambient temperature around the cable. Depending on the length of such regions and its effect on the cable heat dissipation, the current rating of the cable will be reduced. This is based on the assumption that the entire route is characterized by similar condition. Since the configuration and application of underground electric cables demand careful consideration for thermal effects on cable materials, pessimistic approaches are followed to determine the ampacity and reduce cable thermal damages.

Calculating accurate cable ampacities for the system designed is critical as it

determines the system size and power transfer capability. The cable sizing also drives the cost of the project and it is also critical for the system reliability when overloading or transient conditions are expected . Wind and solar power plants particularly, due to their volatile nature, try to optimize cable size using ampacities that closely match maximum generation in order to ensure optimal values are chosen [49].

The cable conductor size is decided based on the maximum current the cable is required to carry i.e the maximum allowable ampacity. Heat dissipation is an important factor considered while determining the maximum ampacity of the cable. The cable insulation thermal efficiency and the surrounding media contribute to the ability of the cable to dissipate the internal heat produced from the conductor. In addition to heat dissipation, there are few factors like load conditions: steady-state, transient and short-circuit scenarios, as well as load factor also affect the allowable ampacity.

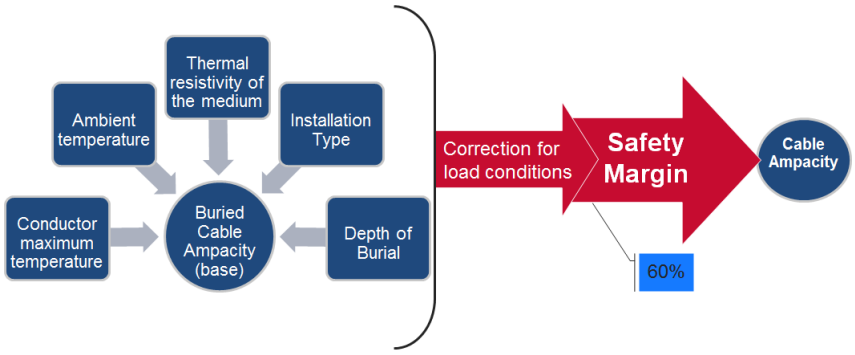

Figure 2.4: Cable ampacity calculation overview

A combination of factors is considered in the calculations of the ampacity. Fig. 2.4 shows the factors influencing ampacity calculation and safety constraints. The power cables installed underground or subsea have higher safety constraints to avoid failures during operation and this approach tends to the over-designing of the cable system that are not fully utilized [50].

The simplified ampacity calculations from the Neher-McGrath formula [17] re-

mains a prevalent reference for ampacity deductions [51] for high-voltage cables. This calculation follows the basic principle that electric current produces thermal heating and transfer to the ambient environment, which requires there to be a difference between the temperatures of the two media. It also adheres to the assumption that in insulated cables, the maximum normal operating temperature is determined by the specific insulation, while in non-insulated cables, the limiting material property is the tensile strength of the cable [51].

The ampacity and ampacity derating of power cables in a distribution network is widely determined by the governing standards – IEEE 834, IEC 60287 [52–56] and regional electric codes such as National Electric Code (NEC) used in the USA [57].

"Considering the number of calculations needed to determine ampacity using the Neher–McGrath method, it is obvious why engineers would prefer using this simplified tabular method" [58]. These standard defined ampacity- tables are still in use for the purpose of sizing the transmission cables in the planning phase by many utilities. It is important to understand that these tables were created with certain base assumptions. These assumptions, for example, include the ambient temperature of the earth being 20°C. "Many locations in the Southwest USA experience the maximum underground soil temperature of 25°C–30°C, which reduces the ampacity by 5%– 8% below the tabulated values" [58].

2.3.1 IEC 60287

One of the most commonly used analytical methods for calculating cable current ratings for land-based cables is outlined in the IEC 60287 standard [52]. According to this procedure, the maximum current, I that can be transmitted along an AC cable buried in a soil is given by the following formula:

$$I = \left[\frac{\Delta\theta - W_d[0.5T_1 + n(T_2 + T_3 + T_4) + (\Upsilon - 1)\Delta\theta_x]}{R[T_1 + n(1 + \lambda_1)T_2 + n(1 + \lambda_1 + \lambda_2)(T_3 + T_4)]} \right]^{0.5} \tag{2.1}$$

where $\Delta\theta$ is the conductor temperature rise above the ambient temperature (°C). R is the AC resistance of the conductor at its maximum operating temperature (Ωm). Υ is the ratio of the thermal resistivities of the dry and moist soil zones ($\Upsilon = r_d \ / \ r_w$). r_d is the thermal resistivity of the dry soil (°C· m/W). r_w is the thermal resistivity of the moist soil (°C ·m/W). θ_{x} is the critical temperature of the soil and temperature of the boundary between dry and moist zones (°C). θ_{a} is the ambient temperature (°C). $\Delta\theta_{\mathrm{x}}$ is the critical temperature rise of the soil. This is the temperature rise of the boundary between the dry and moist zones above the ambient temperature of the soil (θ_{x})-(θ_{a}) (°C). T_1 is the thermal resistance between conductor and sheath, T_2 is the thermal resistance between sheath and armor, T_3 is the thermal resistance of the outer covering. T_4 is the thermal resistance of surrounding medium (ratio of cable surface temperature rise above ambient to the losses per unit length). λ_1 and λ_2 are the sheath and armor ratio compared to the conductor losses. n represents the number cables used. For example, in three single-core cables, n is three.

It is interesting to note that the only term in equation (2.1) that is directly related to the properties of the surrounding medium is T_4. It is, however a crucial factor in determining the actual value of the current rating [59]. By investigating the heat flow in the region around the cable numerically, a more accurate current rating can be calculated by addressing some of the uncertainties associated with the assumption that the heat flow is totally described by the parameter T_4 in this domain.

Ampacity calculation of a cable is complicated particularly in cases where the routing goes through various environments with dynamic thermal conditions. The heterogeneous nature of the soil and existence of heat transfer by convection in water and air requires a two dimensional heat transfer approach to the problem. Temperature distribution in the cable and surrounding is a function of variable soil thermal resistance, location from the ground level along the axis and depth

of burial, radial distance between nearby cables etc. [60]. Though ampacity calculation follows traditional numerical methods presented in the literature and standards, very few works have been presented for the non-uniform nature of the medium surrounding the cables. This includes models presented by the pioneers Neher-McGrath [17], however these are directly applicable to underground cables that are installed in homogeneous environment. The thermal model developed by them is based on many assumptions to make the numerical formula simpler and in that approach one of the assumptions is the uniform surrounding medium. Hence, no geometrical and thermal property changes along the cable was considered. This makes the approach not anywhere close to reality. Hence the problem is reduced to two-dimensional problem from a three-dimensional one. In addition, the problem was further simplified by considering a virtual heat sink above the ground surface where the cable is installed. Hence, the heat transfer problem becomes a one-dimensional numerical formulation and the ampacity formulation was solved directly as an algebraic equation [17].

Most of the accepted standards [52–57] follow the approximate model provided in the Neher-McGrath method. Those standard tables hence follow the same homogeneity principle and does not account for any changes in the characteristics of the surrounding medium along the cable length that directly affects the cable ampacity [61]. These non-uniform conditions are more prevalent in urban areas and in cases where the cable passes through paved parking lots with concrete bases. The heat dissipation will be poor thus increasing the cable internal temperatures [62]. In the work presented in [63], assessment methods to calculate ampacity for underground power cables are shown. It is understood that all the above approaches consider homogeneous environment for the surrounding medium thus limiting the validity of the results.In more conservative approaches and in situations where complex heterogeneous conditions prevail for longer sectors along the cable length, the worst-case approach is followed. Cables are considered to be

installed in the worst thermal environment and cable ampacity derating is done keeping this as a base [64].

No clear direct method or guide is standardized for cable ampacity calculation for small heterogeneous portions having poor thermal properties prevail around the cable [61–65]. This indicates that the cable ampacity values are not constant as defined in the standard tables and in some cases deviations are present. The cables subjected to continuous operations will lead to changes in the ambient environment which will also affect the heat transfer ability of the surrounding and in turn leads to cable damage. Many new methods for estimating power cable thermal performances in underground installation conditions are are presented in [59,66,67]. They follow finite element analysis for power cables in homogeneous soil installed in conduits [61–67].

The water content in the underground soil and its effect on the underground power cables are investigated in many previous works stated above. The significance of the presence of water is that it enhances heat transfer process in the embedded cables. This phenomenon is more relevant for submarine environment where the natural water content is very high. The study of heat transfer mechanisms in these porous sea sediments with high water content will provide valuable insights about the conspicuous differences between submarine and underground cable thermal performances.

2.4 Heat Transfer in Porous Medium

Heat can be transferred in three different ways: conduction, convection, and radiation [68,69]. In solid medium, conduction is the most significant and only means by which the heat flows due to the nature of the spatial relationship between the particles or atoms in the solid. For underground power cables, though soil is porous in nature, majority of standard procedures assume only heat transfer

by conduction. In submarine environment, conductive and convective heat transfers are likely to occur simultaneously (as there is no likelihood of radiative heat transfer in water [38, 39]) in the water-saturated porous sea sediments. This can result in the heat dissipation from the cable that is different from the heat transfer mechanism assumed by the standard methods.

2.4.1 Principles of Heat Transfer Mechanism

According to Fourier's law of thermal conduction, the rate of heat transfer through a body is proportional to the negative temperature gradient and to the area. It is given by [70]

$$q = -k\nabla\theta \tag{2.2}$$

where q ($\mathrm{W/m^2}$) is the heat flux, and $\nabla\theta$ is the temperature gradient. The parameter k ($W/m\cdot^\circ C$) is the thermal conductivity of the heat conduction medium. This is an intrinsic material property that characterises the ability of the body to conduct heat through it. Thermal conductivity depends on material structure, density and the spatial arrangement of the atoms that constitute the medium. For homogeneous mediums, the thermal conductivity can be determined by the material they are composed of. In case of heterogeneous mediums that are composed of different materials, the thermal conductivity is a measure of relative amounts of the thermal conductivities of each constituent. Methods to determine thermal conductivities of such mediums are presented in the Section 2.4.1. The heterogeneity approach for determining the thermal conductivity is more relevant for submarine sediments as they are composed of solid sediment particles and water.

In the context of porous domains in the following sections, the thermal conductivity of the solid sediment matrix will be denoted by k_s and the fluid thermal conductivity will be denoted by k_f respectively. The subscripts will also be followed to refer other physical properties of the sediment and fluid accordingly.

Considering an isotropic condition for the porous medium, we assume a local thermal equilibrium for the matrix i.e. the solid and fluid phases are at the same temperature θ.

$$\theta = \theta_s = \theta_f \tag{2.3}$$

θ_s and θ_f are the respective temperatures of the solid and fluid phase. In order to arrive at the heat balance equation, we also assume that the heat transfer takes place in the solid and fluid phase simultaneously and hence there is no net thermal transfer between the phases. The ratio of the pore volume to the overall volume of the porous medium is denoted by ϵ. The energy balance equation is derived by averaging the heat transfer over a unit volume of the medium. The equation for solid phase is

$$(1-\epsilon)(\rho_s C_s)\frac{\partial \theta}{\partial t} = (1-\epsilon)\nabla \cdot (k_s \nabla \theta) + (1-\epsilon)(Q_{in})_s. \tag{2.4}$$

ρ_s (kg/m$_3$) and C_s (J/kg/°C) are the density and specific heat capacity of the solid and $(Q_{in})_s$ (W/m^3) is the heat generated per unit volume of the solid phase. Similarly, the heat balance equation of the fluid phase is given by

$$\epsilon(\rho_f C_{pf})\frac{\partial \theta}{\partial t} + \rho_f C_{pf}(\vec{v} \cdot \nabla \theta) = \epsilon \nabla \cdot (k_f \nabla \theta) + \epsilon (Q_{in})_f. \tag{2.5}$$

ρ_f (kg/m$_3$) and C_{pf} (J/kg/°C) are the density and specific heat capacity at constant pressure of the fluid. $\vec{v}$ is the fluid velocity and $(Q_{in})_f$ (W/m^3) is the heat generated per unit volume pertaining to the fluid phase. It is to be noted that in the fluid phase equation, due to the fluid flow (represented by v) the convective term is added. This term represents the temperature gradient as a result of the convecting fluid.

Combining equations (2.4) and (2.5), we arrive at common terms that represent the heat transfer in the porous domain. It is given by

$$(\rho_m C_m)\frac{\partial \theta}{\partial t} + \rho_f C_{pf}(\vec{v} \cdot \nabla\theta) = k_{eff}\nabla^2\theta + (Q_{in}). \tag{2.6}$$

The subscript "m" represents the overall heat capacity, (Q_{in}) is the overall volumetric heat generated in the medium and k_{eff} is the overall thermal conductivity of the porous medium.

For incompressible fluids, density changes are negligible and hence

$$\nabla \cdot \vec{v} = 0. \tag{2.7}$$

Under steady-state conditions, the heat balance equation of a porous medium is given by

$$Q_{in} = -k_{eff}\nabla^2\theta + \rho_f C_{pf}\vec{v} \cdot \nabla\theta \tag{2.8}$$

The density and specific heat capacity are multiplied to the convective term to represent the rate of change of convective thermal energy per unit volume of the fluid.

In submarine power cable applications, the source term, Q_{in} in the equation (2.8) represents the overall heat generated within the cable due to the losses in the conductor, dielectric losses, circulating and eddy current losses (in case of AC cables) at the sheath and armor. The thermal losses in the conductor is caused by the electric resistance to the cable current.

The equation (2.8) shows that the heat dissipation from the power cables embedded in submarine environment is dependent on the fluid velocity (if present) in the porous medium. Hence it is important to understand the transport phenomenon in porous domains in order to model the power cable heat transfer accurately.

Effective Thermal Conductivity

Power cables are buried in the submarine environment that are porous saturated sea sediments. Heat and fluid flow in this porous medium depends on its effective

thermal conductivity that combines the solid and fluid phase thermal conductivities. In order to investigate the thermal behavior of the embedded cables, it is essential to gain knowledge about the factors that determine the effective thermal conductivity of the porous medium.

The term "porous" can be associated with a wide range of materials and micro structure. Determining the effective thermal conductivity for such porous medium that constitutes of several materials can be challenging [71]. A method suitable for one type of porous matrix might be completely inapplicable for another type. For porous domains like sea sediments, the effective thermal conductivity is a function of the spatial distribution and configuration of the phases within the medium [72], their respective thermal conductivities [71, 73], and volume proportions. Several methods have been proposed to estimate the effective thermal conductivitiy of the porous medium [71–74].

The upper and lower bounds of the actual effective thermal conductivity of the porous medium can be estimated by making assumptions about the structural arrangement of the individual constituents. The solid phase and fluid phases are assumed to be aligned perpendicular to the heat flow in series combination and parallel in parallel configuration, as illustrated in Fig. 2.5. The effective thermal conductivity in such parallel arrangement is given by the weighted arithmetic mean of the contributions from the solid (k_s) and fluid (k_f) phases [73].

$$k_{eff} = (1-\epsilon)k_s + \epsilon k_f \tag{2.9}$$

This provides the upper bound values for the effective thermal conductivity. Similarly, the lower bound for k_{eff} is given by the series arrangement [73].

$$\begin{aligned} k_{eff} &= \left(\frac{1-\epsilon}{k_s} + \frac{\epsilon}{k_f}\right)^{-1} \\ k_{eff} &= \left(\frac{k_s k_f}{(1-\epsilon)k_f + \epsilon k_s}\right). \end{aligned} \tag{2.10}$$

In this model, k_{eff} is given by the weighted harmonic mean of solid (k_s) and fluid (k_f) phase thermal conductivities. The actual effective thermal conductivity lies in between the upper and lower bound values. There are other weighted

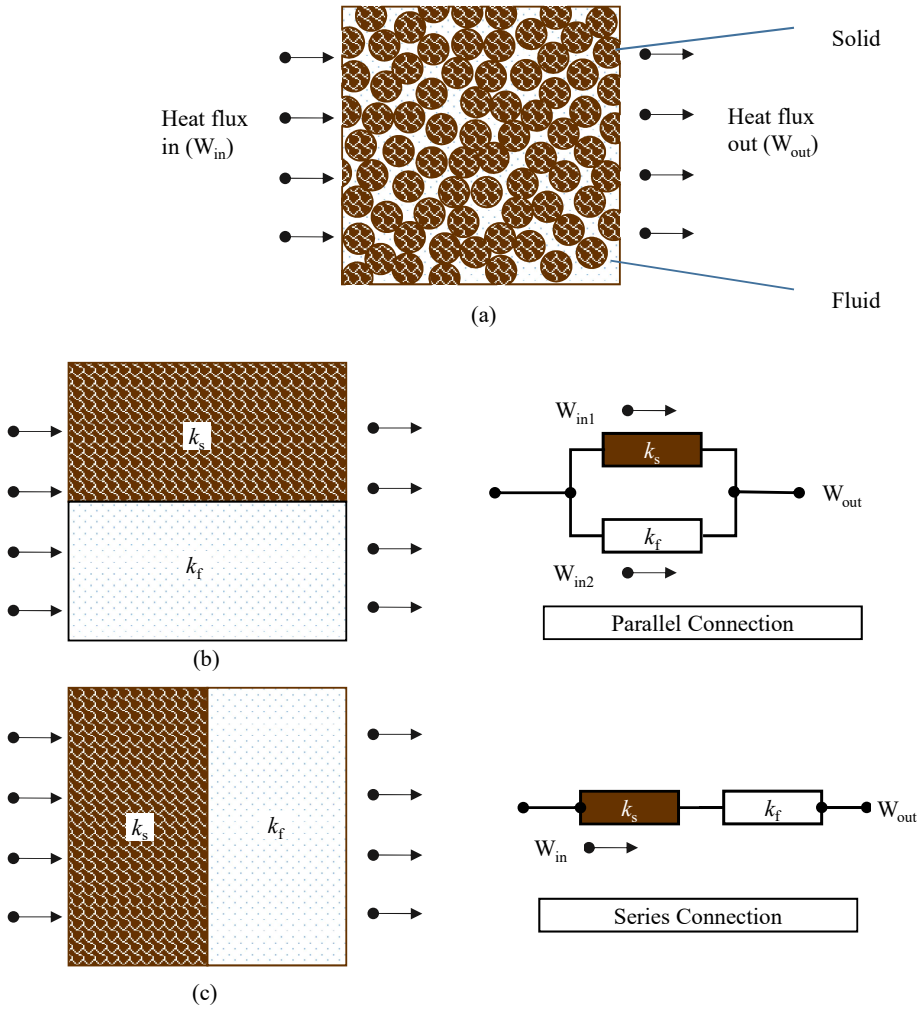

Figure 2.5: Comparison between two different models for estimating bulk thermal conductivity of the porous medium. (a) Typical porous medium structure, (b) assumes that the solid and liquid phases are in parallel, and (c) that assumes they are in series.The heat flows in the direction indicated by the arrows.

mean models have been developed for varying degrees of saturation in the porous medium. Several other models were also developed for specific applications and known material structure of the medium.

For granular porous medium saturated with water, the commonly used method [72, 73, 75, 76] for determining the effective thermal conductivity is given by

$$k_{eff} = {k_s}^{(1-\epsilon)} {k_f}^{\epsilon}. \tag{2.11}$$

This is called the weighted geometric mean model applicable to porous matrix where the structure of the medium is not known. This method may not be appli-

cable when the ratio of solid to fluid phase thermal conductivity (k_s/k_f) is more than 20 [73], examples like dry porous medium saturated with air.

Convection in Porous Domains

In fluid-saturated porous medium, heat transfer takes place by conduction and convection. A number of factors determine the extent by which the convective heat transfer takes place within the porous medium. The parameters that are directly related to the fluid content are porosity (pore volume ratio) and intrinsic permeability, the measure of the ability of the medium to allow fluid flow through it. This is a quantitative property controlled solely by the pore structure.

Rayleigh number is a dimensionless number for a fluid and it is associated with the fluid flow caused by natural convection, also referred as buoyancy-driven flow. It is the product of Grashof number and Prandtl number. Grashof number is the ratio of buoyancy forces (that causes fluid movement due to density changes caused by rise in temperature) and viscous forces (that oppose the fluid motion). Prandtl number is the ratio of momentum diffusivity (μ/ρ_f) to thermal diffusivity ($k_f/\mathrm{C}_{pf}\ \rho_f$).

In porous medium, Rayleigh-Darcy number (Ra) for fluid motion through the pores is defined as the product of Rayleigh number and Darcy number (permeability). Ra for the fluid flow caused by heat generated in a cable of diameter D_e embedded in porous medium is given by

$$Ra = \frac{\kappa\rho\beta g(\theta_s - \theta_{amb})D_e^3}{\alpha\mu}. \tag{2.12}$$

κ is the intrinsic permeability, β is the fluid thermal expansion coefficient. θ_s and θ_{amb} are the surface temperature of the cable and the ambient temperature. α is thermal diffusivity and μ is the kinematic viscosity of the porous medium. g is the acceleration of gravity $= 9.8\ \mathrm{ms}^{-2}$. Ra values above certain critical

values indicate heat transfer by convection. A detailed simulation study using the relevant PDEs will provide more insights about the other associated parameters that may influence the heat transfer in the submarine power cables.

Chapter 3

Analytical Thermal Network Model for External Thermal Resistance of Submarine Power Cables

3.1 Introduction

The thermal conductivity/resistivity of the surrounding medium determines the heat transfer-ability of the installed power cables. Accurate knowledge of the cable heat transfer is essential to calculate the maximum current carrying capacity of the cables. Determining the thermal conductivity of heterogeneous materials like porous medium is difficult as the exact composition should be done. Modeling the heat transfer from saturated porous materials that exhibit both conduction and convection analytically is highly complex. Unlike the resistance to conduction heat transfer that only depends on the thermo-physical properties of the material, resistance to convective heat transfer varies with the amount of heat it is subjected to.

As the computing technique has been developed, scientists have been paying more and more attention to the numerical methods for the studies to determine effective thermal conductivity of porous medium. Among those methods, FEM is the most commonly used method [77] [78]. More importantly, numerical methods can provide more accurate results for studies of the physical properties due to their high-efficiency and ability to solve the local problem such as the nonlinear heat transfer boundary value problem [79]. However, the numerical methods including FEM are complicated due to the large number of data processing compared to the analytical method. Therein, it is significant to find out a simple analytical method to model the heat transfer accurately. This chapter presents an alternative methodological approach for thermal rating of submarine power cables. An analogous thermo-electric network model was developed to include the convective heat transfer that may occur in certain sediment types. FEM analyses were also carried out to validate the proposed approach for various factors that affect the power cable heat transfer.

3.2 Finite Element Method (FEM)

The physical laws for space and time-dependent problems are usually defined as partial differential equations (PDEs). Certain physical models that are expressed as PDEs are difficult to solve using simple analytical methods due to the complex nature of the problem. A discretization method can be used to represent the PDEs with numerical equations approximately. These discrete equations are solved using numerical methods and the solution will be approximate estimation of the fundamental solution of the PDEs. One such numerical method used for computing PDEs is finite element method (FEM).

FEM is an approach to perform the finite element analysis using numerical technique. The history of the FEM and its usage can be found from the scientific publications dating back to the 1940s [80]. Though many works can be found

on finite discrete variation methods much before 1940s, Richard Courant was the first mathematician to introduce finite elements [81]. Later the modern 2-D FEM was published by Clough and his team [82]. The increase and accessibility to computing power led to the prolific usage of the FEM and it has evolved into 3-D and extended-FEM (XFEM) [83] that solves boundary value problems that are discontinuous and having singularities within the mesh elements more accurately.

The discretization of the PDEs involves the decomposition of the continuous geometry into small connected components called elements. The vertices of these elements are the nodes at which the unknown variables will be calculated [84]. The physical model is also bounded by defined accurate boundary conditions. A finite number of defined elements with the nodes sharing vertices with adjacent elements creates the field variable continuity. The solution of the overall system is formed as a matrix of the solution of at each element level. Hence more discretization will lead to higher a computational cost.

FEM is the most prevalent solution used for solving thermal problems relating to underground power cables. The same basic principles are applied here for submarine environment. The major difference in the approach here is both conductive and convective heat transfer are accounted for in the model for analysis. The model is solved numerically by coupled fluid flow and heat transfer PDEs.

3.2.1 Study Cable Design

The internal structure of a 44-kV armored submarine power cable shown in Fig. 3.1 is used for the study. The FEM model aims to illustrate the heat transfer within the cable and the saturated sediment surrounding the cable. The cable under study was modeled to be buried in a homogeneous sediment with density – 2020 kg/m^3. Since the cable length is far larger than its diameter, 2-D FEM studies were carried out assuming geometrical symmetry along the cable length. The cable copper core conductor is shielded by extruded thermos-set semi-conducting

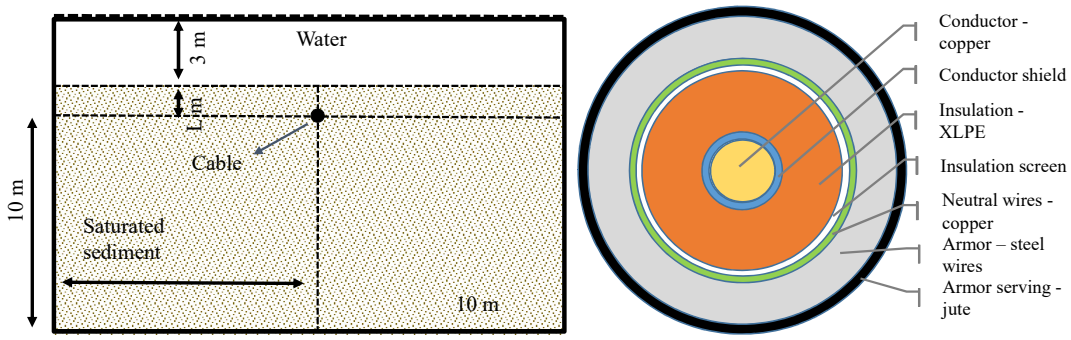

Figure 3.1: Simulation geometry schematic and cross-sectional view of the study-cable structure.

compound. The insulation is cross-linked polyethylene (XLPE) and steel armoring was used, compounded jute and fibrous material were chosen for armor serving [57]. The FEM models were developed and analysed using COMSOL multi-physics 5.4 software.

3.2.2 Geometry and Boundary Conditions

The simulation setup is divided into three parts: 1.) power cable (solid medium), 2.) saturated sea sediment (porous matrix of solid particles and water) and 3.) overlying water (pure fluid medium). The geometry of the simulation area with the embedded cable is shown in Fig. 3.1. The cable is modeled as a heat source with a temperature-dependant electric resistance causing Joule heating. The cable and the porous domains immediately surrounding the cable will be subjected to sharp thermal transients resulting from the heat generated within the cable. Hence, those regions were divided using more refined mesh elements to resolve the PDEs more precisely. Attention was paid to the meshing of the boundary layers between the cable and the porous domain as the interface between the mediums has higher temperature gradients.

The size of the geometry was increased until further increase in the size had negligible effects on the solution. Mesh dependency was eliminated by performing mesh sensitivity analysis.

The top boundary representing the overlying water is modeled as an open boundary condition with constant pressure acting on it [85], [86] that allows heat and fluid flow through it. The bottom and sides are modeled as wall boundary conditions that prevents any heat or fluid flow across these boundaries.

$$n \cdot \vec{v} = 0 \quad \text{and} \quad n \cdot (-k\nabla\theta) = 0. \tag{3.1}$$

The conductive heat transfer inside the cable is defined by Fourier's law of heat conduction and is given by

$$q = -k\nabla\theta \tag{3.2}$$

where q is the local heat flux density ($\mathrm{W/m^2}$) and $\nabla\theta$ is the temperature gradient. The heat transfer in porous media is defined by the mixture of energies in the solid and fluid heat transfer equations [87] and is given by

$$\rho C_p \vec{v} \cdot \nabla\theta + \nabla \cdot q = Q \tag{3.3}$$

where, θ is the temperature (°C). ρ and C_p are the density ($\mathrm{kg/m^3}$) and heat capacity (J/kg/°C) of the fluid at constant pressure. $\vec{v}$ is the fluid velocity (m/s) resulting from the buoyancy-driven flow. The magnitude of the velocity determines the convective heat transfer. Q is the volumetric heat generated ($\mathrm{W/m^3}$) in the cable.

A representative value of 20°C is used for the temperature of the overlying seawater. The velocity of the overlaying water is solved using Navier-Stokes equation for laminar flow. The simulations and analytical solutions were carried out assuming no phase change takes place in the fluid medium. For example at higher temperatures, vaporization or condensation is not considered in the studies.

3.3 Modified Thermal Network Model for Porous Medium

In the previous chapter, the effective thermal conductivity model of porous medium was analysed. The various approaches suggested that the solid and fluid phase

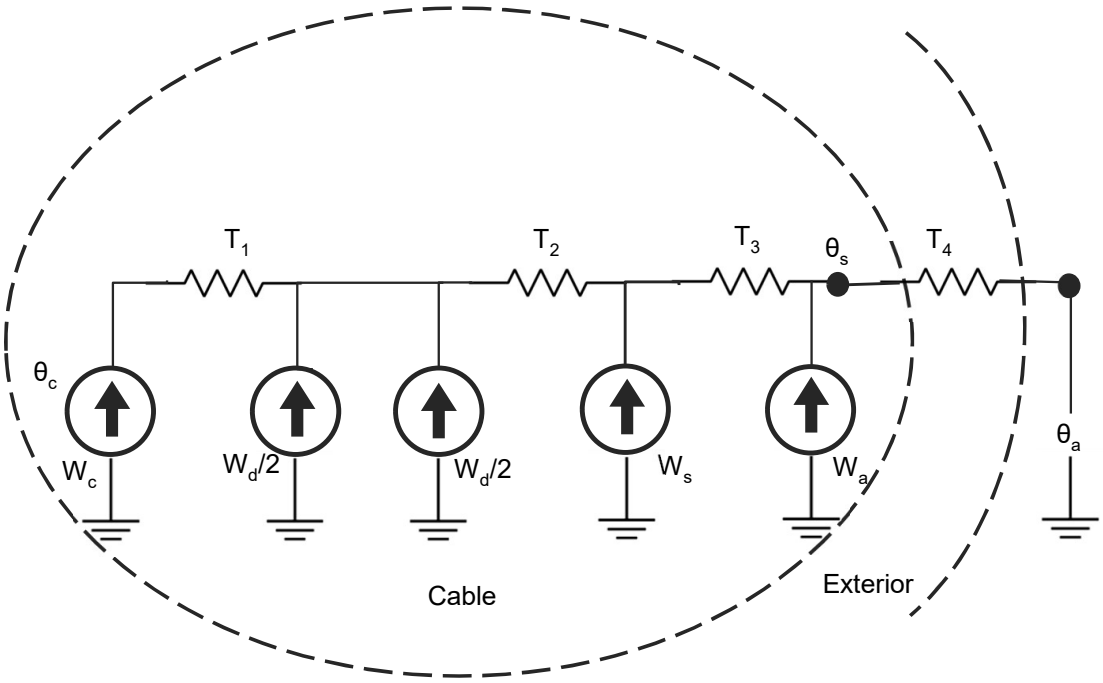

Figure 3.2: Equivalent thermo-electrical circuit for buried power cables. T_4 represents the external thermal resistance as combined resistance to conductive and convective heat transfer

media can be assumed to be arranged in series, parallel, and randomly scattered fashion for the heat flux. A similar approach is followed here. When one of the constituents of the porous domain exhibits heat transfer by convection, then the heat flow process becomes two-phase flow where theoretical estimation of effective thermal conductivity will underestimate the heat transferred by the medium. Hence, a modified thermal network model is developed to decouple the solid and fluid phase thermal conductivities into respective thermal resistances. The thermal analogous model for determining cable temperature rise has proved to produce accurate results [88–90]. The thermal network for buried power cables is shown in Fig. 3.2. W_c, W_d, W_s and W_a are the heat losses in the cable conductor, insulation, sheath and armor respectively. Analogous to current flow in electric circuits, the heat flow in thermal circuits are governed by

$$W = \frac{\Delta\theta}{T} \tag{3.4}$$

where T is thermal resistance of the network and $\Delta\theta$ is the temperature gradient between the nodes. In this analogy, the internal thermal resistances of the cable components are conductive heat resistances of each cable layer. The conspicuous difference between the standard methods and proposed method is the determination of T_4, the external thermal resistance of the surrounding medium.

The cable conductor temperature θ_c for single-core buried cable can be given by

$$\theta_c - \theta_s = W_c\{(T_1 + (1+\lambda_1)T_1) + (1+\lambda_1+\lambda_2)(T_3+T_4)\} + W_d\{0.5T_1 + T_2 + T_3 + T_4\} \tag{3.5}$$

where T_1 is the thermal resistance between the conductor and sheath. T_2 is the thermal resistance between the sheath and armor. T_3 is the thermal resistance of the outer covering. T_4 is the thermal resistance of the surrounding medium (ratio of cable surface temperature rise above ambient to the losses per unit length). λ_1 and λ_2 are the sheath and armor ratio compared to the conductor losses. The conductive heat resistances of the non-metallic cable components are calculated based on the heat flow theory of conduction given by

$$T = \frac{\ln(r_0/r_i)}{2\pi k} \tag{3.6}$$

where r_0 and r_i are the outer and inner radius of the layer and k is the thermal conductivity of the layer material following the equivalent cylindrical modelling [91].

The idea is to find the temperature behaviour of the hottest conductor in a cable installation by the most straight-forward means possible. Hence, the analogy of a single cable is chosen for the study which can be expanded to other cable installation types.

3.4 Model Description

The external resistance T_4 of the physical equivalent thermal circuit shown in Fig. 3.2 is modeled as a result of the combining the solid phase conductive thermal

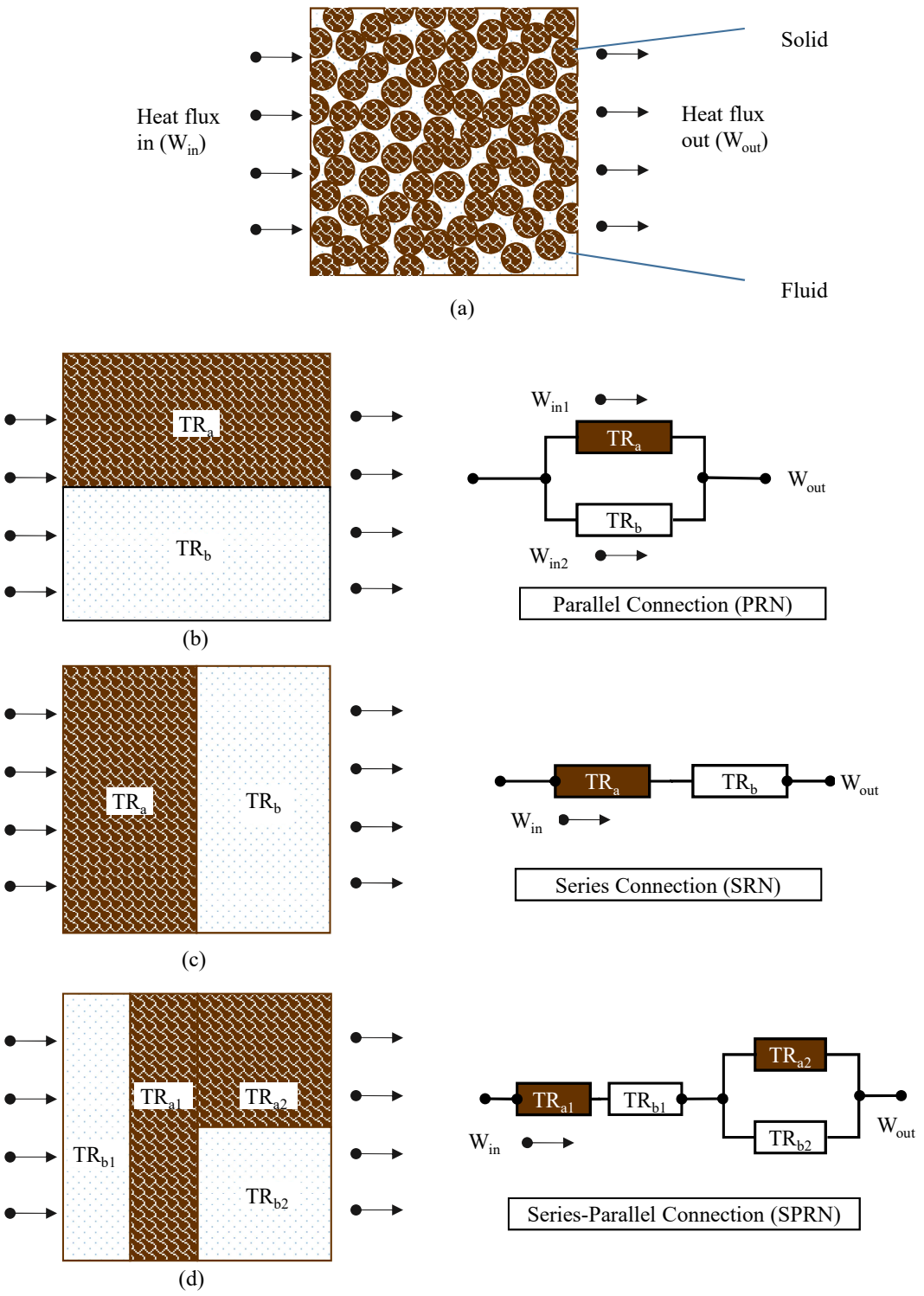

Figure 3.3: Heat Transfer Illustration in Porous Medium for Two-Phase Heat Flow. (b) Parallel Model and Corresponding Parallel Resistance Network (PRN). (c) Series Model and Corresponding Series Resistance Network (SRN). (d) Series-Parallel Model and Corresponding Series-Parallel Resistance Network (SPRN).

resistance and fluid phase convective thermal resistance. To evaluate the effective thermal resistance of the porous medium, the constituents are rearranged such that the solid and fluid phase components are grouped as discrete entities with the given volume fraction (i.e. porosity ϵ). Fig. 3.3 presents the porous domain arrangement for the simplified thermal resistance calculation. Three configurations of the thermal network are used for the study. In the parallel resistance network (PRN), the solid and fluid constituents are parallel to the heat-flux. This arrangement, in theory will enable the porous domain as an effective heat carrier as the equivalent thermal resistance is lesser than the individual thermal resistances. In the series resistance network (SRN), the solid and fluid constituents are perpendicular to the heat-flux which will result in reduced heat transfer as the equivalent thermal resistance is the volume average of the solid and fluid phase resistances. The SRN and PRN forms the upper and lower bounds for the porous domain thermal resistance. A combination of the series and parallel network is also developed to analyse the effect of mixed configuration where solid and fluid volumes are divided into equal parts. In the series-parallel resistance network (SPRN), the thermal resistance of parallel branch TR_{a2} and TR_{b2} is connected with the branch of TR_{a1} and TR_{b1} in the series network.

For PRN, the equivalent thermal resistance is given by

$$\begin{aligned} TR_{eq} &= \left(\frac{1-\epsilon}{TR_a} + \frac{\epsilon}{TR_b}\right)^{-1} \\ TR_{eq} &= \left(\frac{TR_a TR_b}{(1-\epsilon)TR_b + \epsilon TR_a}\right). \end{aligned} \tag{3.7}$$

For SRN, the resulting thermal resistance is weighed arithmetic contributions from TR_a and TR_b

$$TR_{eq} = (1-\epsilon)TR_a + \epsilon TR_b. \tag{3.8}$$

For SPRN, the combination series-parallel arrangement will result in an equivalent

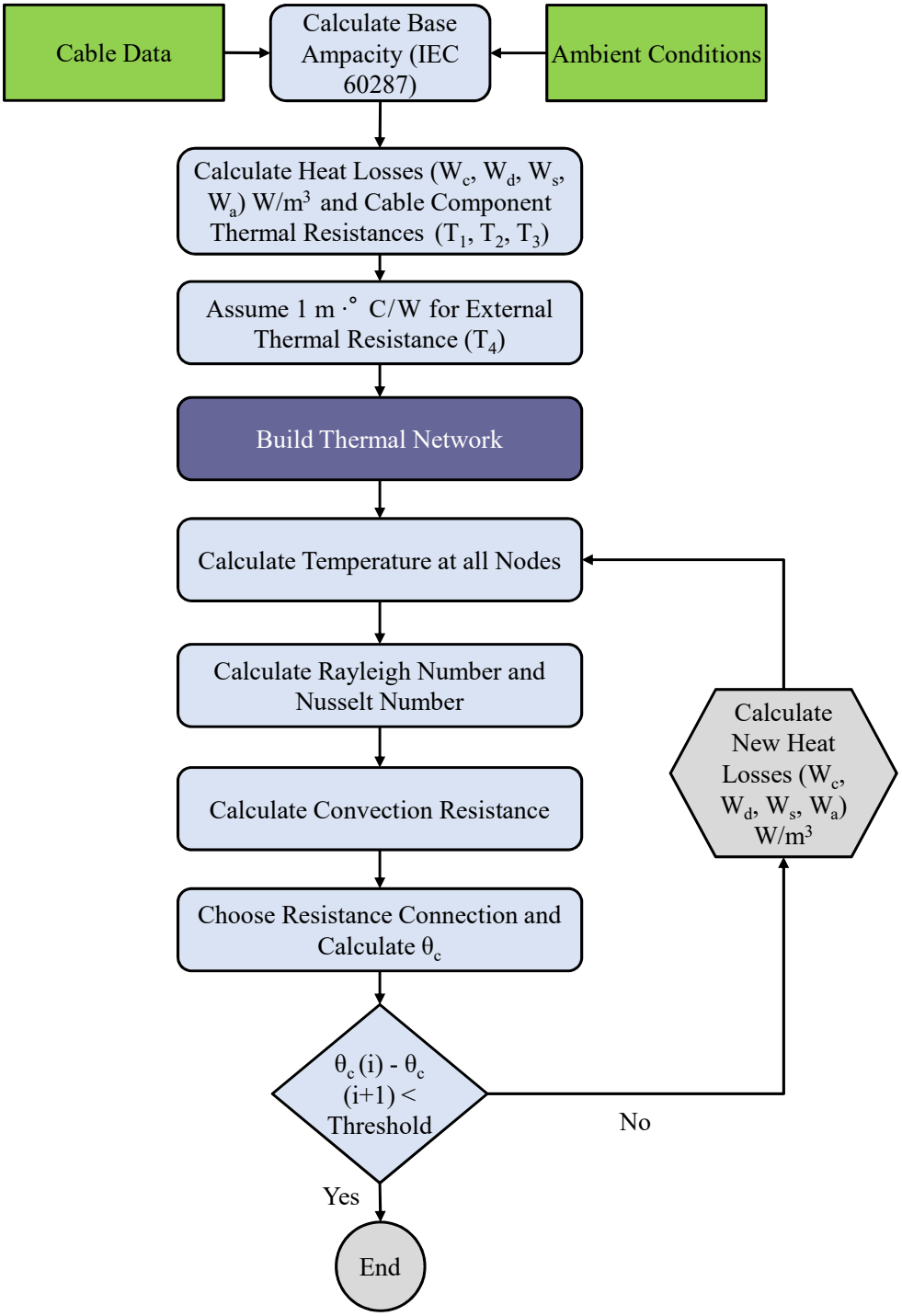

Figure 3.4: Flow diagram of the iterative model to determine the conductor temperature combining the heat transfer by convection and conduction.

thermal resistance given by

$$TR_{eq} = (1-\epsilon)TR_{a1} + \epsilon TR_{b1} + \left(\frac{TR_{a2}TR_{b2}}{(1-\epsilon)TR_{b2} + \epsilon TR_{a2}}\right). \tag{3.9}$$

Here TR_a and TR_b are the conductive and convective thermal resistances of the

solid and fluid phase respectively. The equivalent thermal resistances for the SRN, PRN and SPRN are called iteratively as the convection heat transfer resistance is calculated based on the Rayleigh-Darcy number and the Nusselt number. The Rayleigh number calculation assumes an unbounded porous medium for the image theory, and the model still applies for calculating convective resistance. The conductive resistance follows the image theory as per IEC 60287. The process is presented in Fig. 3.4. The calculation of W_c, W_s and W_a requires the knowledge of Joule losses in copper conductor that is dependent on conductor temperature to compute the electrical resistance. To start with, we assume a sensible temperature (90°C) for the conductor core, 20°C for ambient temperature and 1 m · °C/W for the external thermal resistance T_4. During every iteration, the thermal network is built and nodal temperatures - θ_a, θ_s and θ_c are recalculated. At the end of every iteration when the convergence criterion is not met, we use the new calculated temperature and re-calculate the conductor AC resistance and then adjust W_c, W_s and W_a accordingly and repeat steps until convergence.

The authors of [92] proposed an equivalent thermal conductivity of porous domains that exhibits heat transfer by convection and conduction and is calculated by multiplying the pure thermal conductivity with the Nusselt number factor (1+Nu). This method is also evaluated in the approach for calculating external thermal resistance of the submarine sediment.

3.4.1 Numerical Example

The primary objective of the numerical example is to determine the factors influencing the external thermal resistance T_4 that favors convective heat transfer and conductive heat transfer. The extent to which these factors affect T_4 is dependent on their effect on the conductive and convective heat resistances (T_{cond}, T_{conv}). The conductive thermal resistance bounded by a finite domain is given by

$$T_{cond} = \frac{r}{2\pi}(\ln(u + \sqrt{u^2 + 1})) \tag{3.10}$$

where r is the thermal resistivity of the surrounding medium (m·°C/W); $u(= 2L/D_e)$ is the dimensionless geometry factor from the image theory; L is the depth of burial (m) and D_e is the diameter of the cable (m). The thermo-physical property of the solid phase medium that determines T_{cond} is the thermal conductivity/resistivity of the material and the other factor that directly affects T_{cond} is the distance between the heat source (i.e. cable) and the heat sink (i.e. boundary beyond which the heat from the source will have no effect). In this case it is the depth of burial (L) of the cable. The convective thermal resistance is given by

$$T_{conv} = \frac{1}{hA} \tag{3.11}$$

where h is the convective heat transfer coefficient and A is the total area exposed. h is calculated using the Nusselt number (Nu) and Rayleigh-Darcy number (Ra) [93] given by

$$Ra = \frac{\kappa\rho\beta g(\theta_s - \theta_{amb})D_e^3}{\alpha\mu} \tag{3.12}$$

where θ_s and θ_{amb} are the surface temperature of the cable and the ambient temperature. α is thermal diffusivity and μ is the kinematic viscosity of the porous medium.

The porous medium exhibiting convective heat transfer is directly related to non-dimensional Rayleigh-Darcy and Nusselt number. In a pure convective scenario, the Rayleigh number is associated with the buoyancy-driven flow. It describes the fluid flow regime. The Rayleigh number in certain lower range denotes laminar flow and higher range, turbulent flow [94]. The Nusselt number is the the ratio of the convective heat transfer to the fluid convective heat transfer. It is equal to the dimensionless temperature gradient at the surface, and it provides a measure of the convective heat transfer occurring at the surface [95].

The factors that directly influence the Rayleigh-Darcy number (in turn the convective heat transfer) are the fluid density, intrinsic permeability κ, temperature difference between the surface of the heat source and the ambient, kinematic and dynamic viscosity of the fluid. The parameter of interest here is the intrinsic per-

meability κ which is determined by the pore structure and grain size as the other parameters are material properties of the fluid (i.e water in this case).

In addition to the above parameters, the thermal resistance mix is done using the volume fraction (ϵ) that determines the amount of heat transfer contributed by the solid and fluid phase constituents.

The cable presented in Fig. 3.1 is used for the analysis. The base ampacity is calculated using IEC 60287 using the solid phase thermal conductivities. Appropriate derating to the ampacity values is applied for varying depths of burial. The upper and lower bound thermal resistances (SRN and PRN resistances) are analysed for changes in the influential parameters.

Effect of Depth of Burial and Solid phase Thermal Conductivity

The dependence of the equivalent thermal resistance on the depth of burial and solid phase thermal conductivity was investigated by performing the iterative process shown in Fig. 3.4. When porosity remained constant (in this case, the porosity $\epsilon = 0.4$), the external thermal resistance varies significantly when these environmental parameters alter.

As the calculation of conduction thermal resistance still follows the IEC 60287 which is based on the image theory, the depth of burial determines the temperature gradient between the cable surface and the seafloor. When the distance from the heat sink increases, the heat dissipation rate naturally decreases. Similarly, in a free convective environment, heat transfer about a heat source is dramatically affected when constrained in either horizontal or vertical direction compared to the heat source in an infinite medium [96]. It will be of our interest to observe whether the depth of burial is constraining and the extent of its effects on the convective heat transfer.

Tables 3.1 and 3.2 presents the equivalent thermal resistance values calculated by applying SRN and PRN respectively. The contributions by the solid phase and

fluid phase constituents are analysed to identify the way the parameters influence the respective thermal resistances. Moderately high and low permeability values $\kappa = 10^{-9}$ (m^2) and $\kappa = 10^{-14}$ (m^2) were chosen to differentiate the effect of the presence and absence of heat transfer by convection [97].

The solid phase thermal resistance is much higher than the fluid phase (the fluid phase resistance is almost negligible) for high permeable sediments. In parallel arrangement, the lower bound of the T_4 values also affirm the same. Convection in high permeable sediments contribute to a higher percentage of heat transfer by the fluid phase suggesting that it is the least resistive path for the heat to flow. Contrarily, when the permeability is low (where the fluid is far less mobile), the fluid movement is blocked by the pore nature and it will become a heat conducting body and not advecting body. The fluid phase (water) thermal conductivity is much lower than the solid phase thermal conductivity, resulting in higher heat transferred by the solid phase compared to the fluid phase. The fluid phase contributes to the higher T_4 values in this case.

When k_s is low, in high permeable sediments, fluid phase contributes to higher heat transfer by convection that increases with the increase in depth of burial. This is in contradiction with the conduction heat transfer process where the resistance to heat transfer increases with the increase in depth of burial. Hence, the effective T_4 in SRN and PRN increases with the depth of burial (majorly due to the increase in T_{cond} and negligible convection from fluid phase constituents of low permeable sediment). On the other hand, higher k_s increases the conductive heat transfer by reducing T_{cond}, this is observed for high and low permeable sediments. For example, for a burial depth of 5 metres, T_{cond} contributes to 50.23% when k_s is 0.9 (W/m·°C) compared to being 34.24% heat resistive when k_s is 1.8 (W/m·°C) in the low permeable condition. Though the fluid phase is the least resistive path in high permeable condition, the increase in k_s increases heat transfer contribution of the solid phase constituent. For the above case of two k_s values, heat transferred

Table 3.1: Estimated Thermal Resistances in Series Arrangement for Different Solid Phase Thermal Conductivities and Depths of burial with Porosity $\epsilon = 0.4$.

$\epsilon = 0.4$ Thermal conductivity ($k_s W/m{\cdot}°C$)	Thermal resistance	L = 1 m		L = 3 m		L = 5 m	
		$\kappa = 10^{-9}$ m^2	$\kappa = 10^{-14}$ m^2	$\kappa = 10^{-9}$ m^2	$\kappa = 10^{-14}$ m^2	$\kappa = 10^{-9}$ m^2	$\kappa = 10^{-14}$ m^2
0.9	T_{cond}	0.7395	0.7395	0.9338	0.9338	1.0242	1.0242
	T_{conv}	0.0384	1.6667	0.0375	1.6144	0.0372	1.5225
	T_4	0.4591	1.1104	0.5753	1.2061	0.6294	1.2235
	Solid phase resistance	96.65%	39.96%	97.39%	46.45%	97.64%	50.23%
	Fluid phase resistance	3.35%	60.04%	2.61%	53.54%	2.36%	49.78%
1.2	T_{cond}	0.5546	0.5546	0.7004	0.7004	0.7681	0.7681
	T_{conv}	0.0397	1.6667	0.0385	1.6054	0.0382	1.5045
	T_4	0.3487	0.9994	0.4356	1.0624	0.4762	1.0627
	Solid phase resistance	95.43%	33.30%	96.47%	39.56%	96.78%	43.37%
	Fluid phase resistance	4.55%	66.71%	3.54%	60.44%	3.21%	56.63%
1.8	T_{cond}	0.3698	0.3698	0.4669	0.4669	0.5121	0.5121
	T_{conv}	0.0422	1.6666	0.0406	1.5903	0.0402	1.4755
	T_4	0.2387	0.8885	0.2964	0.9163	0.3233	0.8975
	Solid phase resistance	92.95%	24.97%	94.51%	30.57%	95.04%	34.24%
	Fluid phase resistance	7.07%	75.03%	5.48%	69.42%	4.97%	65.76%

Table 3.2: Estimated Thermal Resistances in Parallel Arrangement for Different Solid Phase Thermal Conductivities and Depths of Burial with Porosity $\epsilon = 0.4$.

$\epsilon = 0.4$ Thermal conductivity ($k_s W/m{\cdot}°C$)	Thermal resistance	L = 1 m		$L = 3$ m		L = 5 m	
		$\kappa = 10^{-9}$ m^2	$\kappa = 10^{-14}$ m^2	$\kappa = 10^{-9}$ m^2	$\kappa = 10^{-14}$ m^2	$\kappa = 10^{-9}$ m^2	$\kappa = 10^{-14}$ m^2
0.9	T_{cond}	0.7395	0.7395	0.9338	0.9338	1.0242	1.0242
	T_{conv}	0.0685	1.6667	0.0723	1.6198	0.0739	1.5293
	T_4	0.1503	0.9512	0.1619	1.1243	0.1668	1.1801
	Conduction	12.19%	77.18%	10.40%	72.24%	9.77%	69.13%
	Convection	87.77%	22.83%	89.57%	27.76%	90.28%	30.87%
1.2	T_{cond}	0.5546	0.5546	0.7004	0.7004	0.7681	0.7681
	T_{conv}	0.0644	1.6667	0.0675	1.6188	0.069	1.5252
	T_4	0.1371	0.7566	0.1475	0.906	0.1521	0.9584
	Conduction	14.83%	81.85%	12.64%	77.61%	11.88%	74.87%
	Convection	85.16%	18.16%	87.41%	22.39%	88.17%	25.14%
1.8	T_{cond}	0.3698	0.3698	0.4669	0.4669	0.5121	0.5121
	T_{conv}	0.06	1.6667	0.0623	1.6218	0.0635	1.5295
	T_4	0.1207	0.5369	0.1299	0.6529	0.1338	0.6977
	Conduction	19.58%	87.11%	16.69%	83.90%	15.68%	81.75%
	Convection	80.47%	12.89%	83.40%	16.10%	84.28%	18.25%

by conduction increased from 9.77 % to 15.68 %. For a given depth of burial, both SRN and PRN results in decreased effective thermal resistance with the increase in solid phase thermal conductivity.

Effect of Porosity and Solid phase Thermal Conductivity

In this section, the effect of varying the pore volume (porosity) and solid phase thermal conductivity on the effective thermal resistance of the porous medium is studied. The assumed depth of burial is 2 meters. Since the depth of burial is constant, the distance between the heat source and heat sink is unaltered. The increase in solid phase thermal conductivity enhances the conductive heat transfer and is expected to decrease the thermal resistance. However, when porosity increases, it means increase in fluid content in the saturated porous media. Fluid flow predominantly affects the heat dissipation and permeability will be the influential factor in determining the heat transfer due to the change in fluid volume. Tables 3.3 and 3.4 present the effective thermal resistances calculated using the SRN and PRN thermal models for varying porosity and solid phase thermal conductivity.

The effective T_4 values calculated for high permeable composition decreases with the increase in porosity. The tendency is observed in both the series and parallel resistance configurations. The decrease in T_4 values for the increase in porosity can be attributed to the availability of a higher volume of mobile that enhanced the buoyancy-driven flow. The calculated percentage contributions by the fluid phase resistances increased slightly with increased porosity due to the increase in fluid volume. The contribution to heat transfer by the solid phase and fluid phase constituents can be understood from the PRN results. When porosity increases, PRN shows that the heat transfer by fluid phase increases significantly due to convection. On the other hand, for low permeable sediments, an increase in porosity results in the increase in T_4 values due to the presence of higher volume of immobile fluid. For a given ϵ value in low permeable sediments, the solid phase

Table 3.3: Estimated Thermal Resistances in Series Arrangement for Different Solid Phase Thermal Conductivities and Porosity Values. The depth of burial $L = 2$ m.

$L = 2$ m Thermal conductivity ($k_s W/m{\cdot}^\circ$C)	Thermal resistance	$\epsilon = 0.3$		$\epsilon = 0.5$		$\epsilon = 0.6$	
		$\kappa = 10^{-9}$ m^2	$\kappa = 10^{-14}$ m^2	$\kappa = 10^{-9}$ m^2	$\kappa = 10^{-14}$ m^2	$\kappa = 10^{-9}$ m^2	$\kappa = 10^{-14}$ m^2
0.9	T_{cond}	0.8621	0.8621	0.8621	0.8621	0.8621	0.8621
	T_{conv}	0.0349	1.6569	0.0412	1.6545	0.0457	1.6532
	T_4	0.614	1.1006	0.4517	1.2583	0.3723	1.3368
	Solid phase resistance	98.29%	54.83%	95.43%	34.26%	92.62%	25.80%
	Fluid phase resistance	1.71%	45.16%	4.56%	65.74%	7.37%	74.20%
1.2	T_{cond}	0.6466	0.6466	0.6466	0.6466	0.6466	0.6466
	T_{conv}	0.0361	1.6558	0.0424	1.6515	0.0467	1.6491
	T_4	0.4635	0.9493	0.3445	1.1491	0.2867	1.2481
	Solid phase resistance	97.65%	47.68%	93.85%	28.14%	90.21%	20.72%
	Fluid phase resistance	2.34%	52.33%	6.15%	71.86%	9.77%	79.28%
1.8	T_{cond}	0.4311	0.4311	0.4311	0.4311	0.4311	0.4311
	T_{conv}	0.0384	1.6536	0.0445	1.6457	0.0485	1.6409
	T_4	0.3133	0.7978	0.2378	1.0384	0.2015	1.1569
	Solid phase resistance	96.32%	37.83%	90.64%	20.76%	85.58%	14.91%
	Fluid phase resistance	3.68%	62.18%	9.36%	79.24%	14.44%	85.10%

Table 3.4: Estimated Thermal Resistances in Parallel Arrangement for Different Solid Phase Thermal Conductivities and Porosity Values. The depth of burial $L = 2$ m.

$L = 2$ m Thermal conductivity ($k_s W/m{\cdot}°C$)	Thermal resistance	$\epsilon = 0.3$		$\epsilon = 0.5$		$\epsilon = 0.6$	
		$\kappa = 10^{-9}$ m^2	$\kappa = 10^{-14}$ m^2	$\kappa = 10^{-9}$ m^2	$\kappa = 10^{-14}$ m^2	$\kappa = 10^{-9}$ m^2	$\kappa = 10^{-14}$ m^2
0.9	T_{cond}	0.8621	0.8621	0.8621	0.8621	0.8621	0.8621
	T_{conv}	0.0654	1.6583	0.0755	1.6565	0.0795	1.6553
	T_4	0.1851	1.0072	0.1388	1.134	0.1249	1.21
	Conduction	15.03%	81.78%	8.05%	65.77%	5.80%	56.14%
	Convection	84.91%	18.22%	91.92%	34.23%	94.26%	43.86%
1.2	T_{cond}	0.6466	0.6466	0.6466	0.6466	0.6466	0.6466
	T_{conv}	0.0615	1.6586	0.0707	1.6561	0.0744	1.6544
	T_4	0.1679	0.7915	0.1274	0.9301	0.1151	1.0191
	Conduction	18.18%	85.69%	9.85%	71.92%	7.12%	63.04%
	Convection	81.90%	14.32%	90.10%	28.08%	92.82%	36.96%
1.8	T_{cond}	0.4311	0.4311	0.4311	0.4311	0.4311	0.4311
	T_{conv}	0.0573	1.6595	0.0652	1.6566	0.0683	1.6542
	T_4	0.1458	0.5541	0.1132	0.6841	0.103	0.7748
	Conduction	23.67%	89.97%	13.13%	79.34%	9.56%	71.89%
	Convection	76.34%	10.02%	86.81%	20.65%	90.48%	28.10%

conductivity strongly determines the contribution of heat transfer by the solid and fluid phases. Higher k_s values favor more heat transfer by conduction in the solid medium because it is the least resistive path for the heat to flow. Though the same phenomenon is observed in high permeable sediments, it is more pronounced in low permeable bodies.

3.5 Results and Analysis

In this section, the FEM numerical model results are used to evaluate the submarine power cable thermal performance and to predict the cable conductor temperature for various parameter combinations. Mainly, the results are used to validate the proposed analytical thermal models. The cable base current ratings were calculated using IEC 60287 for conductor temperature of 90°C. The procedure for conductor temperature calculation using the proposed thermal networks is shown in Fig. 3.4. The permeability range used for the analysis is $10^{-7}(\mathrm{m}^2)$ to $10^{-18}(\mathrm{m}^2)$.

3.5.1 Comparison of SRN, PRN, 1+Nu Models with FEM Simulations

The thermal behavior of the cable was studied by varying key factors namely porosity, permeability, solid phase thermal conductivity and depth of burial. In this section, the conductor temperatures calculated using SRN and PRN are analysed to understand the upper and lower bound values and how well they compare with the FEM results. The more simplified model with the Nusselt number factor (1+Nu) is also included in the results to show the accuracy of the proposed models. Fig. 3.5, 3.6 and 3.7 show the trend of temperature changes for varying parameters. The current was calculated using IEC 60287 (I = 400 A for k_s = 0.9 W/m·°C, I = 438 A for k_s = 1.2 W/m·°C and I = 489 A for k_s = 1.8 W/m·°C). It is to be noted that the temperature changes are in a particular pattern in all the cases. The temperature increases with the decrease in permeability values and

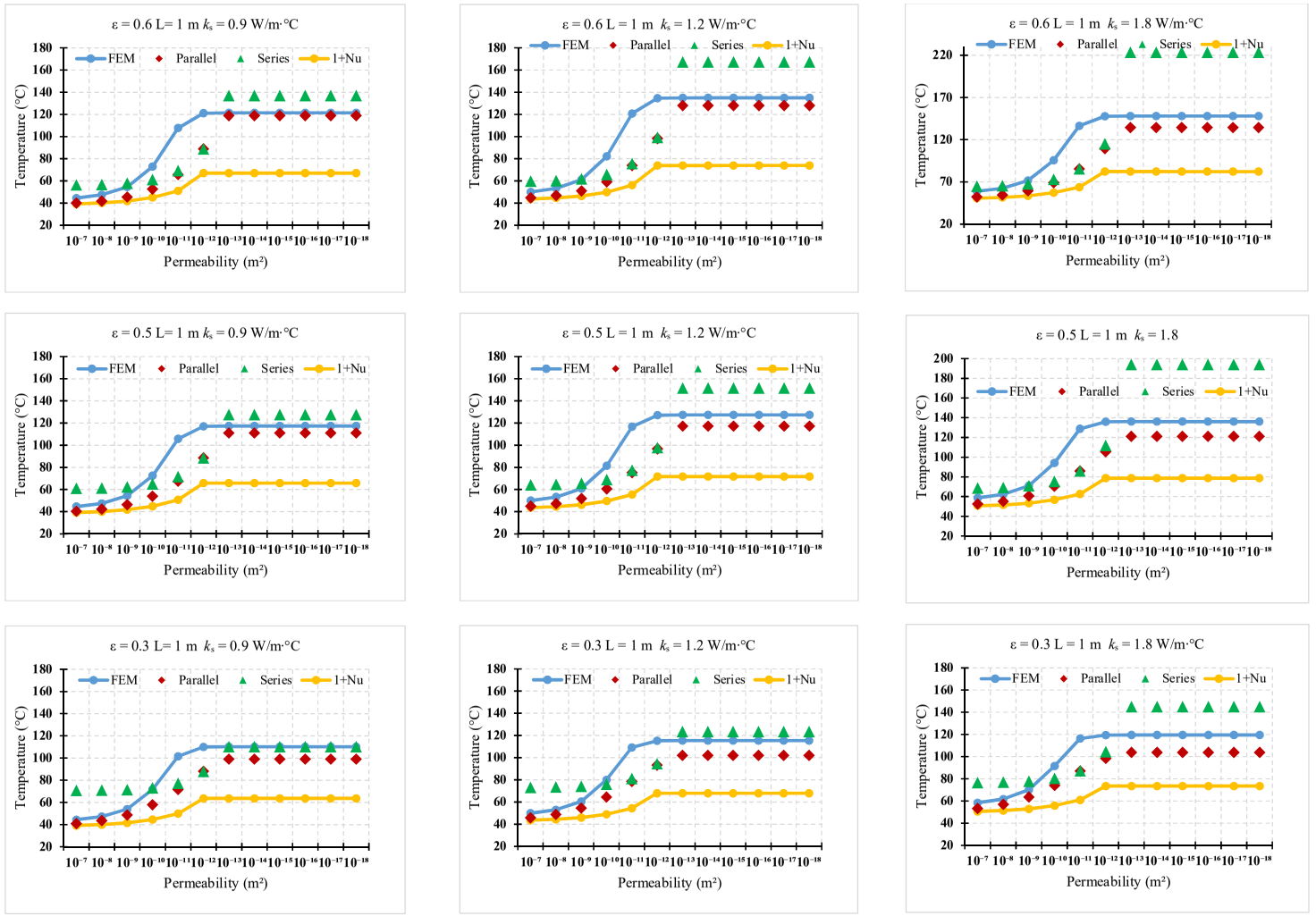

Figure 3.5: Comparison of cable conductor temperature estimated using SRN, PRN, 1+Nu with FEM results for varying solid phase thermal conductivity (k_s) and porosity (ϵ).

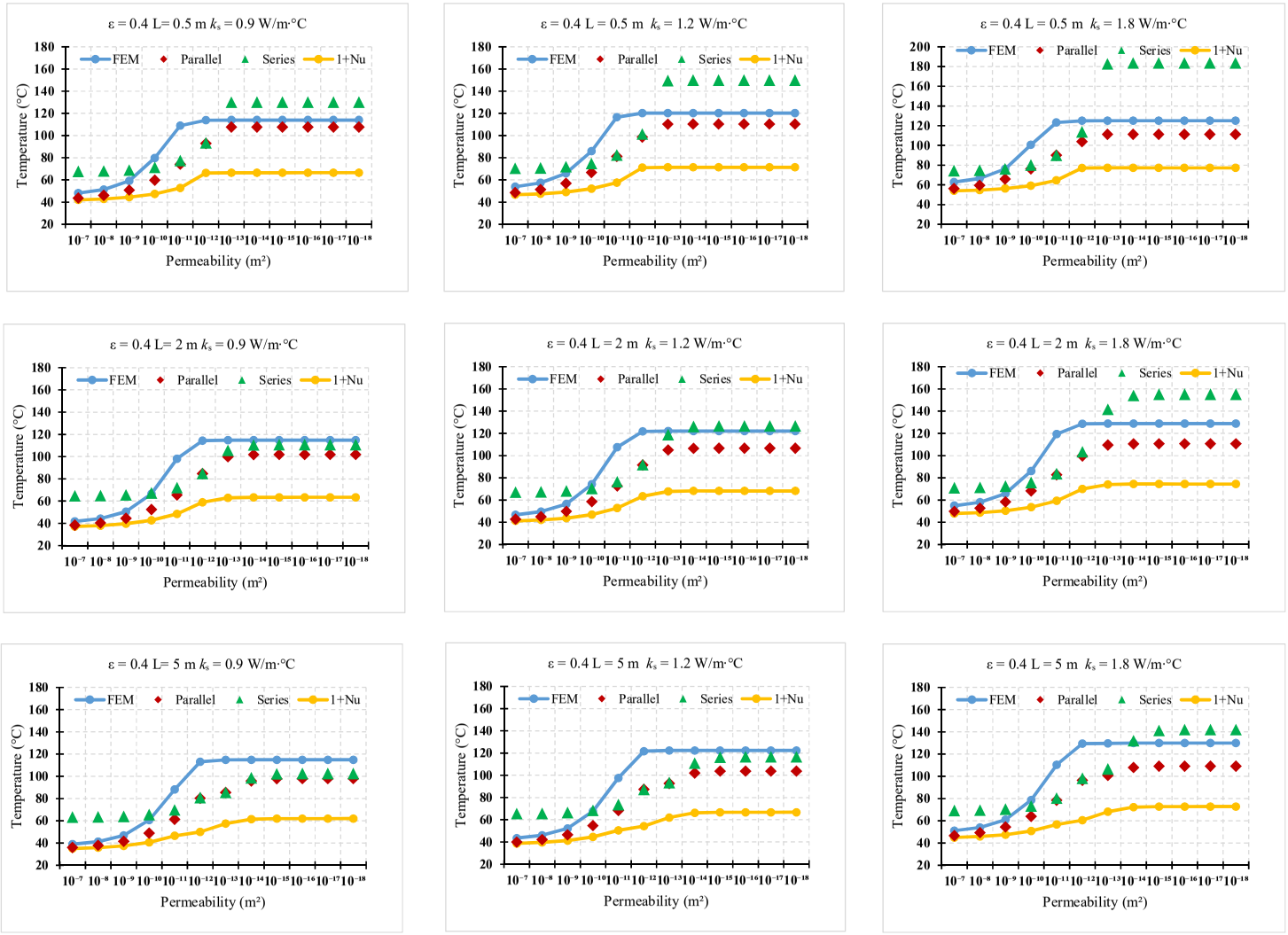

Figure 3.6: Comparison of cable conductor temperature estimated using SRN, PRN, 1+Nu with FEM results for varying solid phase thermal conductivity (k_s) and depth of burial (L).

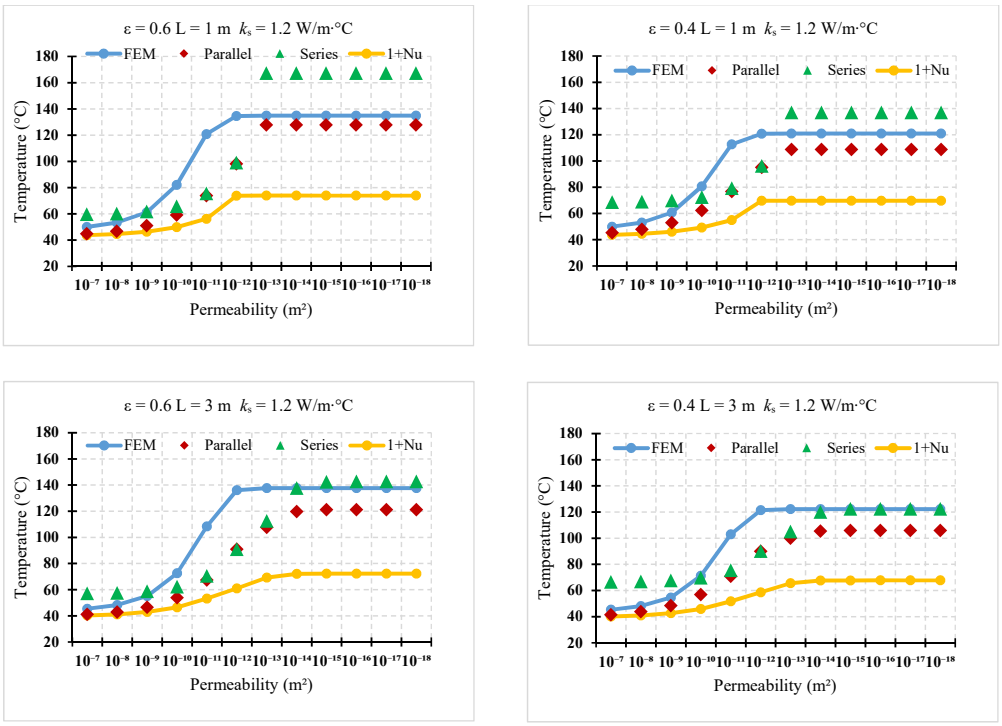

Figure 3.7: Comparison of cable conductor temperature estimated using SRN, PRN, 1+Nu with FEM results for varying depth of burial (L) and porosity (ϵ).

around the permeability values of $10^{-12}(\mathrm{m}^2)$ to $10^{-13}(\mathrm{m}^2)$, temperature becomes insensitive to further decrease in permeability. The findings are in close agreement with [97]. The decrease in temperature can be attributed to the convective heat transfer occurring in the sediments with permeability above certain critical values. The authors of [98] estimated that the minimum permeability value at which convection currents may occur is 20 Darcy.

$$\kappa_{min} = 1.97378 \cdot 10^{-11} \tag{3.13}$$

The transition from convection to conduction only heat transfer can be observed for permeability values below κ_{min}.

Effect of Porosity and Solid Phase Thermal Conductivity

FEM simulations and analytical solutions were performed for varying porosity and solid phase thermal conductivity for a constant depth of burial (at L = 1 m). The 1+Nu model critically underestimates the conductor temperature for all perme-

ability values. Especially for the low permeable section, the deviation from FEM simulations are very high even though the lower bound model was used to calculate the effective thermal conductivity. The temperature calculated using SRN and PRN models follow the FEM results shown in Fig. 3.5. SRN predicts higher temperatures particularly for permeability values that are minimally convecting. The deviation increases with the increase in porosity and very high deviations can be observed for sediments with high solid phase thermal conductivity. The PRN values are in close agreement with FEM results compared to SRN especially for high porous sediments. The transition from partly convective to fully conductive heat transfer occurs for permeability values above $10^{-11}(\mathrm{m}^2)$ for FEM and $10^{-12}(\mathrm{m}^2)$ for the proposed model.

Effect of Solid Phase Thermal Conductivity and Depth of Burial

Fig. 3.6 shows the results for varying the depth of burial and solid phase thermal conductivity for the range of permeability values where porosity is constant $\epsilon = 0.4$. SRN overestimates the conductor temperature for lower burial depths and the deviation is very high for higher k_s values. For example, when $k_s = 1.8$ W/m·°C and L = 0.5 m, the deviation between SRN and FEM is as high as 50%. On the other hand, PRN predicts lower values for conductor temperature compared to FEM. With the increase in burial depth and k_s, the deviation is very high, especially for the lower permeability band.

Effect of Porosity and Depth of Burial

Fig. 3.7 compares the results for changing porosity and depth of burial for a range of permeability values and constant solid phase thermal conductivity (k_s = 1.2 W/m·°C). For highly porous sediments with lower depth of burial, PRN predicts values closer to FEM whereas, SRN estimates temperatures in very close agreement with FEM results for cable installed in less porous sediments in deeper depths of burial.

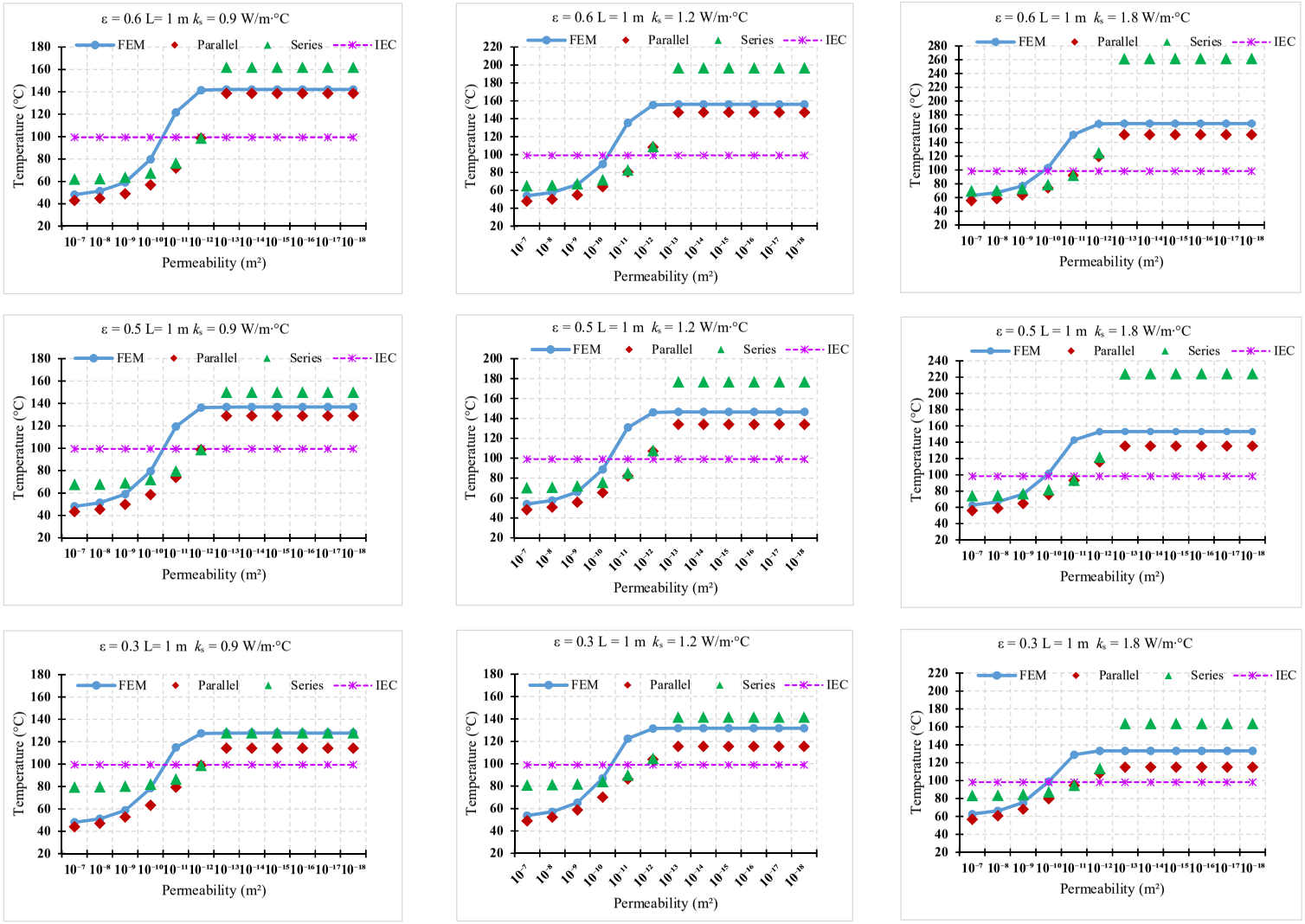

Figure 3.8: Comparison of cable conductor temperature estimated using SRN and PRN with FEM results and IEC 60287 for varying solid phase thermal conductivity (k_s) and porosity (ϵ).

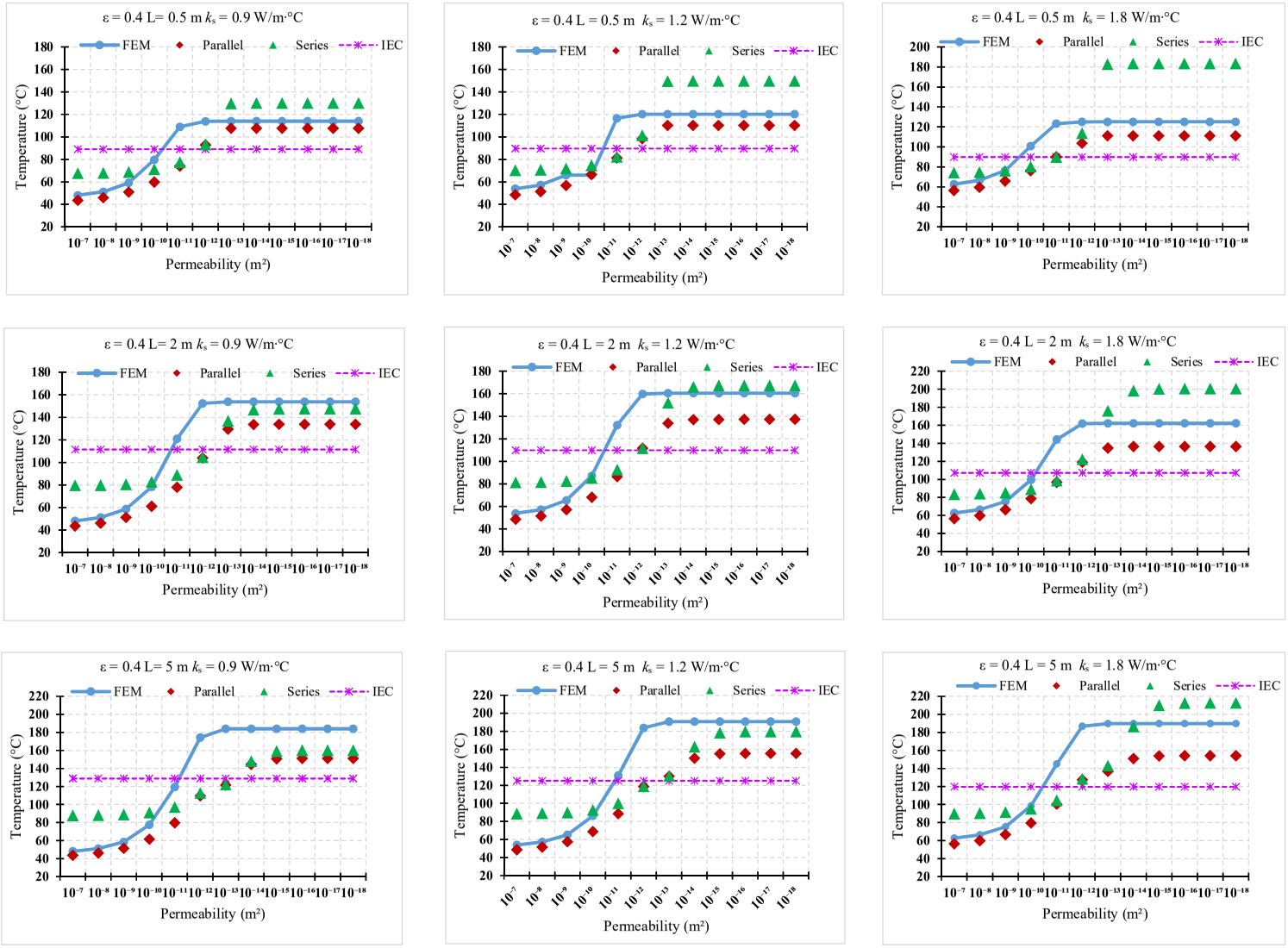

Figure 3.9: Comparison of cable conductor temperature estimated using SRN and PRN with FEM results and IEC 60287 for varying solid phase thermal conductivity (k_s) and depth of burial (L).

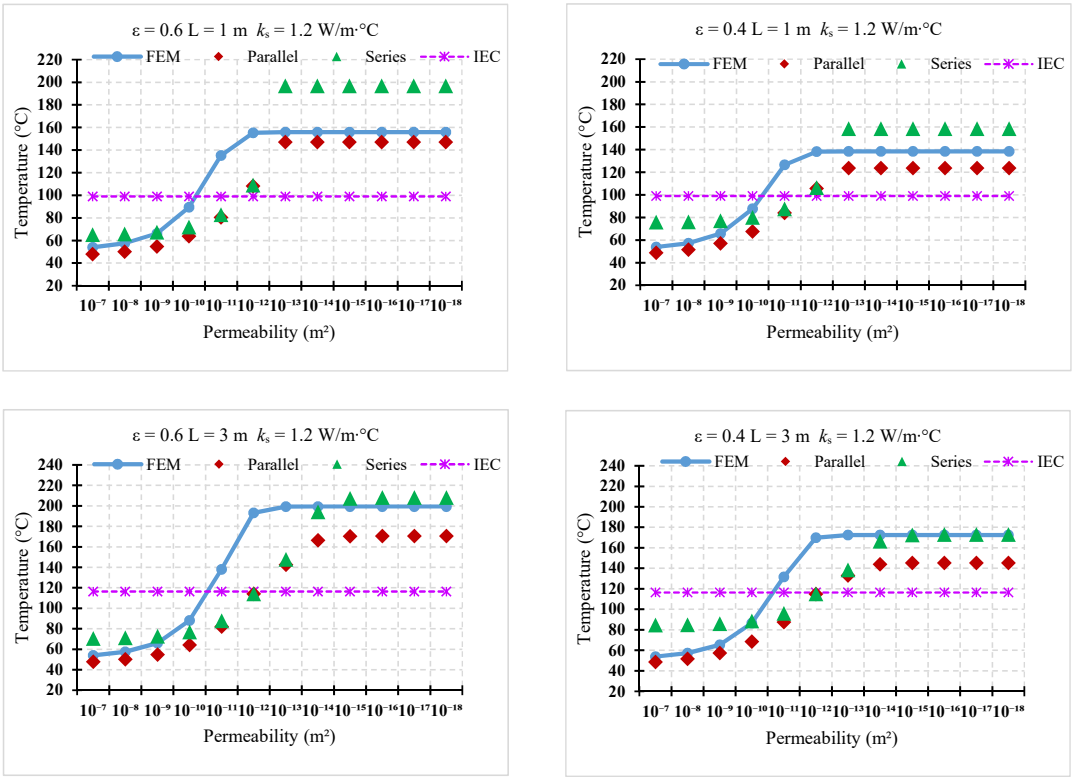

Figure 3.10: Comparison of cable conductor temperature estimated using SRN and PRN with FEM results and IEC 60287 for varying depth of burial (L) and porosity (ϵ).

3.5.2 Comparison of SRN, PRN with IEC and FEM Simulations

The results discussed above indicate that the SRN and PRN models predict conductor temperatures closer to FEM results but the deviations are higher for certain values and combination of parameters. It is also noted that the conductor temperatures estimated for the high permeability band are not affected by the depth of burial changes. In this section, the ampacity value is not derated for the change in depth of burial. Base ampacity calculated (using IEC 60287) for burial depth of 0.5 m is used for all calculations; appropriate corrections were made only for changes in k_s values. The proposed models are compared with conductor temperatures predicted using the FEM and IEC 60287 analytical model.

Effect of Porosity and Solid Phase Thermal Conductivity

In an un-derated condition, the conductor temperature predicted for the high permeability band is the same as the derated condition (see Fig. 3.5 and 3.8). This implies that the cables installed in high permeable sediments can have a higher thermal rating that may be independent of the depth of burial. For changing porosity and solid phase thermal conductivity, PRN predicts conductor temperature values closer to FEM results with a maximum deviation of 12.5 %. SRN on the other hand estimates very high temperatures specifically for the low permeable band. The IEC analytical model predicts constant temperature for all permeability values. However, it is an overestimate for the high permeable band and underestimate for the low permeable band.

Effect of Solid Phase Thermal Conductivity and Depth of Burial

When the depth of burial and solid phase thermal conductivity changes, the conductor temperature for high permeability band remains the same for a given solid phase thermal conductivity. For very high permeability values, PRN and FEM

results are in complete agreement indicating that the convective heat transfer is dominant in this region. Hence the effective thermal resistance from PRN is more suitable (refer to Fig. 3.9). On the other hand, PRN severely underestimates the temperature values for low permeable sediments. SRN is suitable for medium burial depth but the results are affected by the solid phase thermal conductivity values. In most cases, the FEM results are in between the values predicted by SRN and PRN.

Effect of Porosity and Depth of Burial

From the results shown in Fig. 3.10, it is evident that the PRN model predicts temperature values closer to FEM results when the porosity is higher and depth of burial is lower. Contrarily, SRN is closely matching with the FEM results compared to PRN when the porosity is lower and the depth of burial is higher.

The SRN and PRN follow the temperature trends of the FEM simulations. Though the proposed models improved the IEC 60287 analytical model, for some cases, the predicted temperatures are either underestimated or overestimated compared to FEM. An improved model combining SRN and PRN is proposed and the results for the conductor temperature predicted using SPRN are discussed in the following section.

3.5.3 Comparison of SPRN and FEM Simulations

Effect of Porosity and Solid Phase Thermal Conductivity

Fig. 3.11 compares the conductor temperatures calculated using the SPRN model with the numerical method for varying porosity and solid phase thermal conductivity. The SPRN model predicts temperature values that are in very close agreement with the FEM results (for both low and high permeability band). The degree of agreement is higher than that of the SRN and PRN model. This is the result of the mixed configuration. As SPRN is derived from SRN and PRN, the tempera-

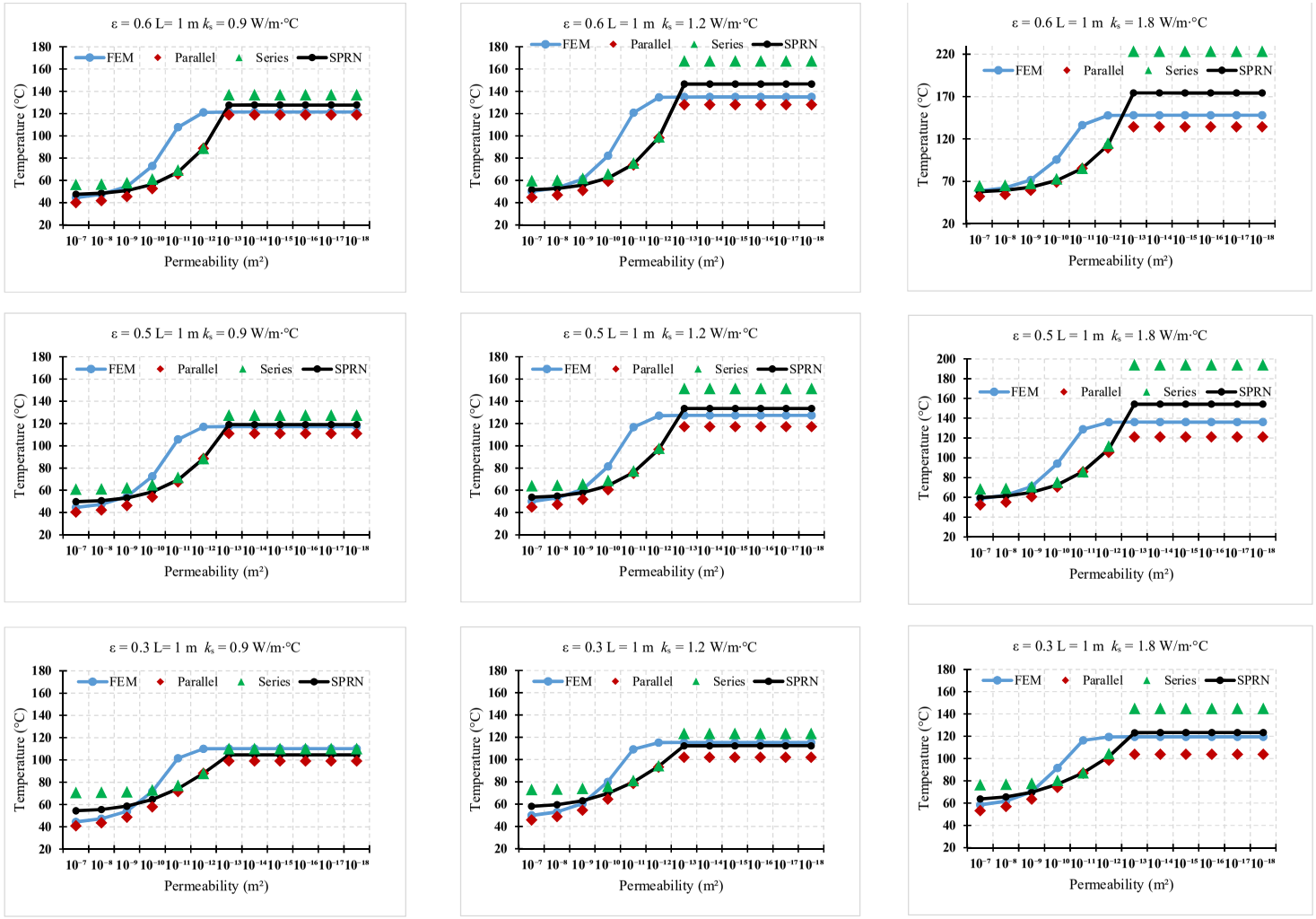

Figure 3.11: Comparison of cable conductor temperature estimated using SRN, PRN, SPRN with FEM results for varying solid phase thermal conductivity (k_s) and porosity (ϵ).

ture deviation at the critical permeability values ($10^{-11}(m^2)$ and $10^{-12}(m^2)$) still remains.

Effect of Solid Phase Thermal Conductivity and Depth of Burial

The temperature predictions for varying depth of burial and solid phase thermal conductivity are presented in Fig. 3.12. The SPRN values are in close agreement with the FEM results but deviations can be observed for lower solid phase thermal conductivity at deeper burial depths. In this case, SPRN underestimates the conductor temperature values compared to the FEM results.

Effect of Porosity and Depth of Burial

By changing the porosity and depth of burial for a range of permeability values, the effect on predicted cable conductor temperatures by SPRN and FEM models are presented in Fig. 3.13. The temperature calculated using SPRN is matching the FEM results compared to the SRN and PRN model results.

The analysis presented above shows that all the three proposed thermal network models are sensitive to the changes in the factors (namely porosity, permeability, solid phase thermal conductivity and depth of burial) that determine the thermal behavior of the submarines cables installed in porous sea sediments. Of the three models proposed, SPRN results correspond well with the FEM results.

The results from the proposed analytical methods are summarized in Tables 3.5 and 3.6. Conductor temperatures estimated for the study cable under steady-state conditions with a burial depth of 1 metre and solid phase thermal conductivity of 1.2 W/m·°C are presented in Table 3.5. The current was calculated using IEC 60287 assuming a conductor temperature of 90 °C. Two permeability values were used for the study - one high permeability value favoring convective heat transfer and one low permeability value corresponding to conduction-only heat transfer. The results show that the conductor temperatures estimated using the

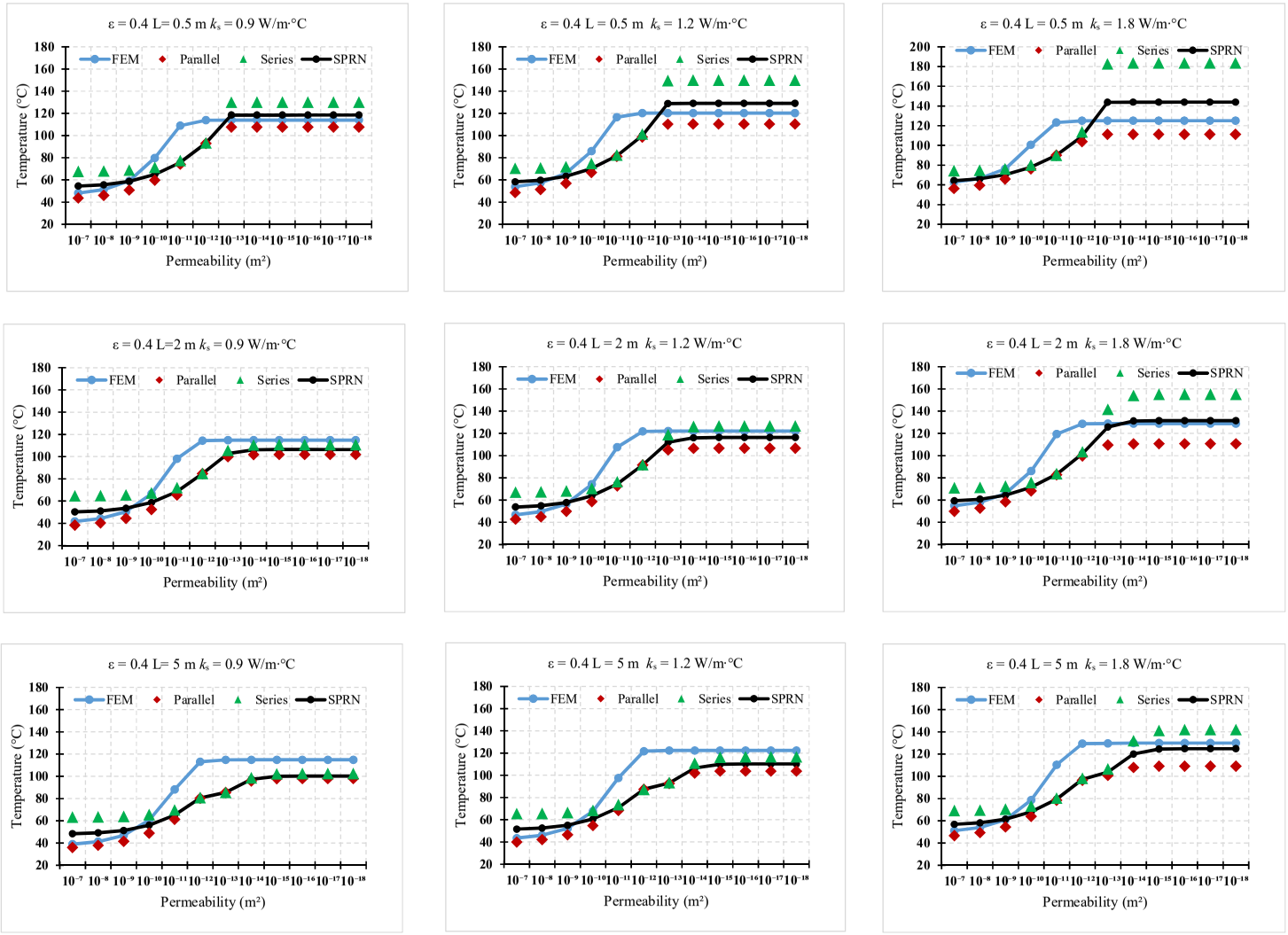

Figure 3.12: Comparison of cable conductor temperature estimated using SRN, PRN, SPRN with FEM results for varying solid phase thermal conductivity (k_s) and depth of burial (L).

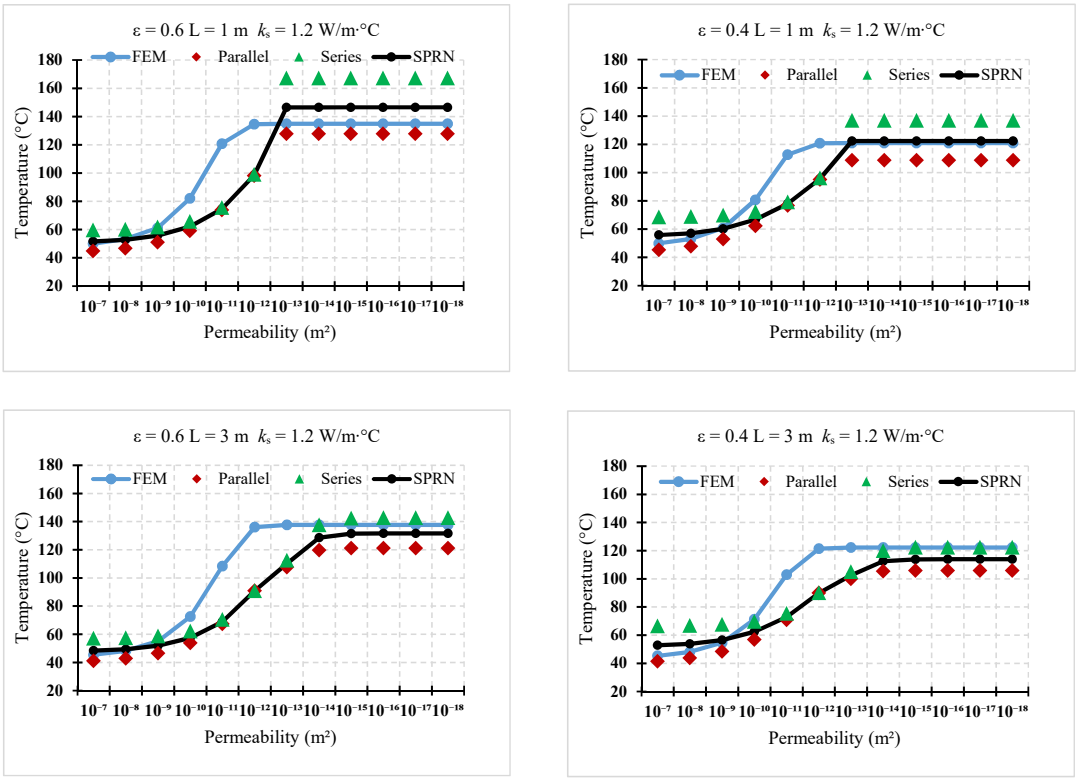

Figure 3.13: Comparison of cable conductor temperature estimated using SRN, PRN, SPRN with FEM results for varying depth of burial (L) and porosity (ϵ).

SPRN method are in close agreement with the FEM results. Similarly, Table 3.6 presents the results for varying solid phase thermal conductivity for two permeability values. The results confirm that the SPRN method is more suitable as the maximum deviation between the values estimated by FEM simulation and SPRN method is 8.6 %.

Table 3.5: Comparision of Conductor Temperatures Estimated using SRN, PRN and SPRN Methods for a Different Permeability and Porosity Values

L = 1 m, k_s = 1.2 W/m·°C		Cable Conductor Temperature (°C)				
Permeability	Porosity (ϵ)	SRN	PRN	SPRN	IEC	FEM
κ= 10^{-9} m^2	0.4	69.86	52.97	60.20	90.00	60.65
	0.6	61.76	50.95	55.68	90.00	56.97
κ= 10^{-12} m^2	0.4	137.00	108.74	122.32	90.00	120.88
	0.6	167.28	127.84	146.55	90.00	134.95

Table 3.6: Comparision of Conductor Temperatures Estimated using SRN, PRN and SPRN Methods for a Different Permeability and Solid Phase Thermal Conductivity Values

L = 1 m, ϵ = 0.4		Cable Conductor Temperature (°C)				
Permeability	k_s	SRN	PRN	SPRN	IEC	FEM
κ= 10^{-9} m^2	0.9	66.86	47.22	55.63	90.00	54.15
	1.8	74.31	61.71	67.18	90.00	70.58
κ= 10^{-12} m^2	0.9	118.79	104.52	111.51	90.00	113.54
	1.8	168.07	111.26	137.51	90.00	126.81

3.6 Thermal Network Configuration for Group of Cables Buried in Submarine Environment

The proposed model is expanded to a group of buried cables separated by a distance. Fig. 3.14 shows the three single-core cables in flat-formation separated by

an equal distance represented by 's'. The inner region is the area subjected to mutual heat transfer and the outer region is unaffected by the heat from adjacent cables.

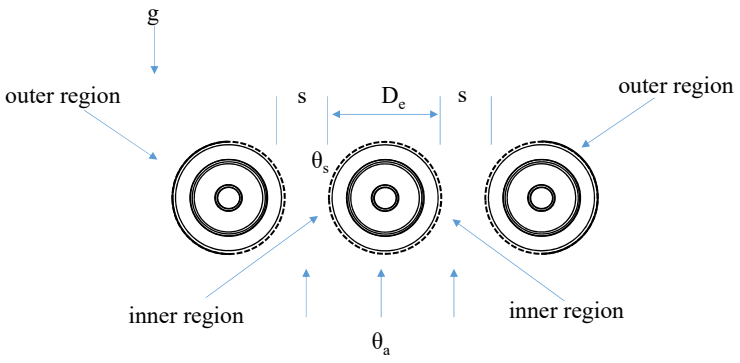

Figure 3.14: Three single cables arranged in flat-formation with equal distance of separation.

The heat balance equation for the three cables is derived from the correlation for convection around two parallel cylinders presented in [99] and is given by

$$q = \left(\frac{s}{D_e}\right)^3 \left(\frac{L_g}{12}\right) k_f(\theta_s - \theta_a) Ra + \left(\frac{Nu}{D_e}\right) k_f(\theta_s - \theta_a) \tag{3.14}$$

The heat flux q is a function of 's', the distance of separation between the cables. Nu is the Nusselt number, and k_f and k_s are the fluid phase and solid phase thermal conductivities. D_e is the diameter and Lg is the length of the cable; since all the calculations are carried for per meter. L_g is considered as 1 meter.

The sensitivity analysis was carried out for the cables in flat-formation to evaluate the validity of SPRN model. The conductor temperature for the centre cable was estimated for varying porosity, permeability, depth of burial and distance of separation. Fig. 3.15 and 3.16 show the results comparing the SPRN and FEM simulation. The proposed model is sensitive to the changes in all the parameters under study. The temperature estimated closely follows the FEM model for high permeable sediments with small deviations where the proposed model values are higher. However, the model predicted temperature values lower than the FEM

results in majority of the cases for low permeable sediments. The model over estimates the convective heat transfer co-efficient following equation (3.14) that results in lower temperature prediction. On the contrary, for deeper burial depths, the models predicts higher temperature than the FEM results. It is also worth to note that conductor temperatures predicted using IEC 60287 for all the above conditions were 90°C.

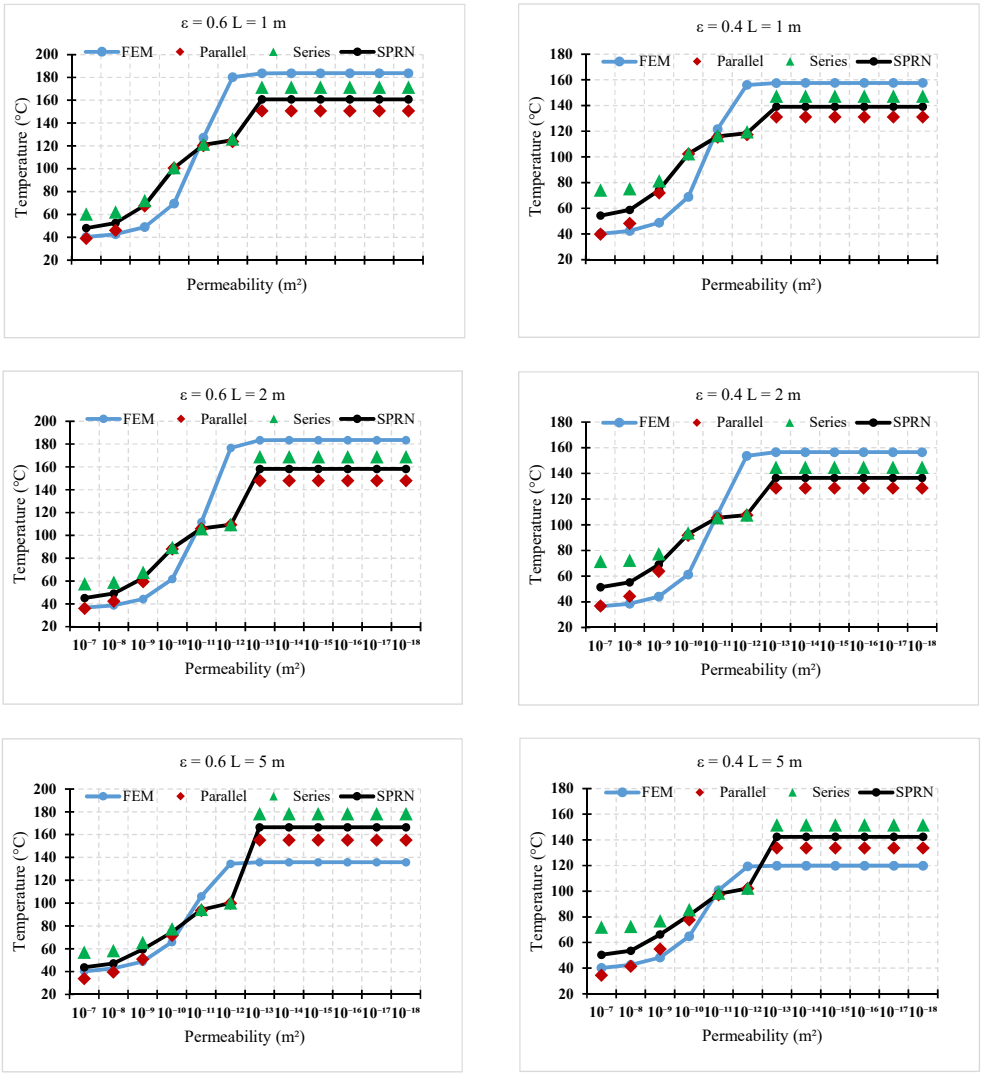

Figure 3.15: Comparison of conductor temperature for cables in flat-formation estimated using SRN, PRN, SPRN with FEM results for varying depth of burial (L) and porosity (ϵ).

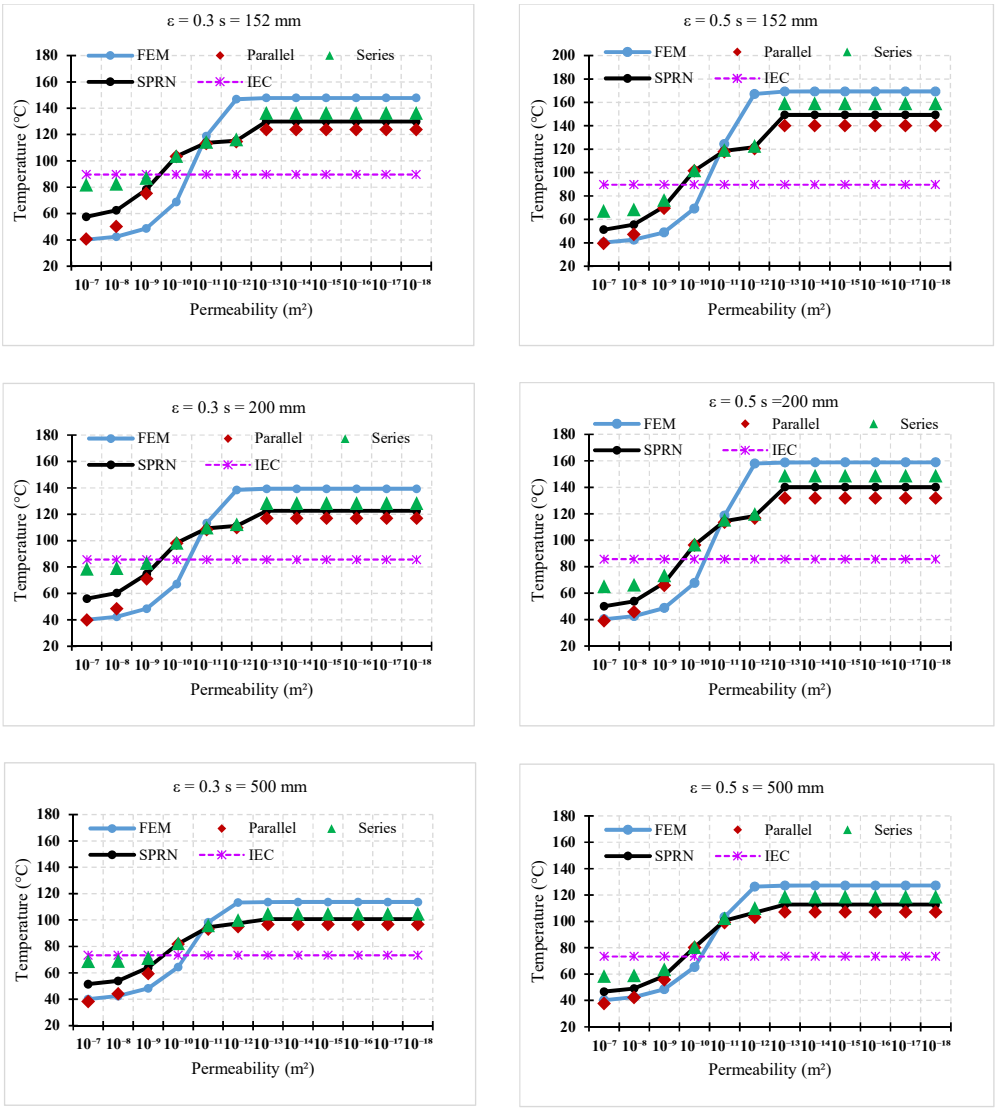

Figure 3.16: Comparison of conductor temperature for cables in flat-formation estimated using SRN, PRN, SPRN with FEM results for distance of separation (s) and porosity (ϵ).

3.7 Summary

The IEC 60287 thermal resistance network model for buried cables is constructed based on conductive heat transfer. This model however may not be completely applicable to the submarine power cables as the installed medium has very high water content that may alter the dynamics of the heat transfer mechanism. A modified thermal network model is proposed for calculating the external thermal resistance by considering the contributions of conductive and convective heat transfer. The factors that influence the combined heat transfer are analysed and their impact on the cable thermal performance is also studied. A finite element model was developed to study the heat transfer using numerical methods and to validate the proposed models.

1. Series (SRN), parallel (PRN) and series-parallel (SPRN) configurations of thermal resistance model were constructed and sensitivity analyses were carried by varying key parameters.

2. The results are in good agreement with the FEM simulations especially the SPRN model.

3. The proposed models are improvements to the IEC 60287 standard as neglects the convective heat transfer. Hence it is insensitive to changes in physical properties of the porous medium like porosity and permeability.

The proposed models will serve as a guidance to understand the parameters that affect the heat transfer in submarine power cables. They will serve to improve the thermal rating of cables installed in submarine environment.

Chapter 4

Ampacity Estimation for Submarine Power Cables Installed in Saturated Seabed - Experimental Studies

The maximum current carrying capacity (ampacity) of power cables depends on the heat transfer-ability of its surrounding medium. Submarine power cable ampacity is calculated conventionally following the international standards defined for underground cables. In reality, the thermal behavior of submarine environments differs significantly from its underground counterpart as the porous sediments are constantly water-saturated. In this paper, finite element method results were used to determine the factors affecting the ampacity in the submarine environment. A method to calculate the ampacity using external thermal resistance considering two series resistances - conductive resistance (of the solid phase sediment) and convective resistance (due to the natural convection in the pore fluid, water) is proposed. An experimental setup was developed to validate the FEM simulations and the numerical method. The results indicated that the inclusion of convective

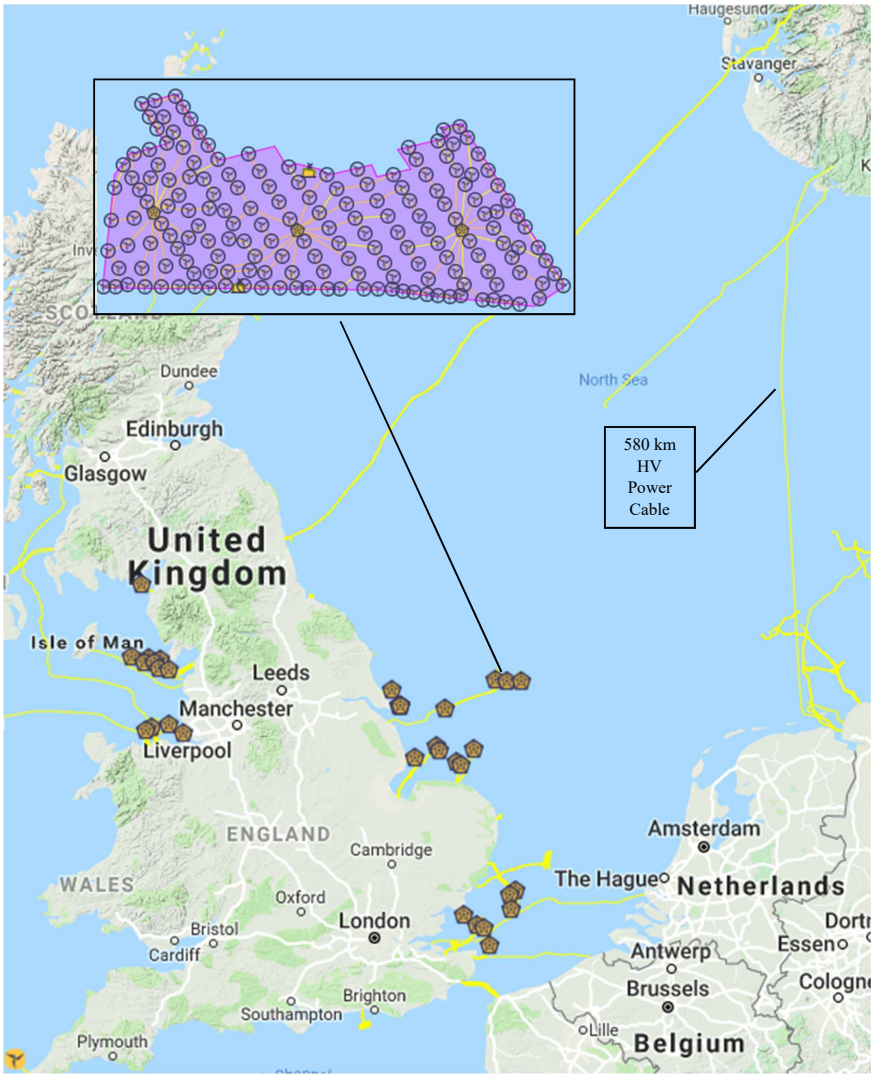

Figure 4.1: Map showing submarine power cable connections of UK and Europe. The inset shows the array of submarine power cable connections of a wind farm. ©KIS-ORCA - Seafish 2019.

heat transfer in the proposed method obtained a more precise ampacity estimate compared to that of the standard methods.

4.1 Introduction

Submarine power cables have been in use for more than a century. Since then, it has evolved significantly in terms of design and efficiency because of the rapid growth in power demand and exploration of off-shore renewable energy sources [100, 101]. The ampacity depends on the physical and thermal properties of the

cable components and also the surrounding medium. The maximum operating temperature of the conductor is a limiting factor. By considering the similarities, submarine power cables may compare well with the underground power cables as both are buried. However, the installation environment exhibits huge differences in thermal properties. The presence of water in the porous sea sediments makes it different from that of the land conditions as the sediments remain fully saturated because of the overlying water. The ampacity calculation is critical for optimal cable sizing particularly for applications like submarine power transmission where the installation and repair costs are extremely high.

Neher and McGrath [17] formulated the ampacity calculation for high voltage cables based on thermal circuits. The contribution by them is very remarkable as it forms the basis for internationally accepted standards like IEEE and IEC [52, 53, 56, 57] for ampacity estimation [59]. In the above approaches, the surrounding medium of the buried cable was considered to be homogeneous for calculating the thermal resistance of the environment. The differences in ampacity values determined using various commonly followed methods are presented in [58] and the authors emphasized the significance of *in-situ* measurements of soil thermal resistivity over the “typical" value approach. The authors of [102–104] presented underground cable ampacity models paying attention to the effects of soil moisture content and soil-drying on the ampacity rating. These works indicate that the soil moisture content and moisture migration have a significant effect on the actual current carrying capacity. Compared to the numerous investigations carried out for optimizing the underground power cable ampacity only very little work can be found on the submarine power cable ampacity. The power-transfer in offshore systems investigated in [105] and [106] followed worst-case thermal effects based on standard approaches that required cable current derating. The submarine power cable manufacturers also indicate that the current rating method is not different from that of the underground cables [107].

The dynamic nature of the submarine environment, deep ocean currents caused by thermohaline circulations, and sediment mobility pose a completely different environment than underground installations. Being porous in nature, submarine sediments exhibit higher thermal heterogeneity [108] due to water saturation. Accurate current ratings require *in-situ* knowledge of the installation conditions and their thermo-physical properties. The buried cable lengths will also act as a key factor in determining the ampacity. Fig. 4.1 shows the map of submarine power cables off the shores of the UK and Europe. The longest cable [109] spanning 580 kilometers connecting the power grids of Norway and Netherlands passes through different sediment types under the seafloor. In this condition, a safe operation must be ensured, and hence worst-case current rating can be used. On the other hand, the wind farms shown in the inset of Fig. 4.1 have comparatively shorter cable connections. These cables will be subjected to uneven loading due to the intermittent nature of wind power and hence optimal current rating will be economical.

The 2-D finite element method (FEM) studies carried out in [97] analyzed the influence of sediment properties on power cable thermal performance and highlighted the differences between the IEC standard model and the FEM results. The results indicated that high permeable sediments exhibit higher heat transfer by convection thus reducing the conductor temperature. The authors of [110] employed a 2-D experimentation to study the heat transfer in sediments using a heating coil. The experimentation results showed the influence of convective heat transfer on the thermal distribution in the coil and the surrounding environment.

The present study proposes an ampacity calculation model for cables in submarine environments considering the thermo-physical properties of the sea sediments. A temperature-dependent electrical resistance model of the conductor was combined with the heat and fluid flow equations to improve the accuracy of the FEM simulation results. Various cable configurations were used to study the impact of

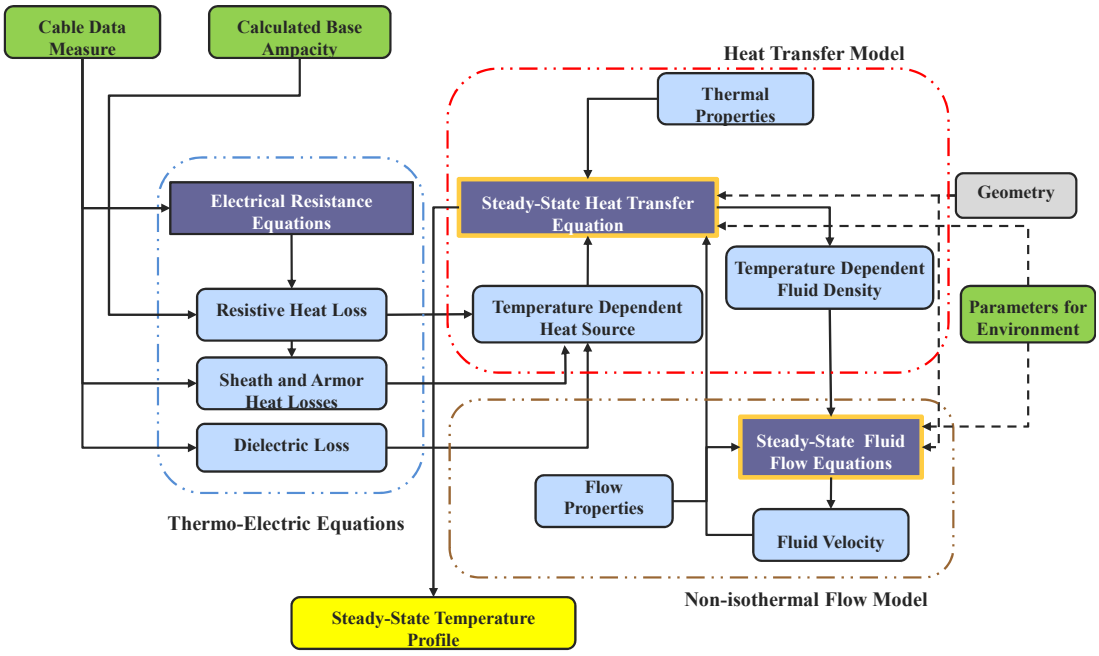

Figure 4.2: Overview of model inputs and outputs and combining the heat transfer by emulating thermo-electric effect and fluid flow interface.

sediment properties on the cable ampacity. An equivalent thermal conductivity method is used to calculate the ampacity and the results are in good agreement with the FEM simulations. A full lab-scale experimentation was conducted to show the validation of the proposed approach.

4.2 Description of the Model

The heat transfer process in the power cables and the surrounding medium was modeled using a finite element method. The conjugate heat transfer between the solid phase cable, water-saturated porous sediment and the overlying water was solved using the COMSOL multi-physics software.

4.2.1 Power Cable Heat Sources

The current flowing through the power cable conductors results in resistive losses that causes heat generation within the cable. Electrical resistances are temperature dependent and the relationship between the resistance and temperature is

given in (4.1) where R_0 is the AC resistance at 20 °C, α_{20} is the thermal coefficient and θ_c is the temperature of the copper conductor. Besides, the dielectric property of the insulation, metallic sheath and armor will also contribute to additional heat generation.

$$R = R_0[1 + \alpha_{20}(\theta_c - 20)] \tag{4.1}$$

Literature survey showed that in FEM models, heat flux boundaries with predetermined values were used to represent cable power losses. In this approach, the heat source was modeled as a function of the real-time temperature.

The thermo-electric effect and the heat balance in the FEM simulation were achieved using the three interdependent physical models shown in Fig. 4.2.

- The electrical equations were used to calculate the temperature dependent joule heating losses that cause the heat generation in the system.
- The corresponding temperature rise was calculated by solving the heat balance equations.
- The temperature rise affects the fluid flow in the porous domain and also in the overlying water which was resolved using the non-isothermal flow equations.

The resulting temperature was used to update the electrical resistance and the process was repeated until the steady-state was reached.

4.2.2 Equations Governing Heat Transfer and Fluid Flow

The heat transfer in porous media is defined by the mixture of energies in the solid and fluid heat transfer equations [87] given by

$$\rho C_p \vec{v} \cdot \nabla\theta + \nabla \cdot q = Q \tag{4.2}$$

where, θ is the temperature (°C). ρ and C_p are the density (kg/m^3) and heat capacity (J/kg/°C) of the fluid at constant pressure. $\vec{v}$ is the fluid velocity (m/s)

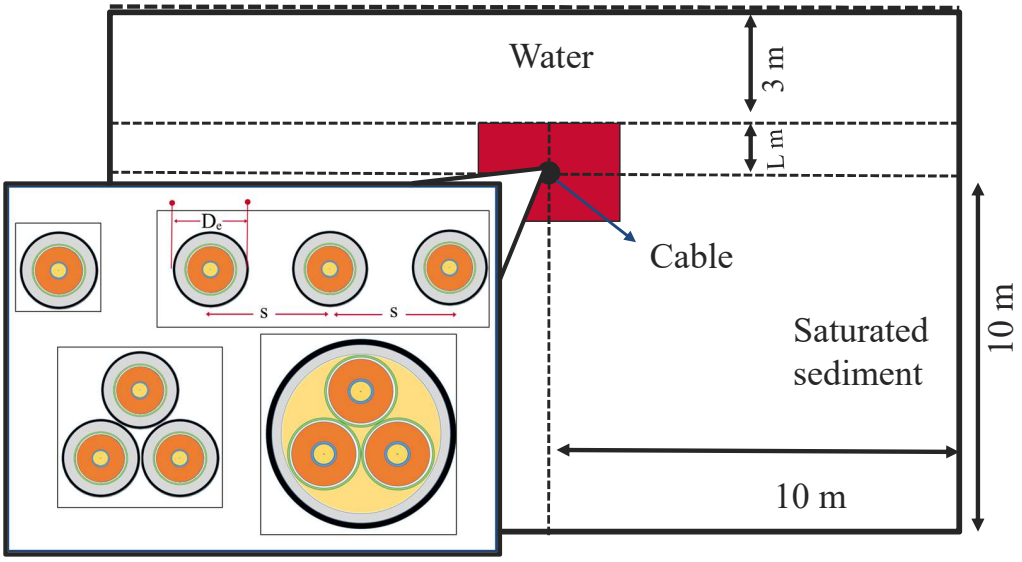

Figure 4.3: FEM geometry setup schematic and cable configurations used for the simulation studies.

which was computed by solving the fluid flow equations in the following section. The magnitude of the velocity determines the convective heat transfer coefficient. Q is the volumetric heat source (W/m^3). The conductive heat flux q (W/m^2) is described as

$$q = -k_{eff}\nabla\theta \tag{4.3}$$

where k_{eff} is the equivalent thermal conductivity ($W/m{\cdot}^\circ C$) of the porous medium which was estimated using the thermal conductivity of the solid and fluid parts of the domain. A simple volume average method is generally used to calculate k_{eff} and is given by

$$k_{eff} = \epsilon k_f + (1-\epsilon)k_s \tag{4.4}$$

where ϵ is the fraction of the volume of pores over the total volume of the porous domain (porosity). k_f ($W/m\cdot^\circ C$) and k_s ($W/m\cdot^\circ C$) are the respective thermal conductivity of the fluid and solid parts. The velocity resulting from the convective heat transfer in (4.2) is defined by the Darcy-Brinkman equation

$$\nabla p - \nabla \cdot \left[\frac{1}{\epsilon}\left\{\mu(\nabla\vec{v} + (\nabla v)^{\theta}) - \frac{2}{3}\mu(\nabla \cdot v)I\right\}\right] + (\mu\kappa^{-1} + \frac{Q_{br}}{\epsilon^2})\vec{v} = g\rho_0(1 - \beta(\theta - \theta_0)) \tag{4.5}$$

where p, μ and κ are the pressure (Pa), viscosity (Pa· s) and intrinsic permeability tensor (m^2) respectively. The intrinsic permeability is a characteristic parameter of the porous medium to allow fluid flow through the pores. The term on the right-hand side of the equation corresponds to the buoyancy forces influenced by gravity and temperature-driven density changes. g is the acceleration of gravity (m/s^2) and β ($1/°C$) is the coefficient of fluid thermal expansion. The density changes were considered only to calculate the buoyancy forces as stated in Boussinesq approximation [111]. The viscous part was included in the equation for the boundary conditions.

Q_{br} (kg/m^3· s) is the mass source component that accounts for the mass deposit or mass creation within the domains. For in-compressible flows, the density remains constant and hence Q_{br} reduces to

$$Q_{br} = \rho\nabla \cdot \vec{v}. \tag{4.6}$$

The model assumes a local thermal equilibrium between the fluid and the solid phases in the porous domain and hence a common temperature term θ was used. Phase transitions in the liquid phases were not included as the sediment was assumed to remain fully saturated irrespective of any temperature variations.

4.2.3 Study Cable Configurations

The simulation studies were carried out on MV submarine power cables. The cable construction described in [112] was implemented in the FEM model. The properties of the cable components are presented in Table 4.1. Commercial submarine power cable arrangement shown in [113], i.e. single-core single cable and three single-core cables in flat-formation and trefoil arrangement and as well as three-core cable were used for the steady-state analysis (see Fig. 4.3). The ge-

Table 4.1: Geometrical Properties of the Cable Components used in the FEM Model

Component	Material	Diameter (1 core / 3 core) (mm)
Conductor	Copper	12
Conductor screen	Cross-linked polyethylene (XLPE)	14.5
Insulation	XLPE	37.2
Insulation screen	XLPE	39.8
Concentric neutral wires / shield	Copper	41.2
Filler	Polypropylene	N/A
Armor	Steel	51.52 / 95.78
Outer serving	Compounded jute	60.5 / 98.8

ometry of the setup shown in Fig. 4.3 contains three parts - saturated submarine sediment, overlying water and study cable. A sensitivity analysis was performed for meshing and simulation geometry. The sides of the simulation setup were increased to an extent such that the surface area changes had no observable effect on the temperature of the region immediately surrounding the cable.

The factors affecting buried power cable ampacities were investigated in several research works conducted before. The key differentiation in submarine conditions is the presence of water inside and above the sediments. The porosity and permeability parameters determine the effect of water content on the heat transfer. So, this study focused on the effect of porosity and permeability values on ampacity. The submarine sediment properties presented in [114] were investigated to choose the value ranges for these parameters. Porosity values of range 0.3 - 0.6 and permeability range of 10^{-18} m^2 to 10^{-7} m^2 were used to analyze the cable conductor temperature. The parameters for ambient conditions and the heat generation in the cable components were calculated based on IEC 60287 to highlight the differences.

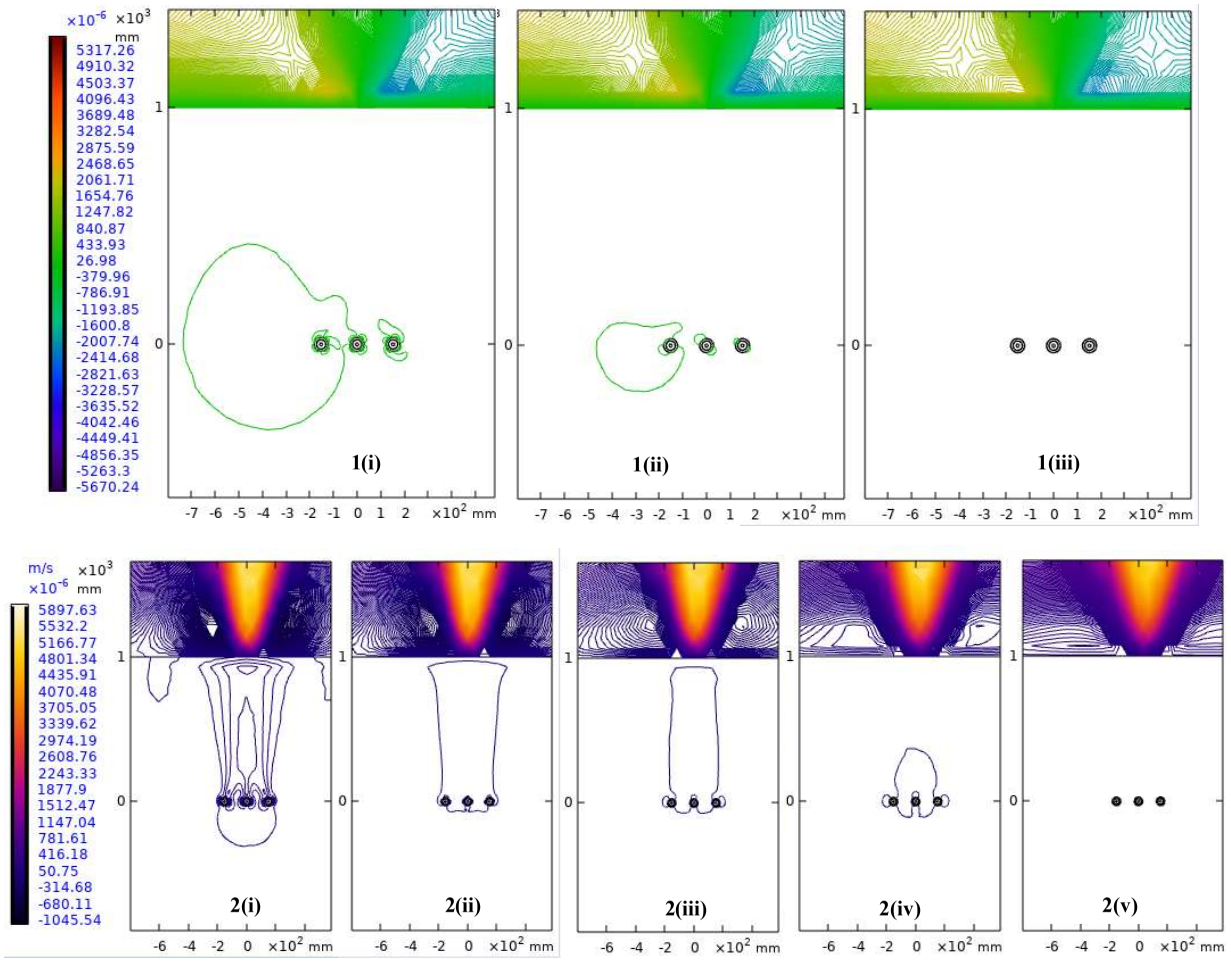

Figure 4.4: Horizontal and vertical velocity components of fluid motion in the sediments for permeability values 10^{-8} m^2 to 10^{-10} m^2 (1(i) - 1(iii)) and 10^{-8} m^2 to 10^{-12} m^2 (2(i) - 2(v)) respectively. The cable burial depth is 1 m and sediment porosity is 0.4.

4.2.4 Parameters for Ampacity Calculation

The ampacity calculation methods specified in IEC 60287 standard include factors that affect the current capacity of the buried cables. The ampacity depends on the ambient and cable conductor temperatures, loss factors for the sheath and armor, thermal resistances of the cable components and the surrounding medium. The thermal resistances of the cable components, sheath and eddy current loss factors can be predetermined based on the cable construction and bonding techniques. The thermal resistance of the surrounding medium is given by,

$$T_4 = \frac{r}{2\pi}\left(\ln(u+\sqrt{u^2+1}) + \sum_{\substack{k=1\\k\neq p}}^{q} \ln\left(\frac{d'_{pk}}{d_{pk}}\right)\right) \tag{4.7}$$

where r is the thermal resistivity of the surrounding medium (m·°C/W); $u(=2L/D_e)$ is the dimensionless geometry factor; L is the depth of burial (m) and D_e is the diameter of the cable (m). d_{pk} and d'_{pk} are the distances from the centre of the pth cable to the centre of cable k and to the centre of the reflection of cable k in the surface above the ground respectively. The summation term is not applicable for single cable configurations. The T_4 calculation in (4.7) was based only on conductive heat transfer but the first term in (4.2) indicates the presence of convective heat transfer in porous domains.

4.3 Steady-state Analysis for Implications on Ampacity

4.3.1 Qualitative Analysis

The heat transfer by convection is a function of fluid velocity in the porous domain. The buoyancy term in (4.5) describes the fluid motion which is a resultant of natural convection that can be observed in Fig. 4.4. The horizontal and ver-

tical velocity vectors are show in Fig. 4.4(1) and Fig. 4.4(2) respectively. The horizontal velocity component is denoted by (u^1) and vertical velocity is denoted by (v^1) represents the fluid motion around the energized cables in flat formation. The simulation area is enlarged to view the velocity vectors closer to the cables. The vertical velocity component was present for permeability values above 10^{-12} m^2. On the other hand, the horizontal velocity component was present only in permeability values above 10^{-9} m^2. The transition from convection to conduction-only heat transfer can be observed in κ values 10^{-11} m^2 and 10^{-12} m^2. Horizontal fluid motion is not present or negligible for these permeability values (see 1(iii) of Fig. 4.4). However, dominant vertical fluid motion observed in 10^{-10} m^2 and a very small magnitude of the vertical velocity in the case of 10^{-11} m^2 (see 2(iv) and 2(v) of Fig. 4.4) contributes to the convective heat transfer. This observation is in agreement with the minimum permeability value required for convective heat transfer show in equation (3.13). In practical cases, permeability values (10^{-11} m^2 and above) can also be used for uprating the cable ampacity in addition to the other physical properties of the sediments.

The permeability (κ), porosity (ϵ) and distance of separation between the cables were varied to determine the extent to which these parameters influence the heat transfer around the power cables. Numerous FEM simulations were carried out to study the convective heat transfer and to establish the relationship between the factors influencing the ampacity.

4.3.2 Varying Permeability and Porosity

Physical properties of the sediments that determine the fluid content and fluid mobility in the sediments i.e porosity and permeability were used in this section to study their impact on the power cable heat generation and dissipation. Simulations were carried out using parameter sweep function across permeability values of range $10^{-18}m^2$ to 10^{-7} m^2 and porosity values of range 0.3 to 0.6 in steps of 10^{-1}.

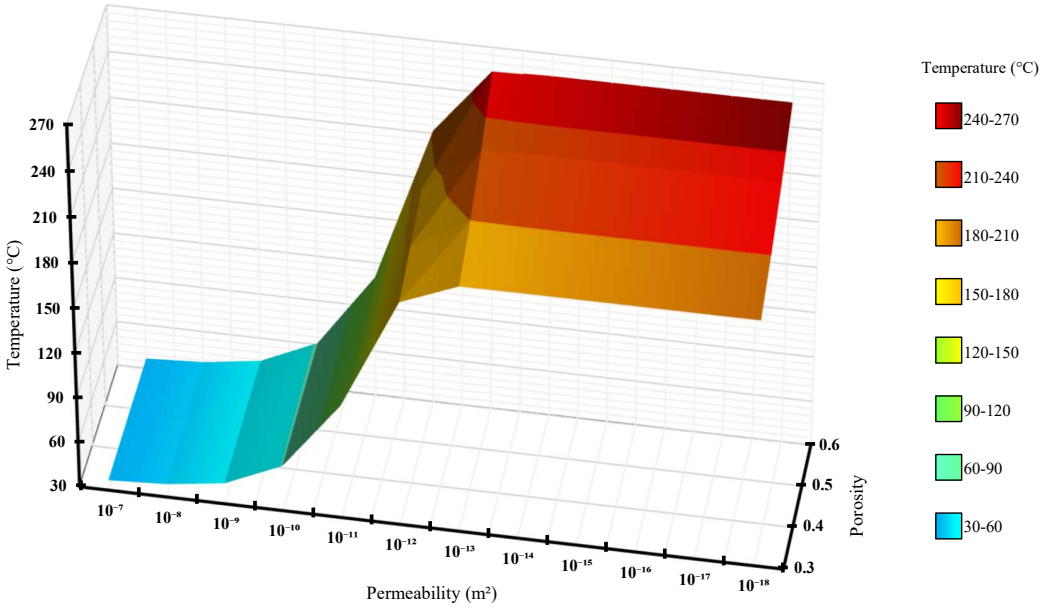

Figure 4.5: Dependence of cable conductor temperature on the sediment permeability and porosity. The solid phase thermal conductivity in this case is 1.2 (W/m·°C) and corresponding burial depth is 1 m.

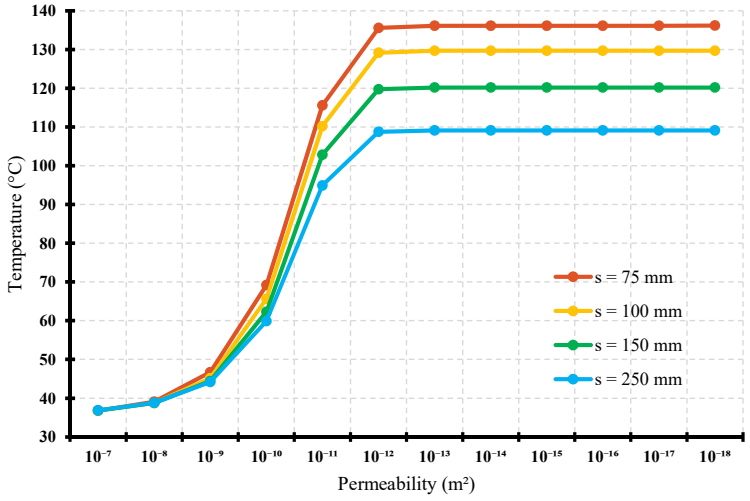

Figure 4.6: Dependence of cable conductor temperature on the sediment permeability and separation distance (s). The solid phase thermal conductivity in this case is 1.2 (W/m·°C) and the corresponding burial depth is 1 m.

The transition from convective to conductive heat transfer can be observed in Fig. 4.5. As the conductive heat transfer becomes predominant for permeability values below $10^{-11}\mathrm{m}^2$, the conductor temperature increased rapidly. This temperature rise can also be seen for increasing porosity values in low permeabilities. It should be noted that highly porous sediments like clay with medium or low permeability

will reduce the heat dissipation from the embedded cable compared to less porous and low permeable environments. Conversely, in high permeable sediments, the change in porosity had no significant effect on the conductor temperature.

4.3.3 Varying Permeability and Distance of Separation Between Group of Cables

In a group of buried cables, the distance between the adjacent cables affect the cable conductor temperatures due to mutual heat transfer. This is included in the IEC standard as shown in (4.7) to derate the cable ampacity by factoring-in the neighboring cables as heat sources.

Fig. 4.6 shows that as the permeability becomes more favorable to convective heat transfer, the distance of separation between the group cables had no significant effect on the cable conductor temperature. This is applicable especially for high and very high permeable sediments. The efficiency of heat transfer by convection in high permeable sediments is not affected by the neighbouring heat sources, as all of the heat is dissipated by convection. This indicates the significance of permeability values in calculating the optimal ampacity.

4.3.4 Implications on External Thermal Resistance T_4

The thermal and physical properties of some submarine sediments support convection where the heat can be dissipated to the environment more effectively. The convective heat transfer observed in favorable sediment properties was translated into analogous equivalent thermal conductivity based on the cable electro-thermal network. Highly permeable sediments exhibited very high equivalent thermal conductivity due to higher convective heat transfer coefficients.

Fig. 4.7(i) shows that the cable configuration and the depth of burial have significant effect on the convective heat transfer. The cable configurations considered were the single cable and cables in flat-formation. The equivalent thermal

conductivity was higher for deeper burial depths and for cables that generated higher amounts of heat. This implies that all of the heat generated was dissipated by convection where the natural convective flux was permeable to flow. On the contrary, when the heat transfer was predominantly by conduction, the effective thermal conductivity was fairly constant across all permeability values and depths of burial irrespective of the cable configurations. This can be observed in Fig. 4.7(ii).

Fig. 4.8 shows the effect of porosity on the sediment heat transfer for single cable, three-core cable and cables in flat and trefoil arrangement. In high permeable sediments, porosity changes did not vary the equivalent thermal conductivity as shown in Fig. 4.8(i). This was observed across all the cable configurations. Although the conductor sizes were the same for all the cable configurations, the heat generated in cables in flat-formation resulted in higher equivalent thermal conductivity compared to those of the other cable configurations because the IEC current derating was higher for trefoil and three-core cables. Porosity alters the effective thermal conductivity of the low permeable sediments. Increase in porosity resulted in reduced effective thermal conductivity (see Fig. 4.8(ii)). The above observations clearly indicate that the external thermal resistance model by IEC will not hold good for porous sediments where the thermal resistivity or conductivity has non-linear relationship with the heat generated.

4.3.5 Impact on Ampacity

A new model is proposed for ampacity calculation to include the heat transfer by conduction and convection. The thermal resistance of the surrounding medium was calculated by incorporating conduction and convection resistances in series arrangement following the weighted average method. This gives the upper bound values for T_4. The resulting T_4 was used to calculate the ampacity value that corresponded to the maximum allowable conductor temperature. For very high

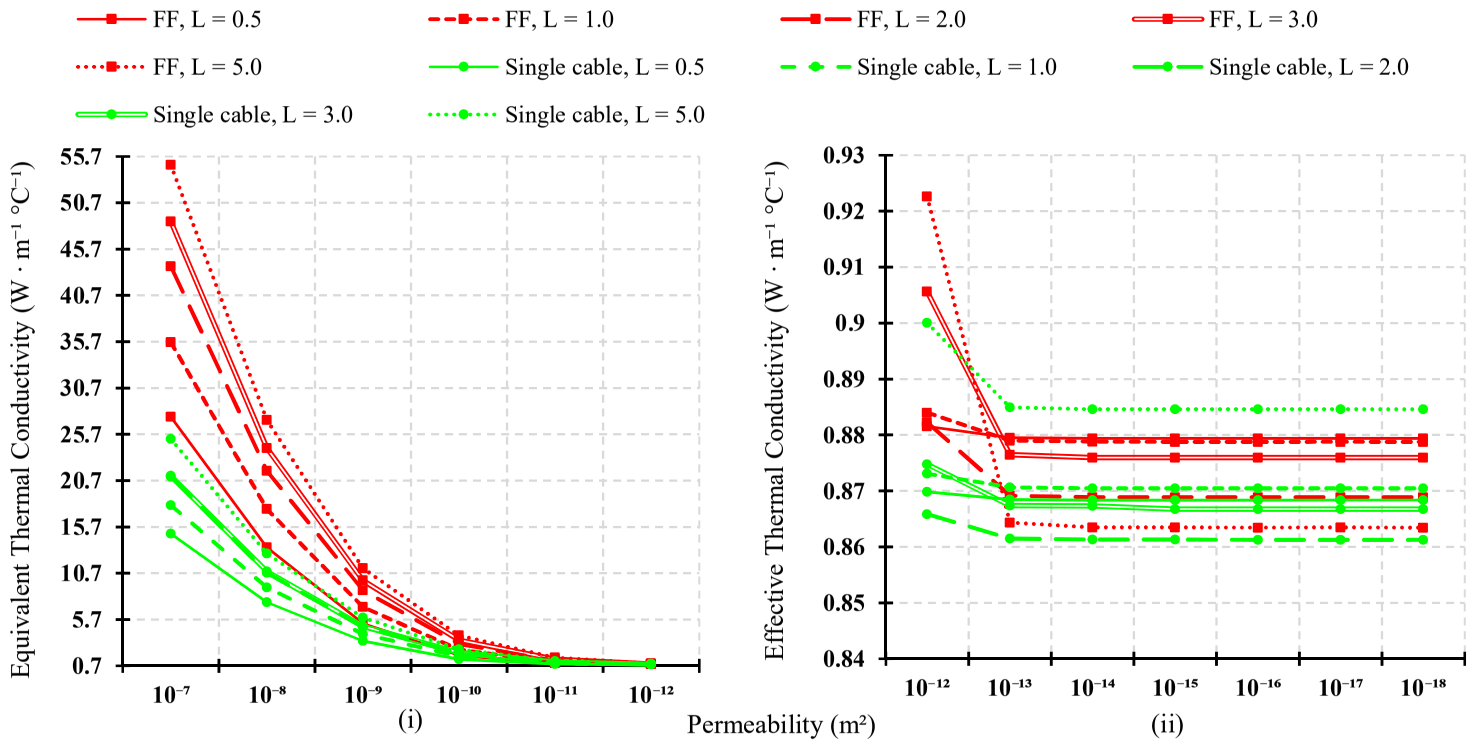

Figure 4.7: Analogous thermal conductivity values calculated based on cable thermal network for varying permeability and depth of burial (L). The solid phase thermal conductivity in this case is 1.2 ($W/m \cdot^\circ C$) and corresponding porosity is 0.4.

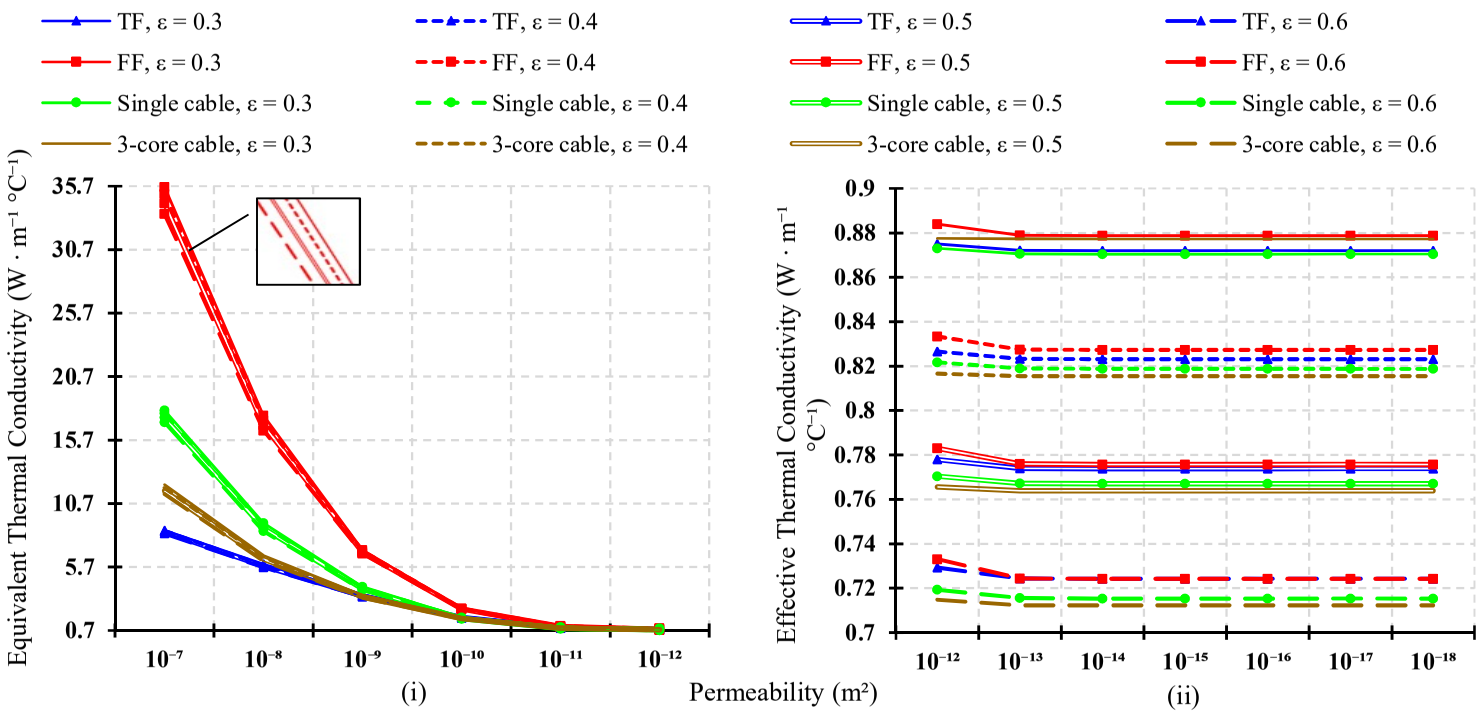

Figure 4.8: Analogous thermal conductivity values calculated based on cable thermal network for varying porosity and permeability. The solid phase thermal conductivity in this case is 1.2 $(W/m \cdot^{\circ} C)$ and corresponding burial depth is 1 m.

Table 4.2: Calculated Ampacity using Proposed Model for Different Depths of Burial and Porosity Values Compared to the IEC Standard for Two Permeability Values (High and Low)

Depth of burial L (m)	Ampacity IEC (A)	Porosity	Ampacity using proposed model (A) $\kappa = 10^{-9}$ m^2	$\kappa = 10^{-14}$ m^2
0.5	438.37	0.4	495.97	349.69
		0.6	532.01	321.16
1	414.35	0.4	476.29	342.47
		0.6	515.89	317.37
2	393.82	0.4	458.75	336.13
		0.6	501.07	314.35
5	380.77	0.4	438.25	334.11
		0.6	483.22	311.71

permeable sediments, though the heat transfer is purely by convection, the upper bound T_4 values were used to determine the worst-case ampacity values. The resistance to the natural convection can be computed as

$$T_{conv} = \frac{1}{hA} \tag{4.8}$$

where h is the convective heat transfer coefficient and A is the total area exposed. h is calculated using the Nusselt number (Nu) and Rayleigh-Darcy number (Ra) [93] given by

$$Ra = \frac{\kappa\rho\beta g(\theta_s - \theta_{amb})D_e^3}{\alpha\mu} \tag{4.9}$$

where θ_s and θ_{amb} are the surface temperature of the cable and the ambient temperature. α is thermal diffusivity of the porous medium. Higher values of Ra indicate heat transfer by convection. The Nusselt number was calculated using Ra as proposed in [93] and [115] and is given by

$$\text{Nu} = 0.3995Ra^{1/2} + 0.78 - 1.9Ra^{-1/2}. \tag{4.10}$$

For critically lower Ra values, the authors of [116] depicted the variation of Nusselt number as a function of Ra for varying burial depths. When the distance between the centre of the cable and the boundaries (side and bottom boundaries) is higher than twice the burial depth, the correlation for the Nusselt number is given by

$$\text{Nu} = (1 + \text{Nu}_\infty^4)^{1/4} \tag{4.11}$$

where

$$\mathrm{Nu}_{\infty} = [1.52 - 1.41\ e^{-0.43(L-1)}]Ra^{1/3}. \tag{4.12}$$

Table 4.2 shows that the external thermal resistance calculated using the proposed method can result in higher ampacity compared to the IEC standards for cables buried in sediments that favor convective heat transfer. For low permeable sediments, the model also takes care of appropriate derating of the ampacity values that will be well within the maximum allowable conductor temperature i.e. 90°C. The ampacity values calculated using the proposed method resulted in ampacity uprating by 13% to 26% for high permeable sediments and derating by -23% to as high as -40% for low permeable sediments compared to the IEC 60287 standard.

4.4 Experimentation

The FEM simulation results and study presented in [112] indicated that the sediment physical properties that influence the heat transfer are porosity and intrinsic permeability. The physical properties of extra-fine sand and silt excavated from the sedimentary areas in the west region of Singapore were examined. Sand was selected for the experiments as the permeability value was higher compared to that of silt and the permeable nature of the sand was suitable to observe heat transfer by conduction and convection around the cable.

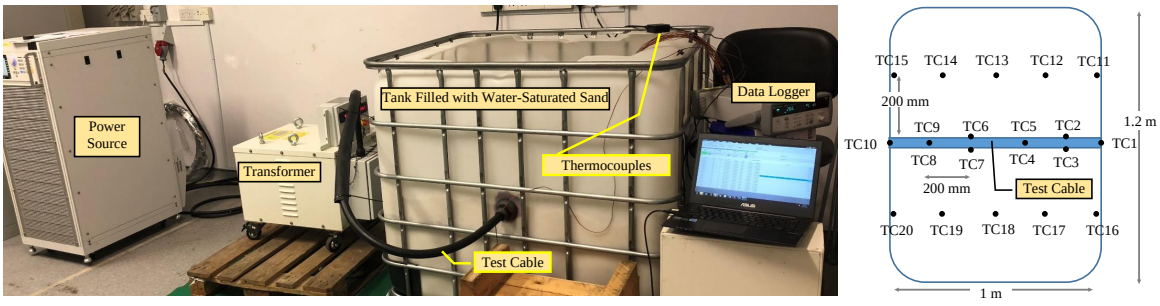

Figure 4.9: Experimentation setup showing cable installed in a tank and illustration showing thermo-couples placement on the surface of the cable and on the soil indicated as TC.

The physical properties of sand measured in the lab tests are given in Table 4.3.

Table 4.3: Physical Properties of Fine Sand used for Experimentation

Physical Property	**Value**
Density (kg/m^3)	1560
Porosity	0.47
Hydraulic Conductivity (m/s)	3.14 x 10^{-4}

Table 4.4: Components and Respective Physical Properties of Test Cable

Component	**Material**	**Size**
Conductor	Copper	185 mm^2
Insulation	Cross-linked Polyethylene (XLPE)	1.6 mm
Sheath	Poly-Vinyl Chloride (PVC)	1.8 mm
Armor	Aluminum Wire Armor (AWC)	1.8 mm
Outer Serving	Poly-Vinyl Chloride (PVC)	2 mm

The hydraulic conductivity (K) is the material property of porous medium and its relationship with the intrinsic permeability (κ), is given by

$$\kappa = (\frac{\rho\mu}{g})K \tag{4.13}$$

A 0.6-kV single-core power cable was used for the experiment. The physical properties of the cable components are given in Table 4.4. The cable was installed in water-saturated sand inside a PVC tank (1.2 m x 1 m x 1.2 m). The test was carried out by short-circuiting the secondary windings of a 12-kVA transformer using the test cable as shown in Fig. 4.9. Accurate measurements of the tank, quantity of sand, water levels, cable insertion height from the ground were made to recreate the geometry in the 3-D FEM model. Ten thermo-couples (TCs) (K-type) were placed on the cable surface along its length at equal distances and ten TCs were embedded in the sand as seen in Fig. 4.9. A current-controlled power source was used to supply the cable current through the transformer.

The cable was subject to a continuous current of 400 A at a constant ambient temperature of 19.5°C. The test was stopped at 100 hours (4.2 days) as the rate of change of measured temperature was around 0.5°C for the last 50 hours. Two sets of experiments were carried out to reproduce the results.

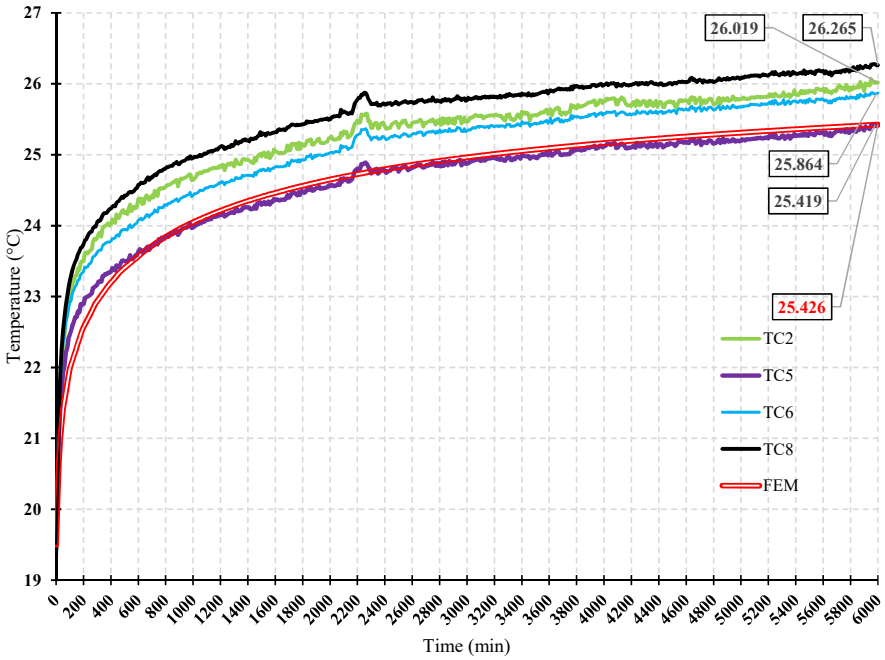

Figure 4.10: Transient simulation results of temperature profile comparing FEM and temperatures measured at positions on the cable surface using the thermo-couples represented as TCs.

4.5 Results and Analysis

A 3-D transient simulation study was carried out on a 32-core processor with a speed of @2.4 GHz and 128 GB RAM. It took 38 hours and 47 minutes to complete the actual 100 hours of experiment using short interval time steps. A dense mesh was created for the entire 3-D model with average element quality of 0.8534 to resolve the complex and sensitive heat transfer and fluid motion in the porous matrix. The results presented in Fig. 4.10 compared the cable surface temperatures of the experiment and the simulated values. The thermo-couples TC2 to TC9 were placed on the cable at positions with 200 mm intervals. At each position, two thermo-couples were placed on the cable surface diagonally opposite to each other. Thus the TCs were able to measure the surface temperature on the top, bottom and sides of the cable along the length. The simulation model was able to calculate the surface temperatures that matched with the measured data with a deviation of 1.7% - 2.3%. A higher temperature deviation was observed for TC2 and TC8 due to their close proximity to the tank walls.

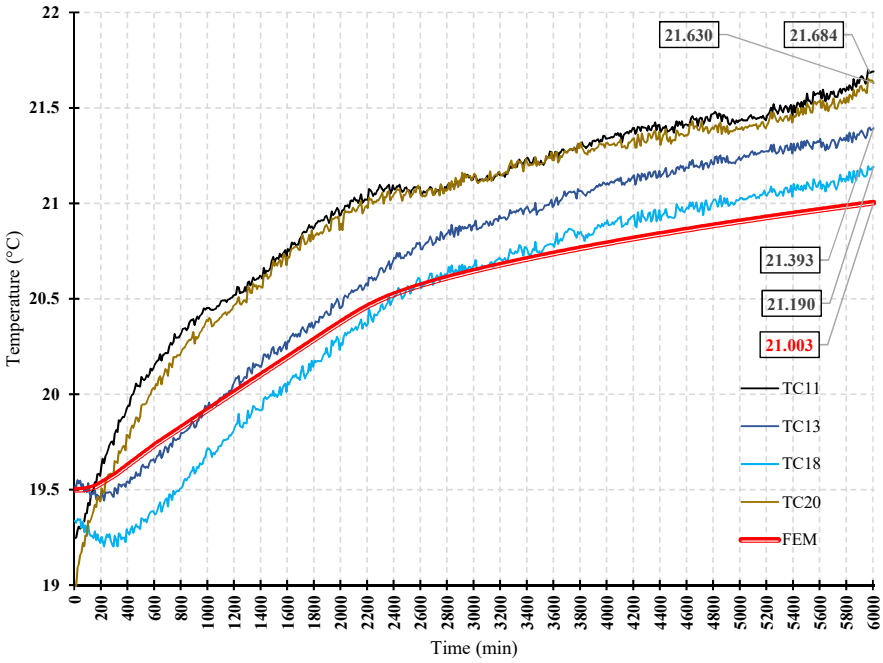

Figure 4.11: Transient simulation results of temperature profile comparing FEM and temperatures measured at positions on the sand that are 200 mm away from the cable axis.

The temperature measured at positions on the sand inside the tank that are 200 mm away from the cable axis is compared with the simulation results in Fig. 4.11. The TCs TC11 to TC20, were placed on the sand. The results show that the deviation between the measured and simulated temperature is less than 3.3%.

The FEM simulation results show the suitability of equations described as the governing laws for the heat transfer and fluid flow in the porous domains. The time constants for the temperature-time curves of the FEM results follow the experimentation curves indicates that the boundary conditions and thermal properties used in the simulations were able to represent the actual ambient conditions of the test.

Thermo-couples were not installed inside the cable conductor to avoid water ingress in the test cable. The conductor temperature was calculated from the measured surface temperature of the cable using well established thermal network models [117]. Fig. 4.12 shows that the FEM simulation and conductor temperature calculated using the proposed model closely matches the estimated cable

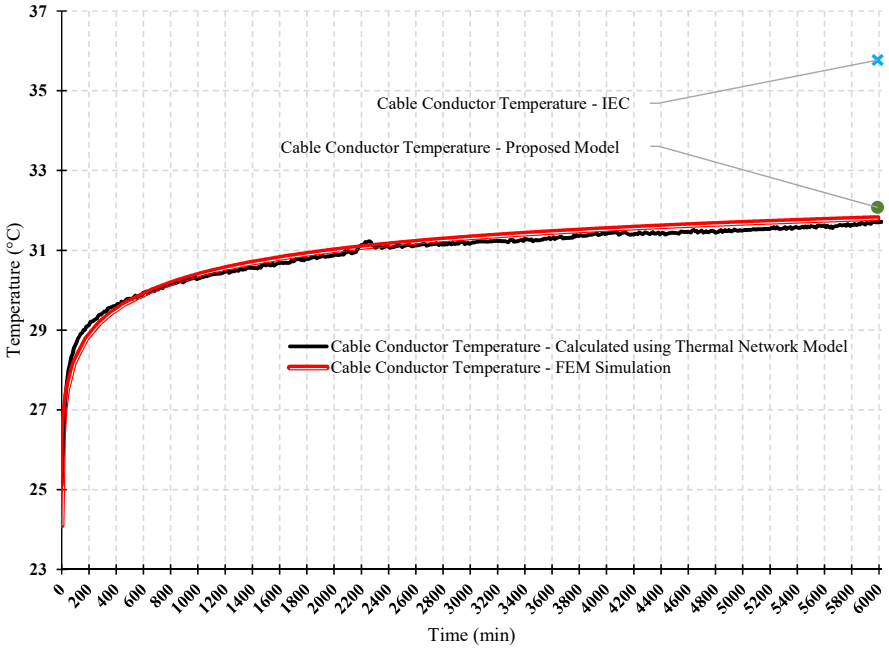

Figure 4.12: Comparison of conductor temperature results from experiment (derived from surface temperature using thermal network model), FEM simulation, proposed model and IEC.

conductor temperature from the experiment. The IEC standard calculation overestimates the conductor temperature for the test setup by 12.8%. For the test cable installed in an environment with the same physical properties and burial depth of 1 meter, ampacity estimated by IEC will be 20% lower than that of the proposed model. The details of the experimentatal setup and more results are presented in Appendix A.

4.6 Summary

The ampacity calculations for submarine power cables using thermal resistance based on conductive and convective heat transfer are presented in this chapter. Various cable configurations were used in the simulation studies to show the suitability of the proposed approach. The experimentation and equivalent finite element model were used to show the validation of the approach. The sediment properties that are usually neglected by international standards were analyzed in the study to show the significant improvement in the ampacity values by incorpo-

rating those parameters.

- Porosity and highly mobile moisture content of the submarine sediments are efficient heat carriers. This contributes to a higher heat dissipation and a higher ampacity.
- Most cable current rating standards including IEC, consider heat transfer by conduction in general. However, this results in incorrect ampacity estimation when significant contribution by convective heat transfer is neglected.
- Using effective thermal conductivity values for low permeable sediments will improve the current rating and avoid the overestimation or underestimation of ampacity values.

In submarine conditions, environmental factors play a major role in determining the cable ampacity. Through *in-situ* measurements, simulation models can be refined for optimal and accurate ampacity rating and for hot-spots detection in condition monitoring applications.

Chapter 5

Effect of Submarine Environment Changes on the Power Cable Thermal Performance

5.1 Introduction

The simulations presented in the previous chapter describe the dissipation of heat from a submarine power cable buried in a sediment that is completely spatially homogeneous in terms of its physical properties and the overlaying water is stationary. Of particular interest was the conclusion that under certain circumstances (particularly when the sediment has a high permeability), convection can play much more of a role in the dissipation of heat than has been traditionally recognised for underground buried cables. While the results of the FEM simulations in Chapter 4 provide a valuable insight into how heat is dissipated from submarine power cables in relatively simple burial scenarios, the applicability of the model to actual cables may be compromised by the assumed environmental conditions.

The marine environments are significantly more dynamic than typical terrestrial environments. For example, migrating bedforms (which can move across the bed

at 10s of metres per year) result in relative increases and decreases in local bed level heights by several metres in the same time period [118]. Hence any rapid burial or excavation of sediment above a submarine power cable will significantly alter the temperature of the cable for a given constant current flow.

The deep seafloor is constantly subjected to changes due water-dominant flows occurring in the deep oceans. The occurrence of turbulent flows termed as "turbidity currents" transports suspended particles and are driven by sediment gravity flow. These are continuous movement of fluid body in a given direction at uniform velocity [119]. The seafloor is also subjected to bottom currents that are also responsible for sediment deposition on the seabed for a sustained period of time. These are thermohaline-induced currents. The range of bottom current velocity measured in different parts of the world's ocean is 0.1 m/s to 2.0 m/s; however exceptionally strong currents with a maximum velocity off 3.0 m/s were also measured in the strait of Gibralet [120].

Whether or not the deep-sea bottom currents affect the thermal behavior of the cables is hard to predict without supplementary investigation. Two potential flow patterns were identified by considering how the flow direction will be aligned with the cable axis and simulation studies were performed to analyse the effect on cable thermal behavior embedded in the sediment.

5.2 Flow Model

The flow above the seafloor decreases the shear resistance of the sediment by increasing the pore pressure. This alters the fluid flow inside the porous sediments [119]. Fig. 5.1 depicts the configuration of the two flow conditions (cross-flow and parallel flow). The FEM model for this scenario was constructed from the one used in Chapter 4 by altering the boundary condition for the water section above the sediment. The flow was defined using the Navier-Stokes equation represented in

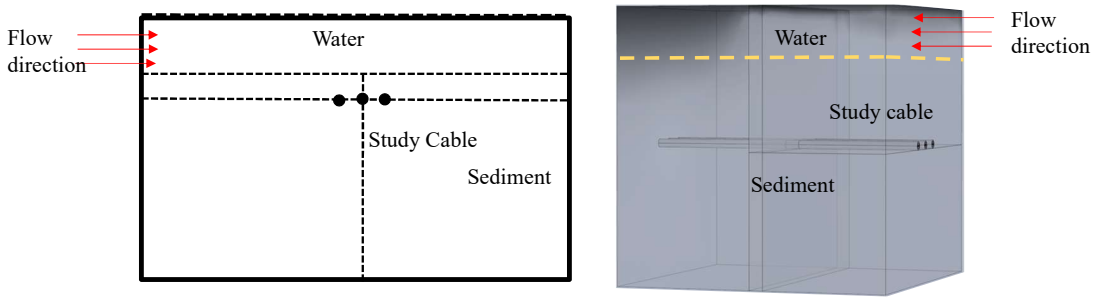

Figure 5.1: Illustration of study configurations for the fluid flow above the seafloor. (i) Cross-flow - perpendicular to the cable axis. (ii) Parallel-flow - flow along the cable axis

PDEs in the numerical model. The boundary at which the fluid enters was defined as a velocity boundary and the boundary at which the fluid exits was defined as a normal pressure boundary. The flow was modelled as fully developed and the flow direction is normal (perpendicular) to the inlet boundary. Representative values of range 0.1 m/s to 2.5 m/s was used for the magnitude of the flow velocity. The power cables in flat-formation was used for the studies to understand whether the mutual heating effects of the adjacent heat sources are altered by the fluid velocity.

5.2.1 Reynolds Number

The Reynolds number define the categories of fluid systems in which the flow velocity and pattern are controlled by the effect of fluid viscosity. The dimensionless Reynolds number determines whether the fluid flow is laminar (steady) or turbulent. It is the ratio between the inertial forces and viscous force and is given by

$$Re = \frac{\rho v L_g}{\mu} \tag{5.1}$$

where ρ is the fluid density, v is the velocity, L_g is the characteristic dimension of the flow regime and μ is the fluid dynamic viscosity. Re values less than 2000 indicates laminar flow, flows with Re values between 2000 and 4000 belong to critical or transitional flow and Re values higher than 4000 indicate turbulent flow [121].

5.3 Cross-flow Condition

The effect of the fluid flow velocity on the cable thermal behavior and its association with other physical properties of the sediment are analysed in this section. As sediment intrinsic permeability determines the convective heat transfer and variations in depth of burial alters the conductive heat transfer, these parameters were chosen for the studies along with the flow velocity of the overlying water. The solid phase thermal conductivity was assumed to be 1.2 W/m·°C and porosity to be 0.4. Several 2-D FEM simulations were carried out and the results are presented in Fig. 5.2.

The maximum conductor temperatures in steady-state conditions predicted by the FEM model for varying sediment permeability, radial flow velocity and depth of burial are shown in 5.2. It is observed that the cables installed in permeable sediments are affected by the fluid flow velocity. High permeable sediments shows localized heating effect due to the thermal perturbations in the mobile pore fluid. The temperature of the cable conductors installed in sediments with transition permeability values ($\kappa = 10^{-11}\text{m}^2$ and 10^{-12}m^2) was not affected by lower velocities but higher flow velocities resulted in lower temperature. When the depth of burial is increased, the above phenomenon was more pronounced indicating that the water flow velocity has significant impact on the heat transfer in porous medium. On the other hand, when the sediment permeability is low (in case of $\kappa = 10^{-14}\text{m}^2$), the cable thermal behavior is unaltered by the cross-flow velocity.

An applicable interpretation of the above results can be obtained by comparing the effects when the cable ratings are adjusted to the maximum allowable conductor temperature (i.e. 90°C). The steady-state rating of the cables proposed in Chapter 3 was used.

Fig. 5.3 shows the cable conductor temperature predicted by FEM for 2 different permeability values ($\kappa = 10^{-9}\text{m}^2$ and 10^{-14}m^2) installed at a depth of 1 meter.

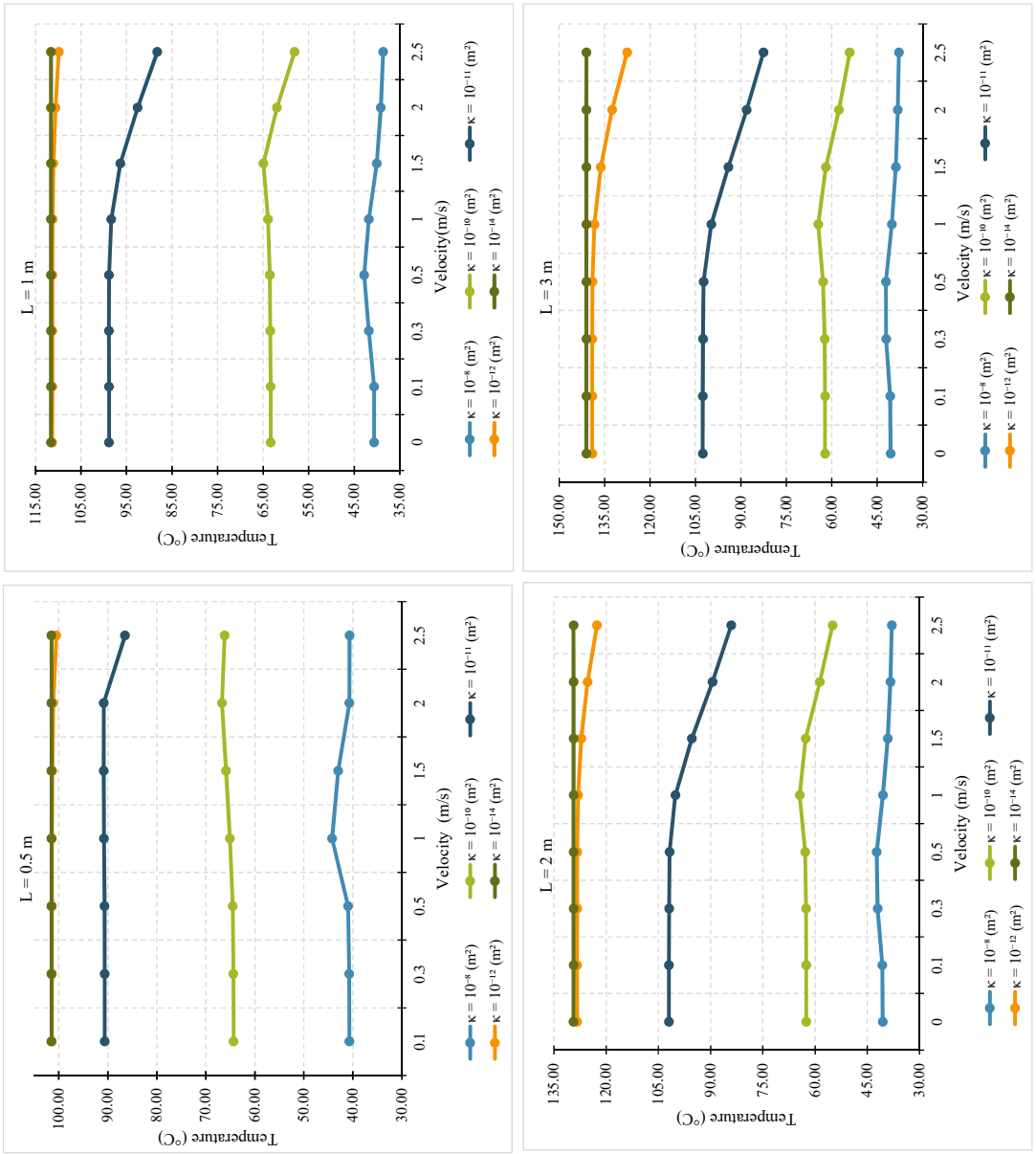

Figure 5.2: Effect of water velocity on the buried cables in cross-flow condition

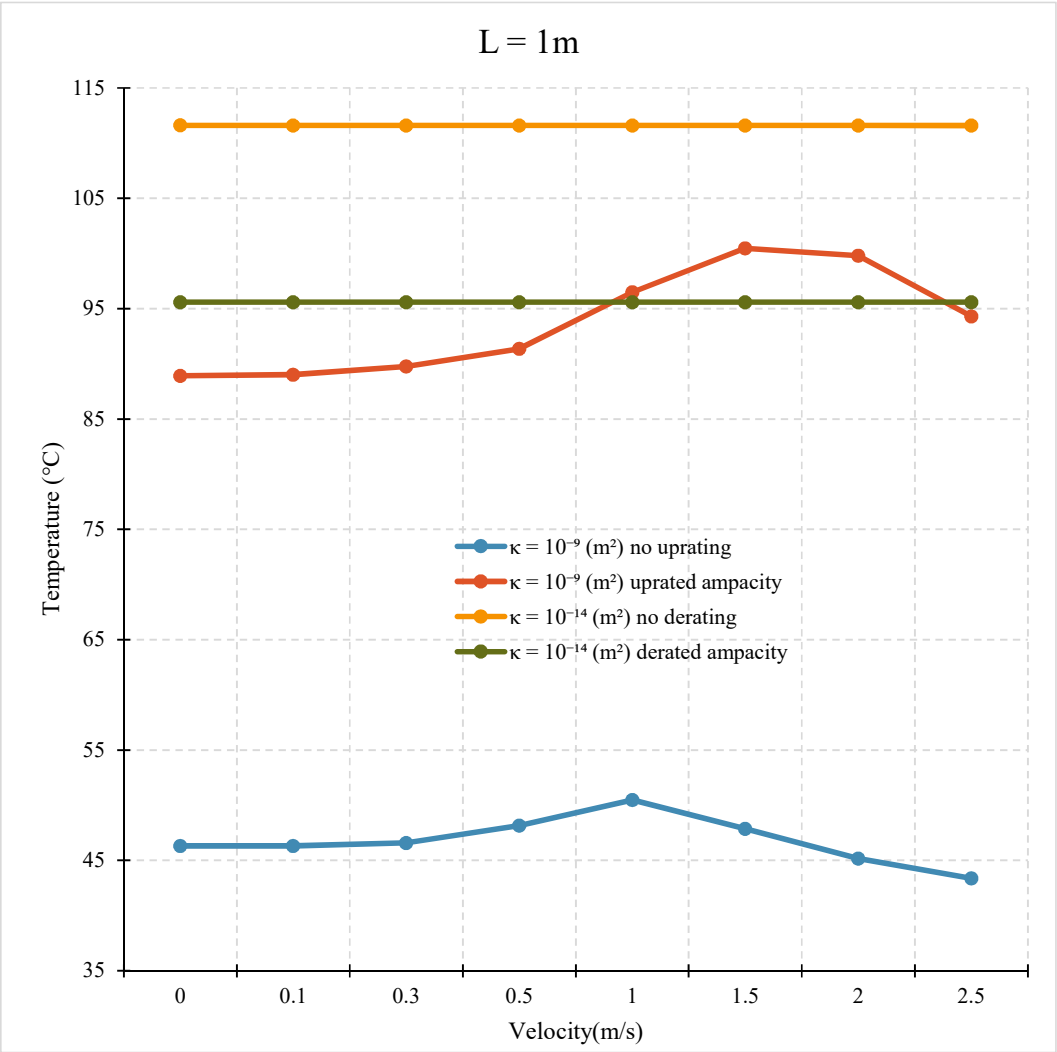

Figure 5.3: Cross-flow effect on cable conductor temperature for uprated/derated current capacity

These values were chosen to differentiate the effect of velocity on the heat transfer by convection and conduction in the porous medium. The temperature of the cable conductors are expected to be at 90°C under no flow condition. However, the flow resulted in higher temperature for cables installed in permeable sediment that favors heat transfer by convection. The increase in temperature can be attributed to the heat flux accumulation resulting from the thermal disturbance of pore fluid caused by the water flow.

5.4 Parallel-flow Condition

The simulation for this section was carried out using 3-D FEM models constructed by extruding the 2-D models. 3-D simulations were performed in order to study the effect of flow velocity on the cable temperature. In reality, the fluid flow can happen over sustainable lengths of the cables. Due to computational cost, the simulation was carried out for cables of lengths of 5 metres, 10 metres and 15 meters. The comparison of results for varying the length of flow are presented in Fig. 5.4, 5.5 and 5.6. The parameter settings for the studies are as follows. Depth of burial = 1 m, porosity = 0.4, and solid phase thermal conductivity = 1.2 W/m·°C.

The cable temperature profile for the high and low permeability sediments is not affected by changing the length of flow (except for small variations in the low permeability sediment for flow length of 5 metres). A common pattern can be observed in the temperature transitions. The cable conductor temperature was lower at the fluid entry point and higher at the exit point for low permeable sediment. This can be correlated to the forced convection by parallel flow over a flat plate. The colder fluid at the entry point will carry away more heat and hence the cable temperature at the entry point is lesser. This temperature decreases with the increase in velocity as velocity increases the heat transfer coefficient of fluids. Conversely, at the exit point the moving fluid after accumulating heat along

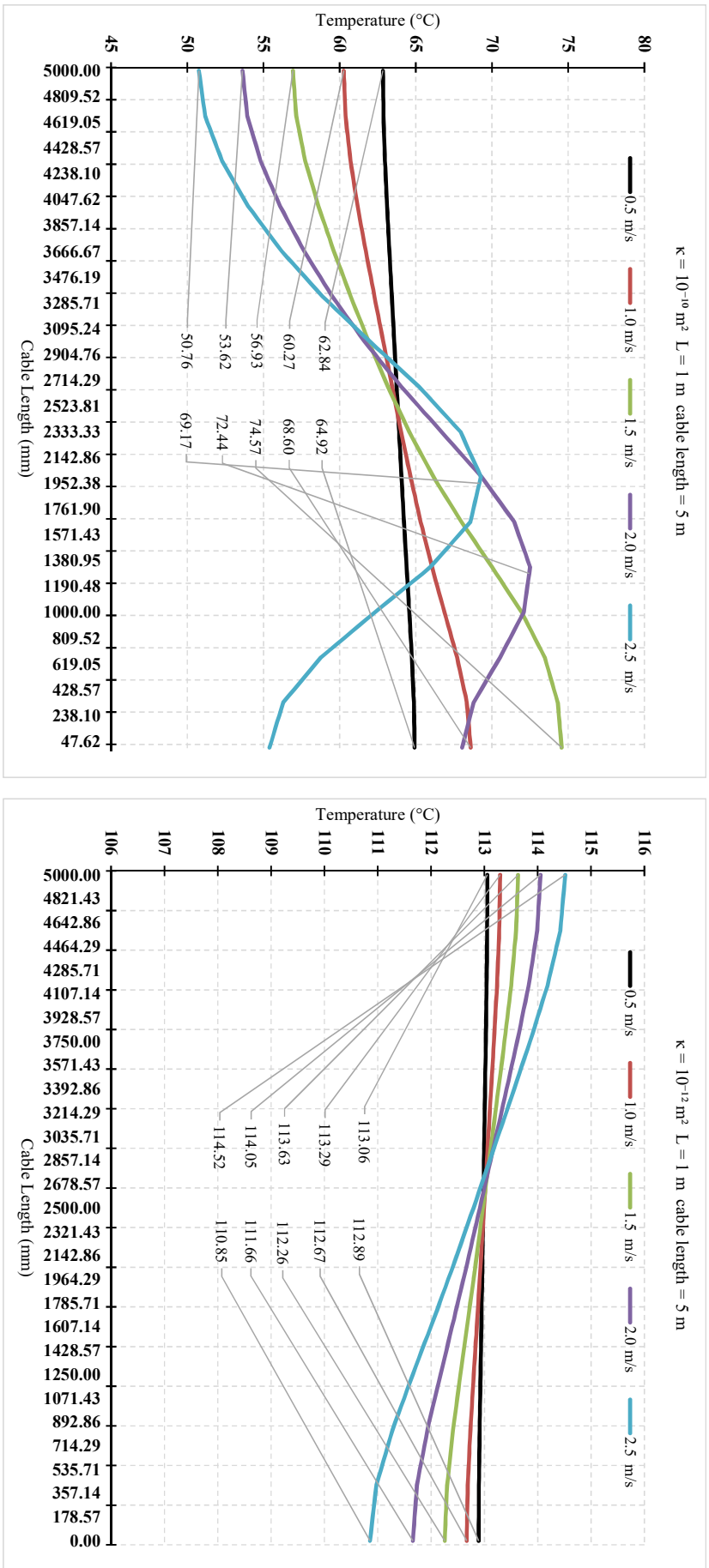

Figure 5.4: Cable conductor temperature for flow velocity along the cable of length 5 meters

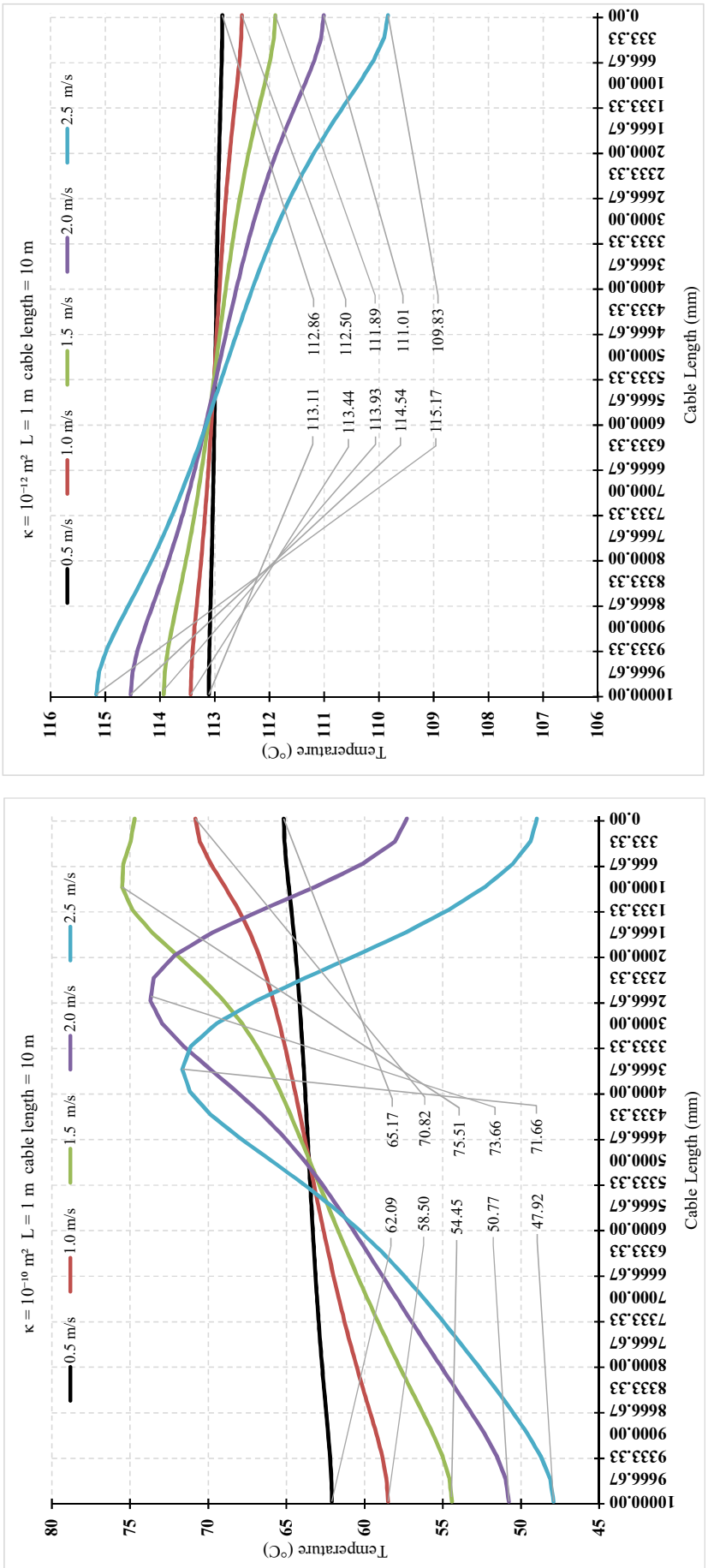

Figure 5.5: Cable conductor temperature for flow velocity along the cable of length 10 meters

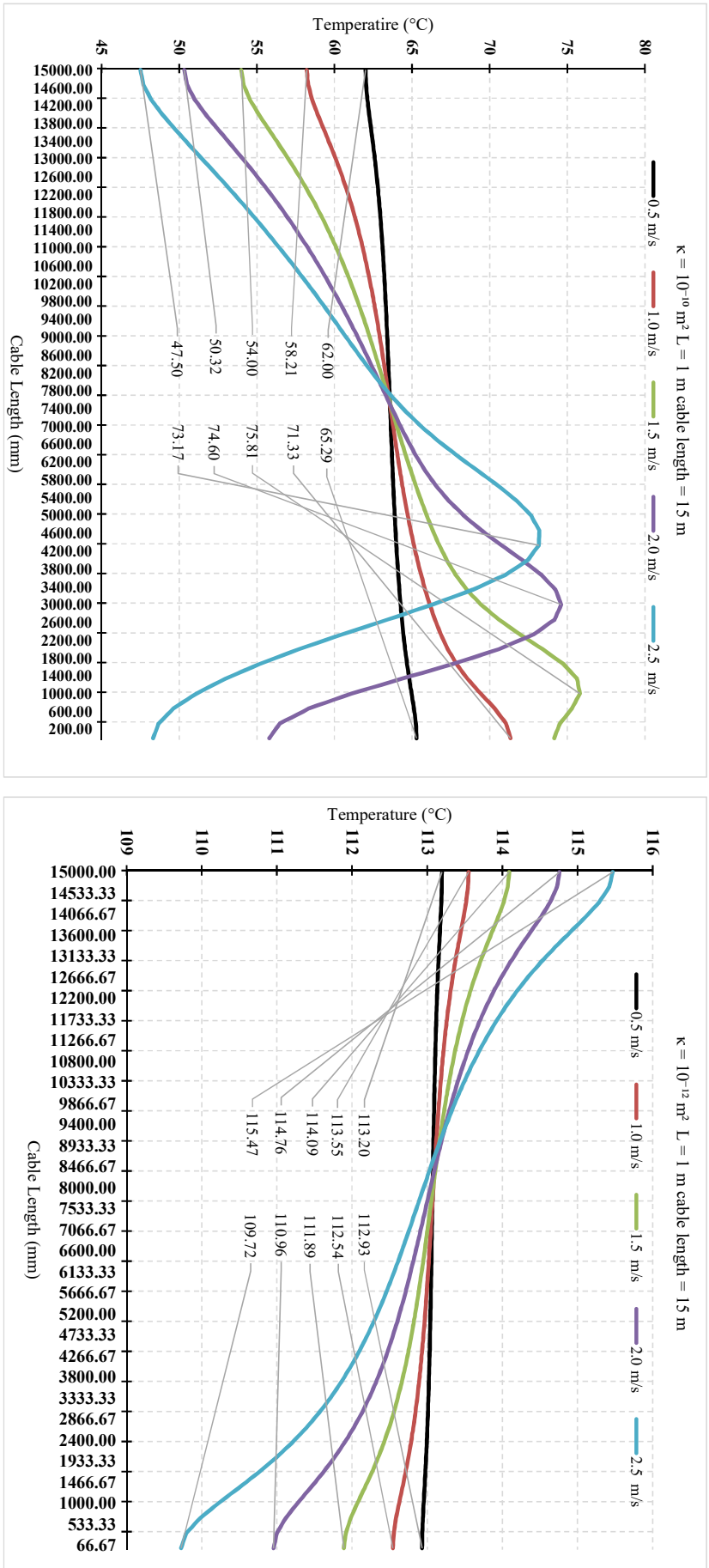

Figure 5.6: Cable conductor temperature for flow velocity along the cable of length 15 meters

the flow length cannot carry away more heat a decrease in temperature difference between the heat source and fluid compared to the entry point results in higher cable temperature. However, the heat transfer mechanism in the high permeable sediment is altered due to the changes in pore pressure. The heat dissipation is not uniform along the cable length and local heating effect due to the water movement is observed.

The axial flow along the cable length for increasing depth of burial (L = 0.5 m, 1.0 m and 2.0 m) and permeability values (10^{-10}m^2 and 10^{-12}m^2) are shown in Fig. 5.7, 5.6 and 5.8. The representative values for near-seabed currents are used. Vertical velocities of sea-water are not considered as it has lesser influence on the buried cable conductor temperature. The low permeable porous sediment temperature profile represents typical heat transfer in conductive medium where the fluid entry/inlet have cooler temperatures due to flow of fluid at ambient temperature and the outlet will have higher temperature due to accumulation of heat along the flow. But the higher permeable porous sediments show completely different temperature profiles than the lower permeable sediments. The fluid exit/outlet has the lowest temperatures and along the length close to the entry/inlet the cable core temperature is higher. This phenomenon is mainly seen in permeability that favour convective heat transfer. This accumulation of heat close to the inlet suggests that the heat flux in the convective zones flow faster towards the entry due to the low thermal resistance path created by water motion.

It is interesting to note that the temperature changes in the cable due to increase in water flow velocity can provide guidance for thermal rating of cables installed under water streams that may have constant flow. The velocity of the water moving above the surface where the cable was installed will be a factor affecting cable thermal performance under steady flow conditions for a longer period of time.

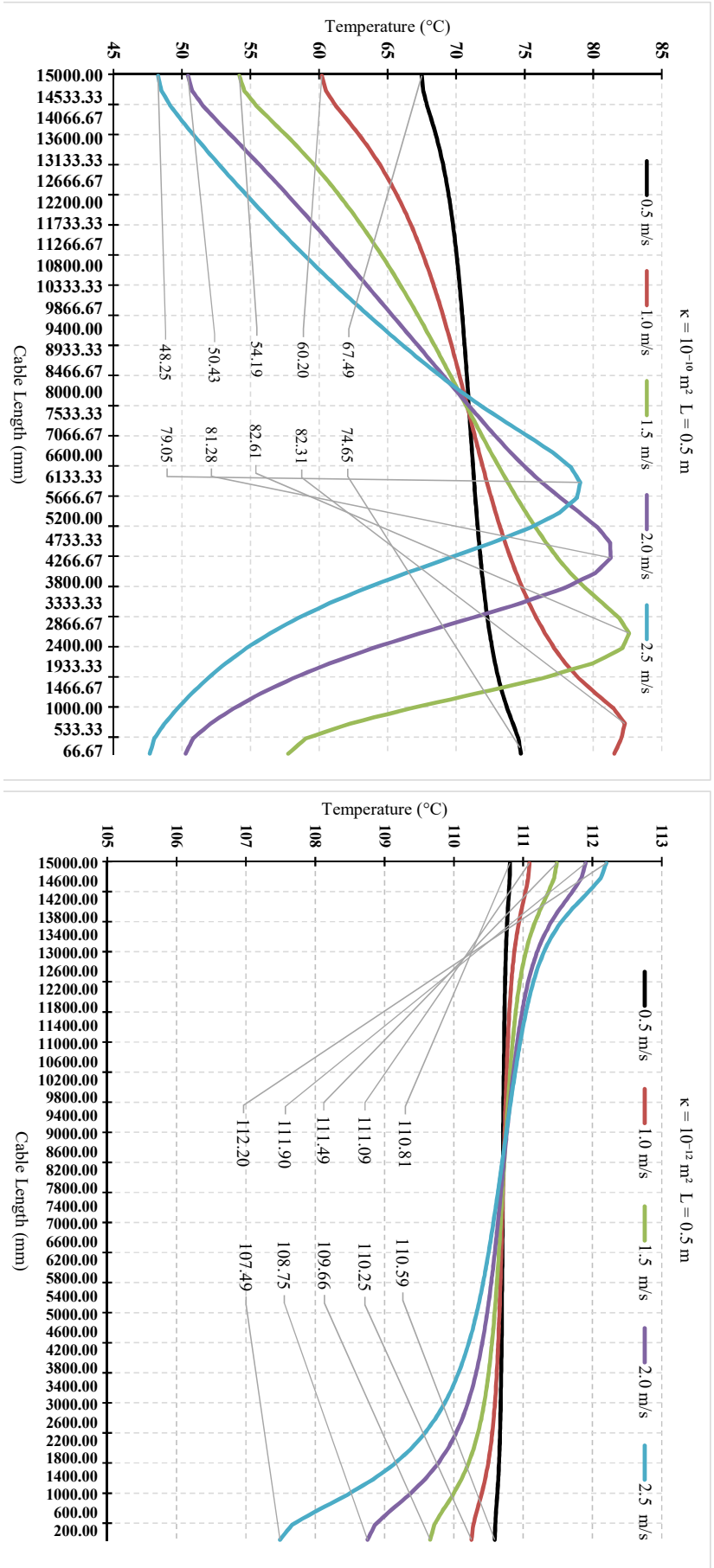

Figure 5.7: Cable conductor temperature for flow velocity along the cable of length buried at depth of 0.5 meter.

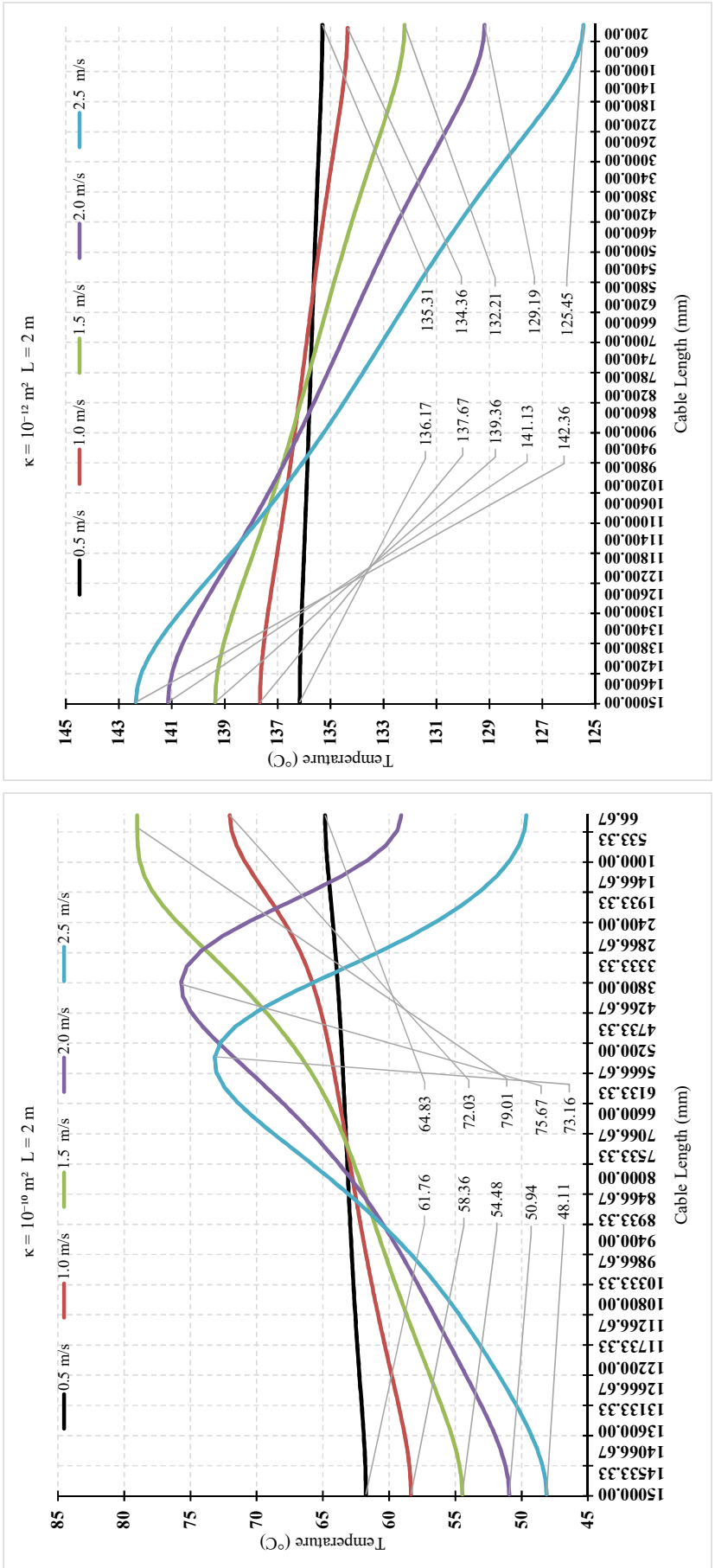

Figure 5.8: Cable conductor temperature for flow velocity along the cable of length buried at depth of 2.0 meters.

5.5 Summary

A summary of the effects of cross-flow and parallel-flow velocities on the cable conductor temperature is shown in Tables 5.1 and 5.2. Two permeability values ($kappa = 10^{-10}$ (m^2) and 10^{-12} (m^2)) were used for the analysis. Table 5.1 shows the FEM simulation results for a depth of 1-metre burial. It is observed that the effect of parallel-flow on cable conductor temperatures is higher compared to cross-flow. In high permeable sediments, the conductor temperature increases with the increase in parallel-flow velocity and the temperatures decreases only for velocities higher than 1.5 m/s. On the other hand, for cables installed in lower permeable sediments, the water velocity above the installation surface has no significant effect on the conductor temperatures.

Table 5.1: Comparison of Cable Conductor Temperatures for Linear and Cross flow at 1 metre Depth of Burial

L = 1 m, k_s = 1.2 (W/m·°C)	Temperature for $\kappa = 10^{-10}$ (m^2)		Temperature for $\kappa = 10^{-12}$ (m^2)	
Velocity (m/s)	Cross-flow	Parallel-flow	Cross-flow	Parallel-flow
0.5	63.52	65.17	111.30	113.11
1	63.91	70.82	111.25	113.44
1.5	64.96	75.51	111.05	113.54
2	61.95	73.66	110.60	114.54
2.5	58.08	71.66	109.87	115.17

Table 5.2: Comparison of Cable Conductor Temperatures for Linear and Cross flow at 2 metres Depth of Burial

L = 1 m, k_s = 1.2 (W/m·°C)	Temperature for $\kappa = 10^{-10}$ (m^2)		Temperature for $\kappa = 10^{-12}$ (m^2)	
Velocity (m/s)	Cross-flow	Parallel-flow	Cross-flow	Parallel-flow
0.5	62.84	64.83	128.33	136.17
1	64.44	72.03	128.08	137.67
1.5	62.73	79.01	127.17	139.36
2	58.63	75.67	125.34	141.13
2.5	54.98	73.16	122.66	142.36

Table 5.2 presents the results of FEM simulations carried out for a depth of burial of 2 metres. When the depth of burial increased, the effect of parallel-flow velocities are more pronounced especially in case of cables installed in high permeable

sediments. In case of low permeable sediments, the effect of cross-flow on cables installed in deeper burial depths is slightly increased. This is due to the fact that the amount of heat generated in these conditions is higher. Hence the flow over the surface will result in heat accumulation at the flow outlet causing the conductor temperature to increase.

Numerical modelling of fluid flow above the cables installed in sea sediment was developed using FEM models. The effect of the fluid velocity on the heat transfer from the cables was studied for two different flow patterns. The results indicate that the cables installed in low permeable sediments were unaffected by the cross-flow conditions. In the parallel-flow condition, the cables may be heated up due to the heat accumulation at the flow exit. The cables in high permeable sediments are affected by the cross-flow conditions especially when the cables carry high current. The non-uniform heat distribution in high permeable sediments might have been caused by the heated fluid being more vigorously advected towards the flow. This in turn would force the cold recharge fluid from the overlying water to enter cooler spots before being drawn along the cable to the warmer spots. It is interesting to consider the implications of the dependence of cable temperature response on the sea water velocity. Unlike the normal forced convective conditions, for cables installed in porous sea sediments, water velocity may not necessarily improve the heat transfer. The study provides an understanding of what can be expected for cables installed in flow regimes and a guidance for the cable thermal behaviour.

Chapter 6

Conclusions and Future Work

6.1 Conclusions

The research work presented in this thesis has been primarily focused on the thermal behavior of submarine power cables and the influence of environmental parameters on the thermal rating of the those cables. This research is more relevant now given the expansion of submarine cable systems due to increasing offshore renewable energy sources and primarily due to the limited work that can be found on this topic compared to the numerous investigation carried out on the thermal behavior of their underground counterparts. Hence, attention was paid particularly on what are the thermal and physical conditions of submarine environment that might differ from the underground conditions and to what extent these new conditions would influence the thermal performance of the cables. Exhaustive literature survey was carried out to understand the thermal processes that are unique to the submarine environment other than their conspicuous similarities with the underground systems that affects the power cable operations.

The literature survey and theoretical background of the problem are presented in Chapter 2. The chapter describes the power cables design, cable thermal rating procedures and methods. Ampacity calculation using IEC 60287 is also intro-

duced in this chapter. The heat transfer mechanisms in porous medium and the differences between the underground and submarine power cable environment are also described in this chapter. Factors that significantly alter the heat and fluid flow in the cable burial medium were investigated and their impacts on the cable thermal behavior are also presented therein. It is understood that the external thermal resistance calculated following standard approaches might not be suitable for submarine power cable ratings.

An analogous thermal resistance network that is suitable for submarine power cable applications is presented in Chapter 3. Simulations studies were carried carried out in parallel to validate the proposed models. The results show that the proposed models are more relevant and effective analytical solutions to predict the cable thermal behavior in submarine conditions.

Chapter 4 introduces the parameters that affect the ampacity calculation of the power cables. An evaluation of these parameters and their impact on the heat dissipation from various cable configurations in submarine environment is also presented in this chapter. The lab-scale experimentation developed to validate the simulation and analytical model results is also described in this chapter.

The submarine environment is dynamic in nature. Presence of water currents near the deep sea can alter the assumptions made in Chapter 4. Chapter 5 extends the FEM simulations to include the water flow above the sea sediments. The thermal performance of the power cables under the influence of moving water is then compared with the cables in stationary water medium above the burial surface. The thermal impacts of the water velocity and orientation of cables with the flow direction are discussed in this chapter.

6.2 Key Contributions

Detailed simulation studies were carried out using finite element method (FEM) modelling to present the distinctive features of thermal transfer in the submarine environment. The foundation of the hypothesis was developed based on the knowledge of exiting methods used for modelling the underground cables, in terms of approach and equations used. The existing methods were modified in the new FEM models, in the view of demonstrating the difference in thermal characteristics of the underground and submarine environment that will result in a different thermal behavior of the installed cables. Therefore, heat transfer from power cables in submarine conditions will require additional specific descriptions to model this thermal behavior.

The relevant PDEs that describe the complex heat transfer mechanisms of the sea sediments, and the thermal interaction of the cable, saturated porous medium in which it is buried and the overlying water were modelled using COMSOL Multiphysics 5.4. One of the insights provided by the FEM simulation study was that the traditional thermal rating of the cables is not suitable for submarine applications. Under certain circumstances, submarine environment exhibit convective heat transfer through the pore fluid that will play a significant role in heat dissipation from the cables. The results are in contradiction with the the thermal behavior predicted using standard approach. These models do not acknowledge convection as a mode of heat transfer in buried cables. The difference in the submarine cable thermal behavior can be attributed to the conjugate thermal and fluid flow in the porous medium thus making the burial environment completely different from the underground setting.

The studies indicate that traditional current rating methods might underestimate the cable ampacity values by neglecting the significant contributions from convective heat transfer. This decreases the cable utilization by conservatively limiting the operating temperature far below the allowable maximum temperature.

1. The ampacity rating models of the submarine power cables can be modified to take into account the convective heat transfer that can significantly reduce the cable temperatures and increase current rating as shown in Table 4.2. Though the cables themselves are not the limiting factors for thermal ratings as seen in the case of J-tubes and beach landings [97], [122], [123] for example, we can take advantage of the favorable thermal environment to increase the transmission line capacity.

2. The calculation methods proposed for the external thermal resistance of porous medium that favors convective heat transfer will help to refine the existing IEC standards for submarine power cable current rating. The methods defined in Chapter 3 can be used to estimate the lower or upper bound (for a more conservative approach) cable temperature that can be expected over the operating period of the cables for dynamic current rating techniques.

3. The convective cooling effects provided by the submarine conditions can help maintain the cable at lower operating temperatures without further current derating. This will help to reduce the thermal degradation of the insulation and increase the cable life expectancy. The thermal life of a cable approximately doubles [10] when lowering the operating temperature by 10°C. This will eventually decrease the temperature-dependent electrical resistance of the metal conductors that causes Joule heating within the cable.

4. The inferences from the studies can be used for a well-informed cable system design. In circumstances, where part or the entire cable route favor convective heat transfer, the proposed analytical models can significantly maximize the cable rating thus improving the cable utilization, and overall system efficiency and cost-effectiveness. The insights provided could also help to plan the cable route. With the *in-situ* information of all the available routes, one path can be preferred over the others that might prove to economical considering the factors discussed above.

6.3 Future Work

6.3.1 Real Time Cable Temperature Monitoring

When installed subsea, cables risk becoming exposed or covered with mud or sand and they are subject harsh conditions like wave an tidal movement, fishing and anchoring of ships that may damage the cable performance and the cable physical and electrical properties [124]. The real-time monitoring of the cable will help to predict and detect damages, and to identify the fault locations accurately. In distributed temperature sensing (DTS) systems optical fiber cables are placed inside the cable sheath or placed over the cable or sometimes laid close to the power cables. In other cases communication cables that run close to the power cables may also be used as optical sensors. The fiber optic cables are placed in a stainless steel tube to prevent cable straining as it can affect the data measurement. DTS systems connects the bundle of optical fibres down which pulses of light are sent.

The working principle of the DTS system is based on the analysis using the back scattered laser pulses sent from the DTS. The scattered pulses can also provide the information about the measurement position on the cable calculated from the time at which they were transmitted from the DTS. The intensity of the back scattered light provides the temperature information. Even finer changes in the intensity can be detected using complex electro-optical devices. Online temperature measurements using DTS systems can be used to provide temperature data for real-time cable ratings that can be used to supplement the conventional steady-state cable current ratings by taking into consideration the prevailing ambient conditions and local thermal conditions, and to justify possible uprating or derating of cable capacity.

The predictions made by the FEM simulations about the cable thermal performance and the heat dissipation in the submarine environment modelled by including the convective cooling effects can be analysed by DTS data of a similar setting

to appreciate the model versatility. The conclusions can be strengthened if the DTS measurements can be combined with the FEM simulations.

6.3.2 Real-Time Ampacity

The real-time cable ampacity rating aims to safely utilize the power cables up to their maximum capacity with real-world limiting factors, so the cable will work within safe limits optimally. The essential difference between conventional cable ampacity rating and real-time rating is the dynamic nature of the calculation, the conventional approach uses static conditions while real-time rating takes into account actual atmospheric conditions. This sometimes result in better ampacity rating [125].

The power transfer efficiency improves with the dynamic ampacity calculation with real-time condition monitoring, optimizing the power flow. The findings from the cable thermal ratings in Chapter 3 can be applied to perform real-time thermal ratings of the cables.

List of Publications

The Author's contribution in this Ph.D thesis are summarised in the following publications:

Journal Publications:

1. **N. Duraisany**, H. B. Gooi and A. Ukil, "Ampacity Estimation for Submarine Power Cables Installed in Saturated Seabed—Experimental Studies," in *IEEE Transactions on Industry Applications*, vol. 56, no. 6, pp. 6229-6237, Nov.-Dec. 2020, doi: 10.1109/TIA.2020.3023398.

2. **N. Duraisany**, H. B. Gooi, S. R. Purimtala, N. Srikanth and A. Ukil, "Equivalent Thermal Resistance Model for Submarine Power Cables," in *Applied Thermal Engineering*. (submitted).

Conference Publications:

1. **N. Duraisamy**, H. B. Gooi and A. Ukil, "Ampacity Estimation for HV Submarine Power Cables Installed in Saturated Seabed," *2018 IEEE International Conference on Power Electronics, Drives and Energy Systems (PEDES)*, Chennai, India, 2018, pp. 1-5, doi: 10.1109/PEDES.2018.8707678.

2. **N. Duraisamy**, A. Ukil, H. B. Gooi and H. Tian, "Ampacity and Electro-Magnetic Modeling for High-Voltage Subsea Cables Installed in Saturated Seabed," *IECON 2017 - 43rd Annual Conference of the IEEE Industrial Electronics Society*, Washington, DC, 2018, pp. 1664-1668, doi: 10.1109/IECON.2018.8592720.

3. **N. Duraisamy**, H. B. Gooi and A. Ukil, "Modeling and analysis of HV cable ampacity for power flow optimization," *IECON 2017 - 43rd Annual Conference of the IEEE Industrial Electronics Society*, Beijing, 2017, pp. 328-332, doi: 10.1109/IECON.2017.8216059.

4. **N. Duraisamy**, and A. Ukil, "Cable ampacity calculation and analysis for power flow optimization," *2016 Asian Conference on Energy, Power and Transportation Electrification (ACEPT)*, Singapore, 2016, pp. 1-5, doi: 10.1109/ACEPT.2016.7811535.

Bibliography

[1] "Columbus Gas Field, United Kingdom." [online], http://www.offshore-technology.com/projects/columbus-gas-field/columbus-gas-field6.html.

[2] "Omnisens Securing Power Cable Integrity." [online], http://www.omnisens.com/docs/AN-013

[3] H. Wagner, "Introduction to wind energy systems," *Institute for Energy Systems and Energy Economy Ruhr-University Bochum, Germany*, Jul. 2014.

[4] "About Submarine Power Cables," International Cable Protection Committee Ltd, Tech. Rep., Nov. 2011.

[5] "Nexans submarine power cables." [online], http://www.nexans.de.

[6] "Prysmian power cables." [online], https://www.prysmiangroup.com.

[7] "Efficient electrical energy transmission and distribution," *International Electrotechnical Commission*, Mar. 2014.

[8] K. Malmedal, "Underground vs overhead transmission and distribution," *NEI Electric Power Engineering*, Jun. 2009.

[9] M. Ardelean and P. Minnebo, "HVDC Submarine Power Cables in the World," EUR 27527 EN, Tech. Rep., 2015.

[10] T. Worxyz, *Submarine Power Cables Design, Installation, Repair, Environmental Aspects*. Springer Dordrecht Heidelberg, 2009.

[11] W. H. Couch, G. H. Hunt, N. D. Kenney, and P. H. Ware, "Modern high-voltage rubber insulation [includes discussion]," *Transactions of the American Institute of Electrical Engineers. Part III: Power Apparatus and Systems*, vol. 74, no. 3, pp. 1387–1398, 1955.

[12] *International Submarine Cables and Biodiversity of Areas Beyond National Jurisdiction: The Cloud Beneath the Sea.* Brill, 2017, pp. 1–72. [Online]. Available: http://www.jstor.org/stable/10.1163/j.ctt1w76vr5.4

[13] H. Brinser, "Submarine power cables," in *OCEANS '76*, 1976, pp. 79–82.

[14] D. Valenza and G. Cipollini, "Hvdc submarine power cable systems-state of the art and future developments," in *Proceedings 1995 International Conference on Energy Management and Power Delivery EMPD '95*, vol. 1, 1995, pp. 283–287 vol.1.

[15] J. J. Gordonnat, "Subsea cable key challenges of an intercontinental power link: case study of australia–singapore interconnector," *Energy Transit*, vol. 4, p. 169–188, 2020.

[16] X. Zhao, L. Yao, J. Wu, J. Xiao, J. Hou, G. Jinghui, and L. Zhong, "Technical and economic demands of hvdc submarine cable technology for global energy interconnection," 2020.

[17] J. H. Neher and M. H. McGrath, "The calculation of the temperature rise and load capability of cable systems," *Power App. and Syst., Part III, Trans. Amer. Inst. Elect. Eng.*, vol. 76, no. 3, pp. 752–764, Apr. 1957.

[18] "RenewableEnergy Market Update, Outlook for 2020 and 2021." International Energy Agency [online], https://www.iea.org.

[19] "Energy Efficiency in the Power Grid." ABB technical report [online], http://www.abb.us.

[20] J. L. D.V. Hertem, O. Gomis-bellmunt, *HVDC GRIDS For Offshore and Supergrid of the Future*. IEEE Press / Wiley Publication, 2016.

[21] H. Brinser, "Submarine power cables," in *OCEANS '76*, 1976, pp. 79–82.

[22] D.McAllister, *Electric Cables Handbook*. Granada Publishing, 1982.

[23] J. Machado, M. V. Neves, and P. J. Santos, "Economic limitations of the hvac transmission system when applied to offshore wind farms," in *2015 9th International Conference on Compatibility and Power Electronics (CPE)*, 2015, pp. 69–75.

[24] "Submarine Power Cables." Subsea Cables UK [online], http://www.kis-orca.eu.

[25] T. Orloff, D. Scott, and D. Shafer, "Transmission System Review Southeast Alaska Intertie," Alaska Industrial Development and Export Authority, Tech. Rep., Mar. 2003.

[26] N. Edlefsen and A. Anderson, "Thermodynamics of soil moisture," *Hilgardia*, vol. 15, no. 2, pp. 31–298, 1943.

[27] G. Groeneveld, A. Snijders, G. Koopmans, and J. Vermeer, "Improved method to calculate the critical conditions for drying out sandy soils around power cables," *IEE Proceedings C (Generation, Transmission and Distribution)*, vol. 131, pp. 42–53(11), March 1984.

[28] G. Anders and H. Radhakrishna, "Power cable thermal analysis with consideration of heat and moisture transfer in the soil," vol. 3, pp. 1280 – 1288, 11 1988.

[29] G. Koopmans, G. van de Wiel, L. van Loon, and C. Palland, "Soil physical route survey and cable thermal design procedure," *IEE Proceedings C (Generation, Transmission and Distribution)*, vol. 136, pp. 341–346(5), November 1989.

[30] J. A. Pilgrim, "Circuit rating methods for high temperature cables," Ph.D. dissertation, University of Southampton, June 2011.

[31] J. R. Philip and D. A. Vries, "Moisture movement in porous materials under temperature gradients," *Eos, Transactions American Geophysical Union*, vol. 38, pp. 222–232, 1957.

[32] J. J. Manyà, M. J. Antal, C. K. Kinoshita, and S. M. Masutani, "Specific heat capacity of pure water at 4.0 mpa between 298.15 and 465.65 k," *Industrial & Engineering Chemistry Research*, vol. 50, no. 10, pp. 6470–6484, 2011. [Online]. Available: https://doi.org/10.1021/ie102462g

[33] K. Weltner, "Measurement of specific heat capacity of air," *American Journal of Physics*, vol. 61, no. 7, pp. 661–662, 1993. [Online]. Available: https://doi.org/10.1119/1.17179

[34] J. R. Welty, C. E. Wicks, R. E. Wilson, and G. L. Rorrer, *Fundamentals of Momentum, Heat, and Mass Transfer*. John Wiley Sons, Hoboken, NJ, USA, 5th Ed., 2008.

[35] M. D. G. Buonanno, A. Carotenuto and D. Villacci, "Effect of radiative and convective heat transfer on thermal transients in power cables," *IEE Proceedings - Generation, Transmission and Distribution*, vol. 142, pp. 436–444(8), July 1995.

[36] M. A. Hanna, A. Y. Chikhani, and M. M. A. Salama, "Thermal analysis of power cables in multi-layered soil. i. theoretical model," *IEEE Transactions on Power Delivery*, vol. 8, no. 3, pp. 761–771, 1993.

[37] S. Purushothaman, F. Leon, and M. Terracciano, "Calculation of cable thermal rating considering non-isothermal earth surface," *Generation, Transmission Distribution, IET*, vol. 8, pp. 1354–1361, 07 2014.

[38] M. Kaviany, *Principles of Heat Transfer in Porous Media.* Springer, NewYork, USA, 2nd Ed., 1995.

[39] R. Siegel and J. Howell, *Thermal Radiation Heat Transfer.* Taylor Francis, NewYork, USA, 4th Ed., 2002.

[40] J. Niu, J. Xu, P. Dong, and G. Li, "Pore water pressure responses in silty sediment bed under random wave action," *Scientific Reports*, vol. 9, pp. 2045–2322, 2019.

[41] D. Stephens and M. Diesing, "Towards quantitative spatial models of seabed sediment composition," *PLOS ONE*, vol. 10, no. 11, pp. 1–23, 11 2015.

[42] S. Bashah, K. C. Galvez, G. P. Eberli, and K. Cantwell, "Control of deep currents on sediment and cold-water coral distribution on the northern manihiki plateau," *Frontiers in Marine Science*, vol. 7, p. 288, 2020.

[43] D. Tayal, *Electricity and Magnetism.* Himalaya Publishing House, Mumbai, India, 2009.

[44] W. A. Thue, *Electrical Power Cable Engineering.* Marcel Dekker, New York, USA, 1999.

[45] T. Worzyk and S. Långström, "Use of aluminum conductors in submarine power cables," in *Jicable'15 B1.1*, Jun 2015, pp. 1 – 6.

[46] *Electrical Design Guide According To IEC Standard.* [onine] http://www.Openelectrical.org.

[47] "525 kV extruded HVDC cable system Doubling power transmission over longer distances." ABB technical report [online], http://https://library.e.abb.com/.

[48] H. Orton, "History of underground power cables," *IEEE Electrical Insulation Magazine*, vol. 29, no. 4, pp. 52–57, 2013.

[49] O. E. Igwe, "Cable sizing and its effect on thermal and ampacity values in underground power distribution," Masters dissertation, Electrical and Computer Engineering, 2016.

[50] A. Bugajev, G. Jankevičiūtė, O. Suboč, and N. Tumanova, "The mathematical modelling of heat transfer in electrical cables," *The Journal of Riga Technical University*, vol. 5, May. 2014.

[51] "IEC Standard Calculation of the Cyclic and Emergency Current Ratings of Cables. Part 1: Cyclic Rating Factor for Cables up to and Including 18/30 (36) kV." IEC Std., 853-1, 1985.

[52] "IEC Standard Electric Cables-Calculation of Current Rating-Part 1: Current Rating equations (100% load Factor) and calculation of Losses- Section 1: General." IEC Std., 287, 2015.

[53] "IEC Standard Electric Cables-Calculation of Current Rating-Part 1: Current Rating equations (100% load Factor) and calculation of Losses- Section 2 Sheath Eddy Current Loss Factors for Two Circuits in Flat Formation,." IEC Std., 287, 1994.

[54] "IEC Standard Electric Cables-Calculation of Current Rating-Part 2: Thermal resistance-Section 1: Calculation of thermal resistance." IEC Std., 287, 1994.

[55] "IEC Standard - A Method for Calculating Reduction Factors for Groups of Cables in Free Air, Electric Cables- Calculation of the Current Rating-Part 2: Thermal Resistance – Section 2A: Protected from Solar Radiation." IEC Std., 287, 1995.

[56] "IEC Standard. Electric Cables- Calculation of the Current Rating-Part 3: Sections on Operating Conditions Section 1: Reference Operating Conditions and Selection of Cable Type." IEC Std., 287, 1995.

[57] "IEEE Standard Power Cable Ampacity Tables." IEEE N.Y. Std., 835, 1994.

[58] C. Bates, K. Malmedal, and D. Cain, "Cable ampacity calculations: A comparison of methods," *IEEE Trans. Ind. Appl.*, vol. 52, no. 1, pp. 112–118, Jan. 2016.

[59] F. de Leon and G. J. Anders, "Effects of backfilling on cable ampacity analyzed with the finite element method," *IEEE Trans. Power Del.*, vol. 23, no. 2, pp. 537–543, Apr. 2008.

[60] A. Mahmoudi, S. Kahourzade, and D. S. S. Lee, "Cable ampacity calculation in heterogenous soil using finite element analysis," in *2011 5th International Power Engineering and Optimization Conference*, Jun. 2011, pp. 416–421.

[61] C. Hwang, J. Chang, and H. Chen, "Calculation of ampacities for cables in trays using finite elements," *Electric Power Systems Research*, vol. 54, no. 2, pp. 75 – 81, 2000.

[62] H. Brakelmann and G. Anders, "Ampacity reduction factors for cables crossing thermally unfavorable regions," *IEEE Transactions on Power Delivery*, vol. 16, no. 4, pp. 444–448, Oct. 2001.

[63] F. Aras, C. Oysu, and G. Yilmaz, "An assessment of the methods for calculating ampacity of underground power cables," *Electric Power Components and Systems*, vol. 33, no. 12, pp. 1385–1402, 2005.

[64] J. Nahman and M. Tanaskovic, "Determination of the current carrying capacity of cables using the finite element method," *Electric Power Systems Research*, vol. 61, no. 2, pp. 109 – 117, 2002.

[65] C.-C. Hwang and Y.-H. Jiang, "Extensions to the finite element method for thermal analysis of underground cable systems," *Electric Power Systems Research*, vol. 64, no. 2, pp. 159 – 164, 2003.

[66] P. Vaucheret, R. A. Hartlein, and W. Z. Black, "Ampacity derating factors for cables buried in short segments of conduit," *IEEE Transactions on Power Delivery*, vol. 20, no. 2, pp. 560–565, Apr. 2005.

[67] M. Al-Saud, M. El-Kady, and R. Findlay, "A new approach to underground cable performance assessment," *Electric Power Systems Research*, vol. 78, no. 5, pp. 907 – 918, 2008.

[68] R. W. Lewis, P. Nithiarasu, and K. N. Seetharamu, *Fundamentals of the Finite Element Method for Heat and Fluid Flow*. John Wiley Sons, Chichester, UK, 2004.

[69] R. Mardiana, "Parameters affecting the ampacity of hvdc submarine power cables," in *2011 2nd International Conference on Electric Power and Energy Conversion Systems (EPECS)*, 2011, pp. 1–6.

[70] A. F. Mills, *Heat Transfer*. Richard D. Irwin, Inc., New York, USA, 1st Ed., 1992.

[71] J. K. Carson, S. J. Lovatt, D. J. Tanner, and A. C. Cleland, "Thermal conductivity bounds for isotropic, porous materials," *International Journal of Heat and Mass Transfer*, vol. 48, no. 11, pp. 2150 – 2158, 2005.

[72] G. C. J. Bart, "Thermal conduction in non homogeneous and phase change media," Ph.D. dissertation, Delft University of Technology, Netherlands, Dec 1994.

[73] W. Woodside and J. H. Messmer, "Thermal conductivity of porous media. i. unconsolidated sands," *Journal of Applied Physics*, vol. 32, no. 9, pp. 1688–1699, 1961.

[74] A. Revil, "Thermal conductivity of unconsolidated sediments with geophysical applications," *Journal of Geophysical Research: Solid Earth*, vol. 105, no. B7, pp. 16 749–16 768, 2000.

[75] M. A. Lovell, "Thermal conductivities of marine sediments," *Quarterly Journal of Engineering Geology and Hydrogeology*, vol. 18, no. 4, pp. 437–441, 1985.

[76] F. Brigaud and G. Vasseur, "Mineralogy, porosity and fluid control on thermal conductivity of sedimentary rocks," *Geophysical Journal International*, vol. 98, no. 3, pp. 525–542, 09 1989.

[77] R. Askari, S. Taheri, and S. H. Hejazi, "Thermal conductivity of granular porous media: A pore scale modeling approach," *AIP Advances*, vol. 5, no. 9, p. 097106, 2015.

[78] B. Ghanbarian and H. Daigle, "Thermal conductivity in porous media: Percolation-based effective-medium approximation," *Water Resources Research*, vol. 52, no. 1, pp. 295–314, 2016.

[79] E. Canot, R. Delannay, S. Mansour, M. Muhieddine, and R. March, "Effective thermal conductivity of a wet porous medium - presence of hysteresis when modeling the spatial water distribution for the pendular regime," *Journal of Heat Transfer*, vol. 138, pp. 1–7, 09 2016.

[80] E. Stein, *History of the Finite Element Method – Mathematics Meets Mechanics – Part I: Engineering Developments*. Berlin, Heidelberg: Springer Berlin Heidelberg, 2014, pp. 399–442.

[81] R. Courant, "Variational methods for the solution of problems of equilibrium and vibrations," *Bull. Amer. Math. Soc.*, vol. 49, no. 1, pp. 1–23, 01 1943. [Online]. Available: https://projecteuclid.org:443/euclid.bams/1183504922

[82] M. J. Turner, R. W. Clough, H. C. Martin, and L. J. Topp, "Stiffness and deflection analysis of complex structures," *Journal of the Aeronautical Sciences*, vol. 23, no. 9, pp. 805–823, 1956.

[83] T.-P. Fries, *Extended Finite Element Methods (XFEM)*. Berlin, Heidelberg:

Springer Berlin Heidelberg, 2018, pp. 1–10. [Online]. Available: https://doi.org/10.1007/978-3-662-53605-6_17-1

[84] J. Reddy, *Introduction to the Finite Element Method*. McGraw-Hill Education, 1993. [Online]. Available: https://books.google.com.sg/books?id=2NOlPwAACAAJ

[85] *Convection in Porous Media*. John Wiley Sons, Ltd, 2004, ch. 8, pp. 240–264. [Online]. Available: https://onlinelibrary.wiley.com/doi/abs/10.1002/0470014164.ch8

[86] *Computational Fluid Dynamics: Physical Law based Finite Volume Method*. John Wiley Sons, Ltd, 2016, ch. 8, pp. 251–269. [Online]. Available: https://onlinelibrary.wiley.com/doi/abs/10.1002/9781119369189.ch8

[87] J. Bear and Y. Bachmat, *Introduction to modeling of transport phenomena in porous media*. Dordrecht, Boston : Kluwer Academic Publishers, 1991.

[88] F. Scarpa and M. De Rosa, "Transient heat conduction in wires with heat sources; lumped and distributed solution techniques," *Heat Transfer Research*, vol. 47, pp. 753–765, 01 2016.

[89] I. Baker and F. D. Leon, "Equivalent circuit for the thermal analysis of cables in non-vented vertical risers," *Iet Science Measurement Technology*, vol. 9, pp. 606–614, 2015.

[90] G. J. Anders, *Special Considerations for Real-Time Rating Analysis and Deeply Buried Cables*, 2005, pp. 211–246.

[91] R. J. Millar and M. Lehtonen, "A robust framework for cable rating and temperature monitoring," *IEEE Transactions on Power Delivery*, vol. 21, no. 1, pp. 313–321, 2006.

[92] Z. Huang, J. A. Pilgrim, P. Lewin, S. Swingler, and G. Tzemis, "Thermal modelling and analysis for offshore submarine high-voltage direct current

cable crossings," *IET Generation, Transmission Distribution*, vol. 9, pp. 2717–2723(6), December 2015.

[93] V. N. Kurdyumov and A. Liñán, "Free and forced convection around line sources of heat and heated cylinders in porous media," *J. Fluid Mech.*, vol. 427, pp. 389–409, 2001.

[94] M. Zeneli, A. Nikolopoulos, S. Karellas, and N. Nikolopoulos, "Chapter 7 - numerical methods for solid-liquid phase-change problems," in *Ultra-High Temperature Thermal Energy Storage, Transfer and Conversion*, ser. Woodhead Publishing Series in Energy, A. Datas, Ed. Woodhead Publishing, 2021, pp. 165 – 199.

[95] T. L. Bergman, A. S. Lavine, F. P. Incropera, and D. P. DeWitt. John Wiley Sons, Ltd, 2002.

[96] M. A. Atmane, V. S. Chan, and D. B. Murray, "Natural convection around a horizontal heated cylinder: The effects of vertical confinement," *International Journal of Heat and Mass Transfer*, vol. 46, no. 19, pp. 3661 – 3672, 2003. [Online]. Available: http://www.sciencedirect.com/science/article/pii/S0017931003001546

[97] T. J. Hughes, T. J. Henstock, J. A. Pilgrim, J. K. Dix, T. M. Gernon, and C. E. L. Thompson, "Effect of sediment properties on the thermal performance of submarine HV cables," *IEEE Trans. Power Del.*, vol. 30, no. 6, pp. 2443–2450, Dec. 2015.

[98] C. W. Horton and F. T. Rogers, "Convection currents in a porous medium," *Journal of Applied Physics*, vol. 16, no. 6, pp. 367–370.

[99] J. Stafford and V. Egan, "Configurations for single-scale cylinder pairs in natural convection," *International Journal of Thermal Sciences*, vol. 84, pp. 62 – 74, 2014. [Online]. Available: http://www.sciencedirect.com/science/article/pii/S1290072914001082

[100] Y. Wu, S. Chang, and P. Mandal, "Grid-connected wind power plants: A survey on the integration requirements in modern grid codes," *IEEE Trans. Ind. Appl.*, vol. 55, no. 6, pp. 5584–5593, 2019.

[101] L. Wang, C. Lin, H. Wu, and A. V. Prokhorov, "Stability analysis of a microgrid system with a hybrid offshore wind and ocean energy farm fed to a power grid through an hvdc link," *IEEE Trans. Ind. Appl.*, vol. 54, no. 3, pp. 2012–2022, 2018.

[102] C. Bates, D. Cain, and K. Malmedal, "Including soil drying time in cable ampacity calculations," *IEEE Trans. Ind. Appl.*, vol. 52, no. 6, pp. 4646–4651, Nov 2016.

[103] K. Malmedal, C. Bates, and D. K. Cain, "The heat and buried cable conundrum: A method to help determine underground cable ampacity," *IEEE Ind. Appl. Mag.*, vol. 22, no. 5, pp. 20–31, Sep. 2016.

[104] K. Malmedal, C. Bates, and D. Cain, "On the use of the law of times in calculating soil thermal stability and underground cable ampacity," *IEEE Trans. Ind. Appl.*, vol. 52, no. 2, pp. 1215–1220, March 2016.

[105] E. Thibaut and B. Leforgeais, "Selection of power from shore for an offshore oil and gas development," *IEEE Trans. Ind. Appl.*, vol. 51, no. 2, pp. 1333–1340, Mar. 2015.

[106] J. Song-Manguelle, M. Harfman Todorovic, S. Chi, S. K. Gunturi, and R. Datta, "Power transfer capability of HVAC cables for subsea transmission and distribution systems," *IEEE Trans. Ind. Appl.*, vol. 50, no. 4, pp. 2382–2391, Jul. 2014.

[107] "XLPE submarine cable systems." ABB Rev.5, https://new.abb.com/docs/default-source/ewea-doc/xlpe-submarine-cable-systems-2gm5007.pdf.

[108] C. Müller, R. Usbeck, and F. Miesner, "Temperatures in shallow marine sediments: Influence of thermal properties, seasonal forcing, and man-made heat sources," *Appl. Ther. Eng.*, vol. 108, pp. 20 – 29, 2016.

[109] J. Skog, K. Koreman, B. Pääjärvi, T. Worzyk, and T. Andersröd, "The norned HVDC cable link - A power transmission highway between norway and the netherlands," in *Proc. of Energex*, Stavanger, Norway, Jun. 2006.

[110] C. E. L. Thompson, C. Emeana, J. Dix, T. Henstock, T. Hughes, T. Gernon, and J. Pilgrim, "The thermal regime around buried submarine high-voltage cables," *J. Geophys. Int.*, vol. 206, no. 2, pp. 1051–1064, May 2016.

[111] H. Sakamoto and F. A. Kulacki, "Buoyancy Driven Flow in Saturated Porous Media," *ASME. J. Heat Trans.*, vol. 129, no. 6, pp. 727–734, Jun. 2006.

[112] N. Duraisamy, H. B. Gooi, and A. Ukil, "Ampacity estimation for HV submarine power cables installed in saturated seabed," in *Proc. 2018 IEEE International Conference on Pow. Elec., Driv. and Ener. Sys. (PEDES)*, pp. 1–5.

[113] L. Wang, B. Kuan, C. Yu, H. Wu, S. Zeng, A. V. Prokhorov, H. Mokhlis, and C. K. Huat, "Effects of submarine-cable types and parameters on performance of a future-scheduled offshore wind farm connected to taiwan power system," *IEEE Trans. Ind. Appl.*, vol. 56, no. 2, pp. 1171–1179, 2020.

[114] P. J. Kamann, R. W. Ritzi, D. F. Dominic, and C. M. Conrad, "Porosity and permeability in sediment mixtures," *Groundwater*, vol. 45, no. 4, pp. 429–438, 2007.

[115] D. B. Ingham and I. Pop, "Natural convection about a heated horizontal cylinder in a porous medium," *J. Fluid Mech.*, vol. 184, pp. 157–181, 1987.

[116] K. Himasekhar and H. H. Bau, "Thermal convection around a heat source embedded in a box containing a saturated porous medium," *ASME J. Heat*

Trans., vol. 110, no. 3, pp. 649–654, Aug 1988.

[117] D. A. Douglass and A. . Edris, "Real-time monitoring and dynamic thermal rating of power transmission circuits," *IEEE Trans. Power Del.*, vol. 11, no. 3, pp. 1407–1418, 1996.

[118] K. J. Van Landeghem, J. H. Baas, N. C. Mitchell, D. Wilcockson, and A. J. Wheeler, "Reversed sediment wave migration in the irish sea, nw europe: A reappraisal of the validity of geometry-based predictive modelling and assumptions," *Marine Geology*, vol. 295-298, pp. 95 – 112, 2012. [Online]. Available: http://www.sciencedirect.com/science/article/pii/S0025322711002738

[119] T. Mulder, "Chapter 2 - gravity processes and deposits on continental slope, rise and abyssal plains," in *Deep-Sea Sediments*, ser. Developments in Sedimentology, H. HüNeke and T. Mulder, Eds. Elsevier, 2011, vol. 63, pp. 25 – 148. [Online]. Available: https://www.sciencedirect.com/science/article/pii/B9780444530004000020

[120] G. Shanmugam, "Chapter 4 - bottom-current reworked sands," in *New Perspectives on Deep-water Sandstones*, ser. Handbook of Petroleum Exploration and Production, G. Shanmugam, Ed. Elsevier, 2012, vol. 9, pp. 129 – 219. [Online]. Available: https://www.sciencedirect.com/science/article/pii/B9780444563354000047

[121] E. Shashi Menon, "Chapter five - fluid flow in pipes," in *Transmission Pipeline Calculations and Simulations Manual*, E. Shashi Menon, Ed. Boston: Gulf Professional Publishing, 2015, pp. 149 – 234. [Online]. Available: http://www.sciencedirect.com/science/article/pii/B9781856178303000055

[122] J. Pilgrim, S. Catmull, R. Chippendale, R. Tyreman, and P. Lewin, "Offshore wind farm export cable current rating optimisation," in *European*

Wind Energy Association Oshore 2013, 2013, pp. 1 – 10.

[123] R. D. Chippendale, J. A. Pilgrim, K. F. Goddard, and P. Cangy, "Analytical thermal rating method for cables installed in j-tubes," *IEEE Transactions on Power Delivery*, vol. 32, no. 4, pp. 1721–1729, 2017.

[124] E. R. J. Rowsell, M. Niklès, "Condition Monitoring and Optimization of Subsea Energy Cables Using Optical Fiber Sensing," Tech. Rep., 2013. Omnisens, Morges, Switzerland. www.omnisens.com.

[125] "Overhead lines dynamic line rating based on probabilistic day-ahead forecasting and risk assessment," *International Journal of Electrical Power Energy Systems*, vol. 110, pp. 565 – 578, 2019.

Appendix A

A.1 Experimental Setup Design

A.1.1 Overview

The heat dissipation from the power cables installed in submarine environment and the temperature regimes around the cables were analysed numerically and analytically in the work presented in the previous chapters. This section will analyse the actual cable thermal performance using laboratory experimentation. As part of a broader approach to investigating the thermal environment around submarine power cables, a 3-D tank experiment has been designed and constructed in one of the laboratories at the Energy Research Institute at NTU (ERI@N). The motivation behind this was to develop an alternative strategy for evaluating the thermal behaviour of submarine power cable systems by providing a physical analogue of the FEM models. In the context of the predictions made by the FEM model in Chapters 3 and 4, it was hoped that the experimental results would deliver valuable supporting evidence (from a physical basis) for the phenomena observed in the model.

The analogous submarine environment was created by filling a test chamber with saturated sandy soil. A 600 V armoured power cable was embedded in it and the thermal behavior was studied under different loading conditions. Equivalent 3-D finite element models were developed in COMSOL Multi-physics 5.4.

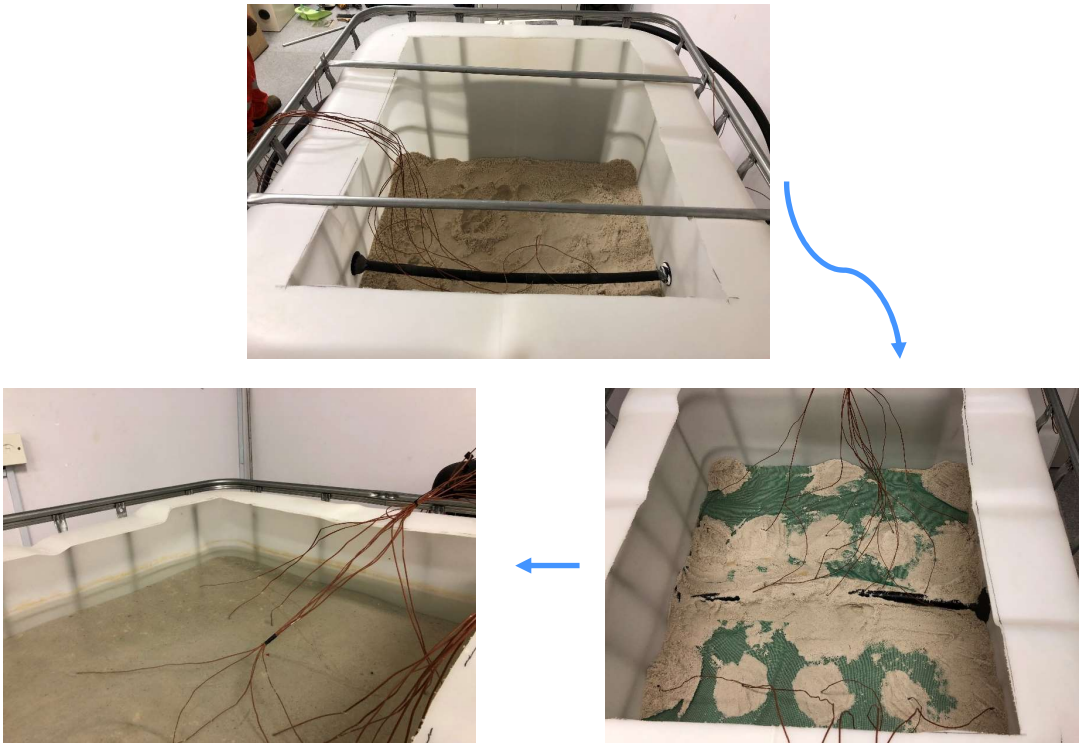

Figure A.1: Experimental test tank filled with sand and water. The study-Cable instrumented with thermo-couples can be seen on the top. Bottom right is the thermo-couple grid installed away from the cable on the soil.

A.1.2 Test Chamber Design

The test chamber is a large industrial grade intermediate bulk container (IBC tank). The tank is made of high-density polyethylene (HDPE) and the tank structure was supported by galvanised steel-grid. The thermal conductivity of HDPE is in the range of 0.45 - 0.52 W/m·°C making it a good insulator for preventing heat dissipation from the body of the tank. Fig. A.1 shows the test chamber with instrumentation, embedded test cable and saturated soil. The dimension of the tank are 1.2 m x 1.0 m x 1.2 m.

The studies conducted in the previous chapters indicated that the intrinsic permeability is a key parameter that enables the convective heat transfer in the saturated sediments and thereby influencing the thermal performance of the embedded cables. For the experimentation, two different soils (fine sandy soil and silty clay) were evaluated to identify the suitability.

A.1.3 Soil Testing

The permeability of the soils were measured using constant-head test and falling-head test procedures.

Constant-Head Test

The granularity of the sandy soil was higher compared to the silty clay and hence the constant-head test method was found suitable for determining the hydraulic conductivity. The procedure established the representative values of the coefficient of permeability by measuring the laminar flow of water through the sand.

Figure A.2: Test setup for constant-head permeability test.

Fig. A.2 shows the laboratory setup for conducting the constant-head tests. The soil sample was compacted and placed in the permeameter that saturates the soil

Figure A.3: Test set-up for falling-head permeability test

using water. A steady flow of water is established through the sample and flow quantity was measured for set intervals of time. The flow rates provides the hydraulic conductivity of the sample and the procedure was repeated for two to three times. The intrinsic permeability was calculated using the hydraulic conductivity. For the sandy soil sample, the constant-head testing results measured the permeability value to be $3.14{\cdot}10^{-11}$ m^2 (by averaging over 3 tests).

Falling-Head Test

For the silty-clay sample, the falling-head method was used to measure the intrinsic permeability. Fig. A.3 shows the test preparation and apparatus used for the silt sample. The test was carried out in a falling head test chamber. Before beginning the test, the sample was compacted and saturated in standpipe filled with de-aired water. The permeameter was then placed in the chamber. The inlet nozzle connected to the standpipe allows the seeping water to flow through the sample. The flow rate was measured few times and the average hydraulic conductivity is

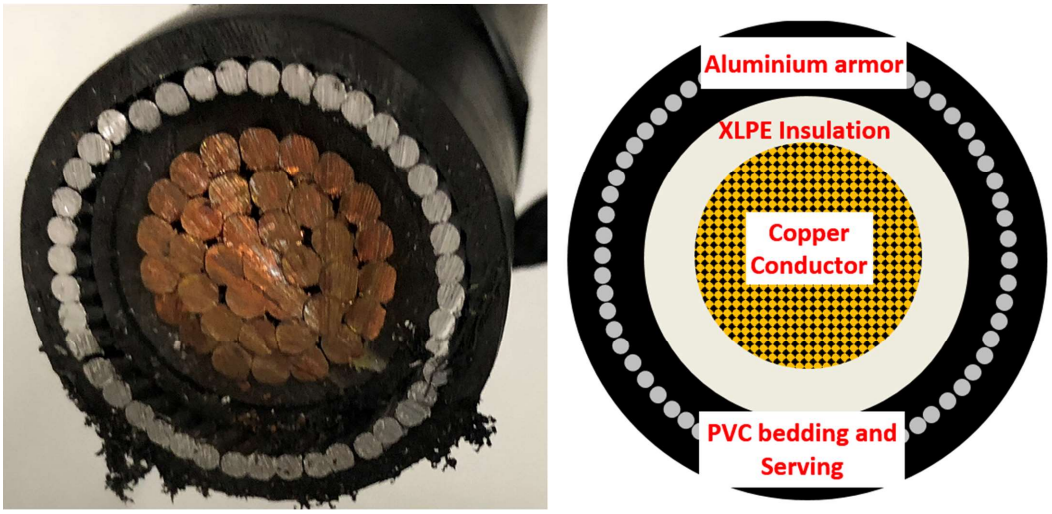

Figure A.4: Cross-sectional view of the steel-wire-armored copper cable used for the experimentation

determined using the flow rate. In this case, the intrinsic permeability was found to be $8.34{\cdot}10^{-16}$ m^2.

The numerical methods suggested that the heat transfer by convection occurs in permeability values higher than 10^{-12} m^2. As our interests lies in understanding and validating the claim, sandy soil was found more suitable to be used for the experimentation.

The tank was filled with the sandy soil up to half the tank capacity, then the study cable was laid in the container and the soil was filled again to cover up to 300 mm above the cable axis. The soil was compacted to avoid voids that may alter the measured porosity. The sand-fill was then saturated using water. Water was filled up to 200 mm above the soil surface. The test set-up was left undisturbed for one day to ensure that the filled water to completely saturate the sand.

The 0.6-kV cable shown in Fig. A.4 was laid in the tank (representing submarine environment) and connected between the secondary windings of 12-kVA transformer by short-circuiting the terminals. The cable physical properties and soil specifications are presented in Chapter 4. The study-cable was subjected to varying load current in order to examine the thermal behavior in transition conditions.

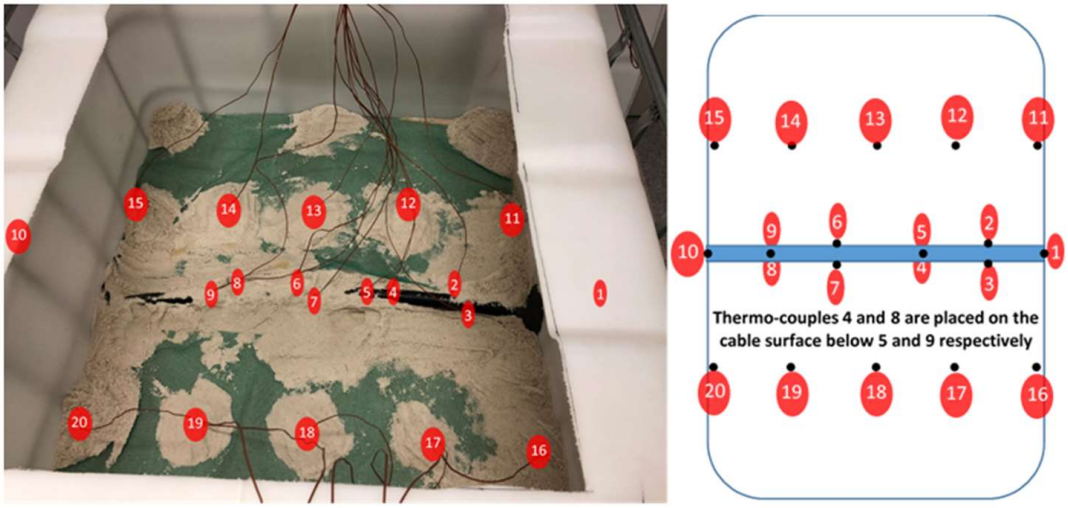

Figure A.5: The positions of thermo-couples on the cable surface and on the sand

20 thermo-couples were used to record the temperature data during the experimentation. 10 thermo-couples were placed on the cable surface to cover temperature measurements on the top, bottom and sides. 10 thermo-couples were placed on the sand at distance of 200 mm away from the cable axis on both sides. The illustration in Fig. A.5 shows the details of the thermo-couple positions.

A.1.4 Verification of the FEM Models

In addition to the results presented in chapter 4, the cable was subjected to additional tests to establish confidence on the numerical method. The cable was energized for 100 hours using continuous current of 400 A. The cable was then de-energized and allowed to cool down. Fig. A.6 shows the heating up and cooling down of the study-cable surface. The results show that the FEM model was able to represent the cable environment accurately and PDEs used in the numerical method corresponds to the heat transfer in the test scenario.

Load Current Variations

The test conditions were modified to study the cable thermal behavior under varying load currents. The cable was energized with a continuous current of 200A

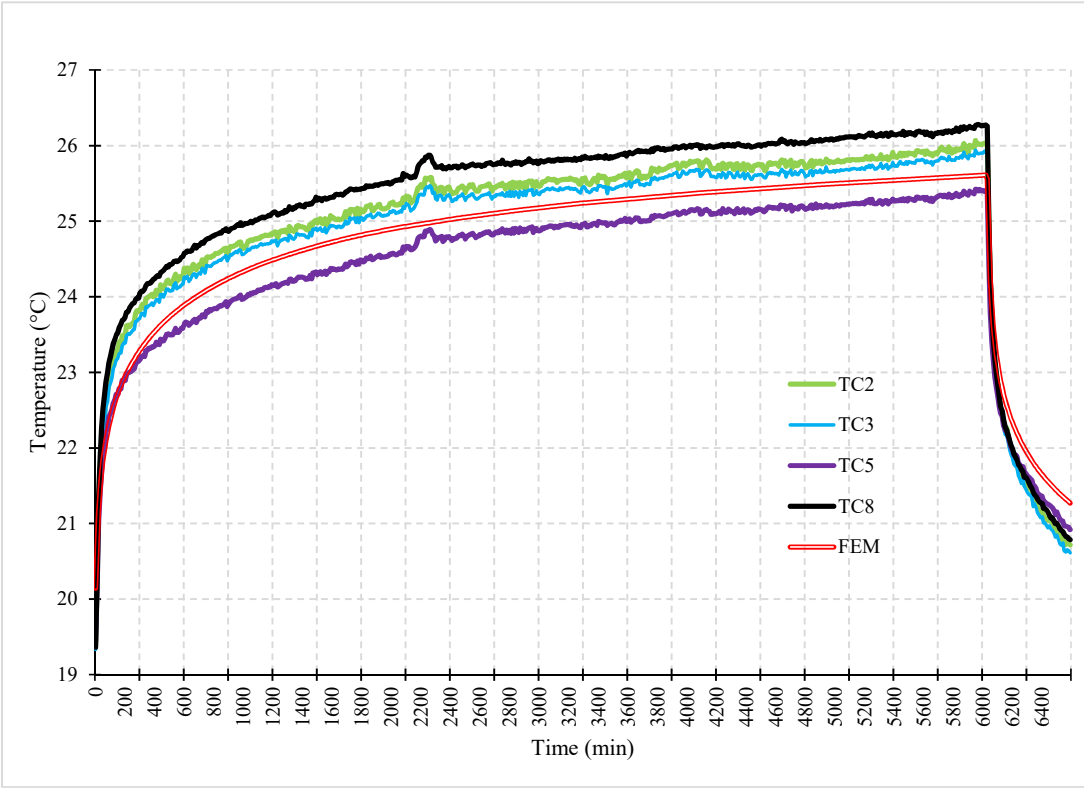

Figure A.6: Temperature data of the study-cable heat-up and cool-down time compared to the time dependent FEM model results depicting the time taken for the cable surface to heat up and cool down

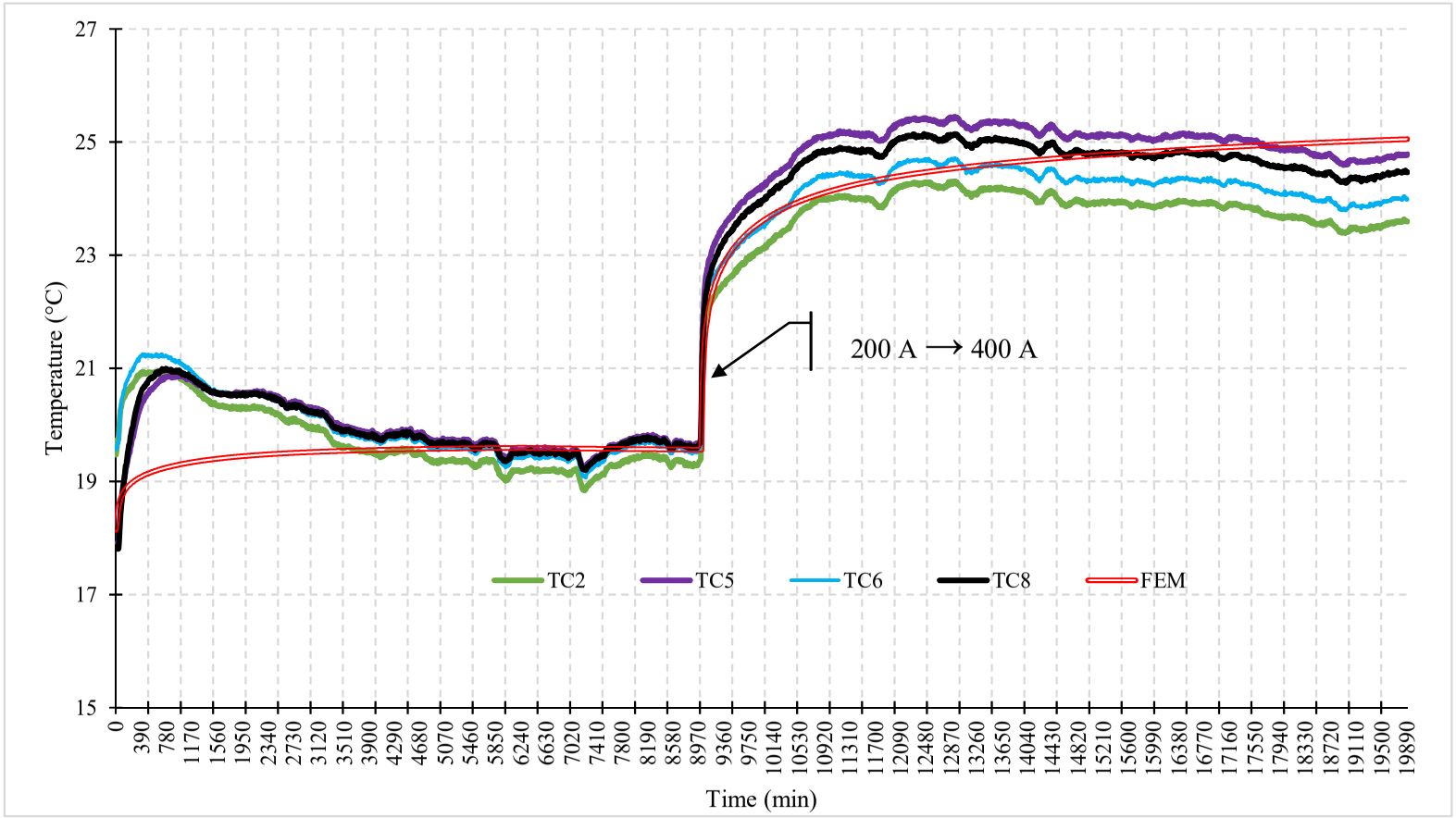

Figure A.7: Temperature data of the study-cable surface temperature recorded during the change in load current compared with the FEM model results

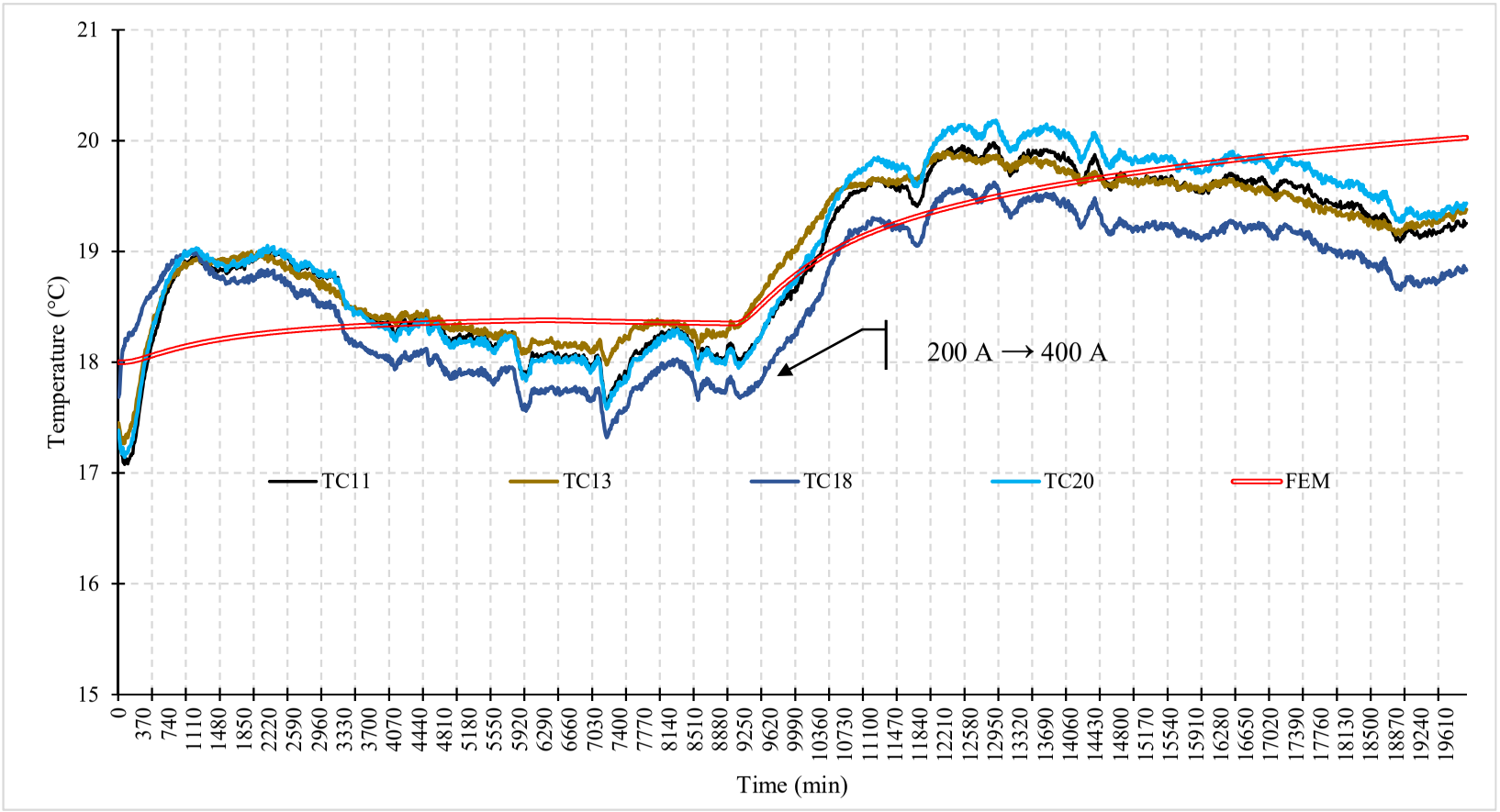

Figure A.8: Temperature data measured from the thermo-couples embedded in sand during the change in load current compared with the FEM model results

and the experiment was carried out until steady state was achieved after 160 hours. Then the cable energising current was increased to 400 A and temperature data were recorded for another 160 hours.

Fig. A.7 and A.8 show the respective temperature measured on the cable surface and soil thermo-couples during the change in load current. In the laboratory setup it was challenging to maintain a constant ambient temperature for a long period of time (this experiment was conducted for 13 days and 17 hours). Due to fluctuations in the ambient temperature, perturbations can be observed in the measurements. The results show that the temperature predicted by FEM model is in close agreement with the actual measured data expect for the initial surge in temperature. However, when the surface temperature reached steady state, the FEM results matched the actual measured data. The sudden temperature rise around 9200 minutes was due to the increase in load current from 200 A to 400 A. The FEM response time for the change in temperature is in very good agreement with the temperature transient measured at the cable surface. It is encouraging to note that the FEM model predictions are mirrored in the experimentation and vice-versa. The set of experiments conducted verified that the PDEs used for representing the heat transfer mechanism in the submarine power cables holds good and the results support the possible convection heat transfer occurring in the porous medium.

Appendix B

A.2 Time Dependent FEM Simulations

A.2.1 Overview

A time dependent model was developed to extend the scope of the original framework as described and used in Chapters 3 and 4 to explore some of the topics mentioned above. Part of the motivation for this originated from a curiosity to learn how the temperature response of a cable buried in a low permeability sediment (with conductive heat dissipation only) might differ from one buried in a highly permeable sediment that, in a steady state, supports both conductive and convective heat transfer. Also of interest were the timescales required for the establishment of a stable, convective system.

A.2.2 Developing a 2D Time Dependent FEM Model

In Section 2.4.1 the expression in equation (2.6) was derived, providing a description of heat transfer through porous media from a combination of conductive and convective processes. In the steady-state models described previously, the time derivative term in equation (2.6) is identically zero. The form of the heat transport equation that is implemented in the time independent FEM models is consequently given by equation (2.8). However, when time dependence is being considered, the term on the left hand side of equation (2.6) includes some new parameters that are not necessary in the time independent picture. As mentioned in

Section 2.4.1, the density and specific heat capacity parameters in the convective component, the rightmost term of equation (2.6), refer exclusively to properties of the permeating fluid (as only the fluid will be involved in the convection of heat). However, the density and specific heat capacity in the time derivative term on the left hand side of equation (2.6) are properties of the bulk medium. A more explicit way of writing equation (2.6) is:

$$(\rho_m C_m)\frac{\partial \theta}{\partial t} + \rho_f C_{pf}(\vec{v} \cdot \nabla\theta) = k_{eff}\nabla^2\theta + (Q_{in}). \tag{A.1}$$

The density and specific heat capacity of the solid phase of the burial medium are set to ρ_s = 2650 kg/m$_3$ and C$_s$ = 700 J/kg/°C respectively (approximately representative of a range of actual sediment types). The bulk properties ρ_m and C$_m$ are taken as simple arithmetic combinations of the separate phases, similar to the model for bulk thermal conductivity.

Equation (A.1), combined with the form of Darcy's law formed the basis of the time dependent FEM model.

A.2.3 Heat Up Time

The first time dependent FEM simulations to be run used the same geometrical configuration (described in Chapter 3) for the cable components and surrounding burial medium as the early time independent models (with a burial depth of 1 m). These simulations investigated the time taken for cables buried in sediments with different permeabilities to heat up from an ambient temperature of 20°C to their steady-state temperature (given a heat generation profile identical to the one used in the steady-state simulations described in Chapter 3, with ampacity of 375 A according to the IEC 60287 standard). The times taken to reach equilibrium were inferred from inspection of the time dependent FEM model data by identifying the first interval (increasing logarithmically in time) for which the change in the

conductor temperature was less than 0.25% of the difference between the maximum steady state (the values for which were taken from the time independent FEM simulations with identical environmental conditions) and ambient temperatures.

Results

The results presented in Chapter 3 showed that the dissipation of heat from cables buried in highly permeable sediments is much more effective, and results in considerably lower characteristic cable temperatures than for their counterparts buried in lower permeability sediments. The results from the first time dependent FEM models (Fig. A.9) reveal that cables buried in low permeability sediments require a long time to heat up to a state of thermal equilibrium with their environment (many months, or sometimes longer). Conversely, cables in highly permeable sediments may take as little as a single day to heat up completely.

The initial heat up of the cable conductors occurs at the same rate in each case shown in Fig. A.9, regardless of the permeability of the burial sediment. Only when the temperature of the cable conductors approaches the permeability dependent steady state temperature (as defined by the temperatures obtained from the time independent FEM simulations) does the rate of heating begin to slow down. This behaviour is likely (at least partially) attributable to the time taken for the cable components to heat up from their initial ambient temperature. A temperature gradient must be established across the entire cable before heat can be conducted through it, and into the surrounding environment.

Once through the serving, the rate at which heat can be dissipated is determined by the environmental conditions. If the dissipation of heat through the surrounding sediment is perfectly efficient, the temperature at the outer surface of the cable will be maintained at ambient. An equilibrium will quickly be reached as the amount of heat lost to the environment rapidly approaches the amount generated within the cable. A cable buried at depth in a highly permeable sediment has

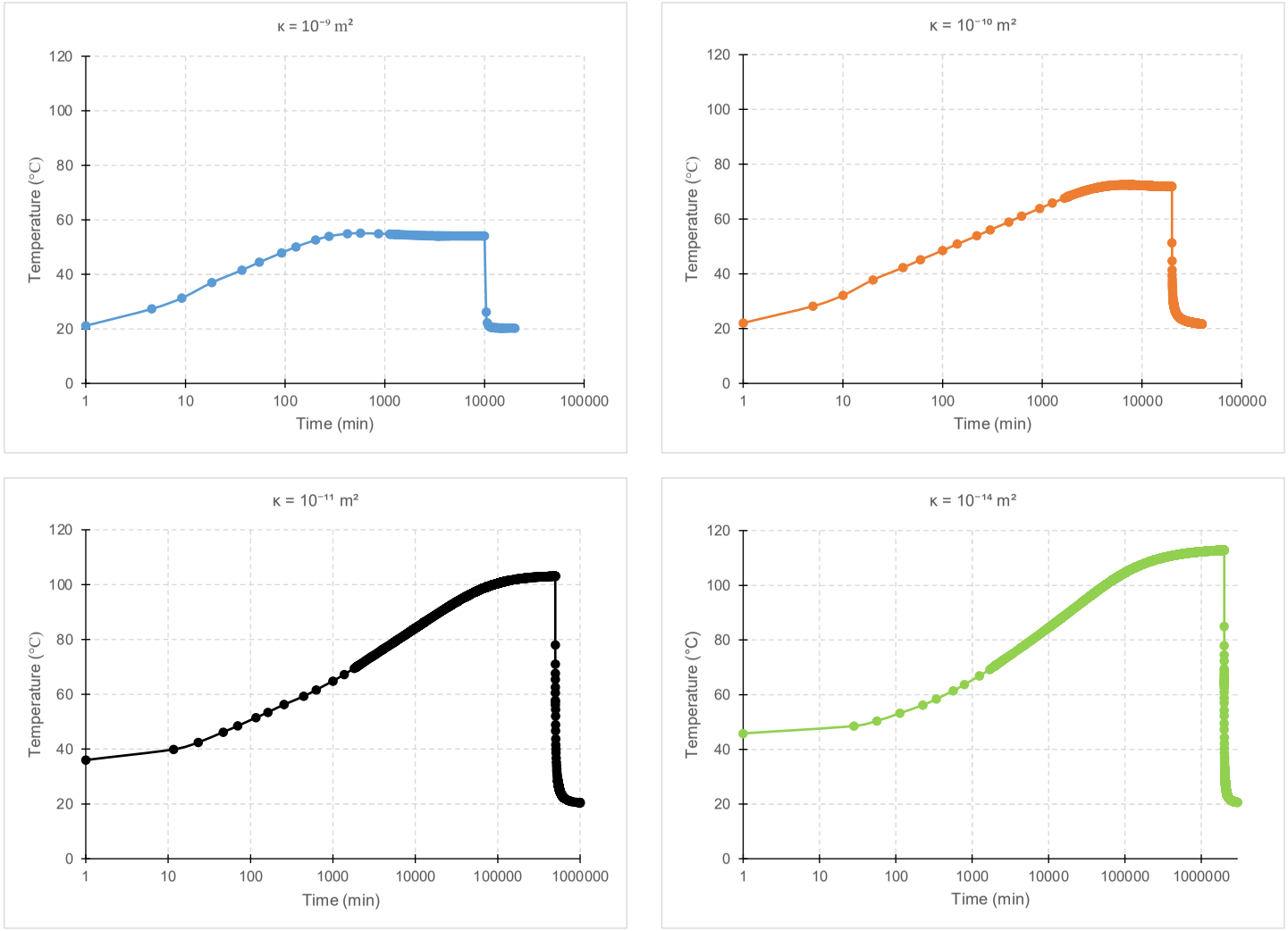

Figure A.9: Results from a time dependent FEM model illustrating the difference in the time taken for the conductors of cables buried in sediments with different permeabilities to heat up from ambient, to a steady state temperature and cool down to ambient.

a comparable heat up time to one whose outer surface is artificially maintained at an ambient temperature by enforcing a constant temperature boundary at the cable surface. Both scenarios fulfilled the criteria detailed above for estimating the point at which thermal equilibrium has been reached after a similar length of time in the FEM model. This indicates that the dissipation of heat through a highly convective sediment is relatively effective. In this case, the time taken to heat the cable components up (to temperatures sufficient to conduct all of the internally generated heat out into the surrounding environment) accounts for the majority of the time required to reach a state of thermal equilibrium.

Heat dissipation in less permeable sediments is less effective. Not all the heat conducted through the serving can be dissipated immediately, this results in the heating of the sediment surrounding the cable. To reach a steady state, temperatures inside the cable must rise further to maintain a gradient with the surrounding sediment capable of dissipating the heat being generated within the cable. This increases the length of time needed for a state of thermal equilibrium to be reached.

A.2.4 Cool Down Time

The simulations were extended to investigate the time taken to cool the cable (the design used was identical design to the previous models) from a state of thermal equilibrium with its surroundings to an ambient temperature of 20°C for a number of different sediment permeabilities. The initial temperature field within the simulation was specified by a corresponding solution to the steady state FEM simulations (detailed in Chapter 3) according to the sediment permeability being modelled. The heat generated within all cable components was set to be identically zero for the duration of the simulation. This corresponds to setting Q_{in} = 0 in equation (A.1) by making the cable current as 0 A. The model was then allowed to cool for a total of 10^7 s of simulated time.

Results

Illustrated in Fig. A.9 are the cool down times from equilibrium to ambient for a range of sediment permeabilities. In a similar manner to the results from the cable heat up simulations, the temperature response times for cables buried in highly permeable sediments were much more rapid for the cooling phase. Despite this, the difference in cooling times is not quite as extreme as the difference between heat up times for cables buried in sediments with differing permeabilities. Even the most permeable sediment shown in Fig. A.9 takes less time to approach ambient from a steady-state. Cross-referencing with heat up time, it can be seen that this is about quarter an order of magnitude more time than was required to heat up a cable buried in a similar environment to a steady state.

A.2.5 Discussion

The temperature response of submarine power cables depends greatly on the permeability of the sediment into which they are buried. As with the steady state simulations, the greatest change in behaviour occurs during the transition from conductive to convective heat dissipation. The maximum time required for a cable to heat up will occur for a sediment that does not support any convective heat dissipation at all (this is illustrated by the consistency in heat up times between the $10^{-14}(\mathrm{m}^2)$ and $10^{-11}(\mathrm{m}^2)$ permeability sediments in Fig. A.9). The shortest possible time taken to reach thermal equilibrium will occur in the hypothetical case in which the outer serving of the cable is maintained at ambient temperature by a perfectly efficient convective cooling effect within the burial medium.

The similarity in the temperature response (particularly the heat up times) between cables buried in highly permeable sediment, and those with a surface at ambient temperature indicates that the dissipation of heat through highly convective sediments is very effective. The heat up time for cables in these sediments is primarily dictated by the heat up time of the internal cable components. By con-

trast, for conductive sediments, the dissipation of heat through the surrounding sediment accounts for a much larger proportion of the total time required to reach a state of thermal equilibrium.

Using a percentage change in the temperature of the cable conductors to gauge whether the simulated cable had reached a state of thermal equilibrium revealed that the heat up and cool down times differed for cables buried in high permeability sediments. The choice of this metric is not altogether unwarranted, as the temperature of the cable conductors is of primary importance when considering implications for the current ratings of submarine power cables. However, this may not result in a representative impression of how heat is dissipated from the cable as a whole. It is interesting to consider the implications of the dependence of the temperature response in the wider context of the day to day operation of submarine power cables. The temperature of cables buried in convective sediments will respond quickly to changes in their current load. Care must be taken to acknowledge the asymmetry between the heat up and cool down periods for cables buried in highly permeable sediments to ensure that they are sufficiently cooled after a period of overloading.